Chapter 1

Introduction

1.1. Background

1.1.1 Necessity of alternative energy

International energy consumption is projected to rapidly soar, especially due to the economic growth of the non-OECD region (Energy Information Administration International Energy Outlook, 2007). On the other hand, in the best-case scenario, the world's crude oil reserves are projected to begin declining in 2018 (Robelius, 2007). Although other fossil fuels such as natural gas and coal account for a large part of the energy supply (about 34.6% of the total energy supply in Japan in 2003), these fossil fuels are also limited. One reason that the current oil price remains high is the gap between the global demand and the supply of energy resources (Medium-Term Oil Market Report, 2006), which is already shrinking, will become tighter in the future. On an aside, climate change, which is especially represented by global warming, is caused by the rapid increase in atmospheric CO_2 (Climate Change, 2001), and burning fossil fuels for energy produces CO_2, which is released into the atmosphere. Hence, it is critical to produce energy without increasing the amount of atmospheric CO_2.

Alternative energy resources are generally defined as energy resources except fossil fuels, and consist of solar photovoltaic, wind power, biomass, etc. Because these energy resources do not increase the amount of CO_2 in the atmosphere, they have received much attention as a solution to global warming. However, these alternative energy sources are expensive compared to fossil fuels, and comprised approximately 1.36% of the total energy consumption in Japan in 2003. Nevertheless, continuous

research and the introduction of the alternative energy have been conducted and proposed by many countries (Renewables Information, 2006) due to the current sharp rise in oil prices and the awareness of global warming.

1.1.2 Alternative energy introduced in Japan and the future perspective

To date, Japan has been regularly introducing alternative energy. Figure 1.1 shows the transition of the introduced amount of alternative energy in Japan between 1990 and 2003, and the future perspective in 2010. The alternative energy in Figure 1.1 includes solar photovoltaic, solar heat, wind power, bio-waste & biomass, and black liquor & waste wood. Black liquor & waste wood are mostly recycled in the pulp industry and their introduced amount has remained steady at a high level. Recently, the amount of solar heat has been declining, while those from solar photovoltaic, wind power, and bio-waste & biomass have been increasing. Particularly, the amount of bio-waste & biomass has increased rapidly, and the perspective shows that the amount of bio-waste & biomass accounts for about 41.5% of alternative energy in 2010. According to Table 1.1, the prospective amount of solar photovoltaic energy available in Japan has the highest potential. In the long run, solar photovoltaics should dominate the alternative energy industry, but in the short run, bio-waste & biomass, which might be introduced more easily, are projected to be the major resources of alternative energy in Japan (Figure 1.1).

Japan's primary energy consumption corresponded to 596,800 ML in oil equivalents during the fiscal year of 2003. The total amount of alternative energy introduced in that fiscal year was 8,100 ML in oil equivalents. Consequently, alternative energy accounted for 1.36% of the total primary energy consumption in the fiscal year of 2003. However, in the fiscal year of 2010, the prospective amount of consumed primary energy is 626,600 ML in oil equivalents, while the prospective amount of introduced alternative energy is 14,100 ML in oil equivalents, which means that alternative energy should account for 2.25% of the total primary energy consumption. Thus, it is not an exaggeration to say that whether this goal is achieved or not depends on the introduced amount of bio-waste & biomass in the fiscal year of 2010.

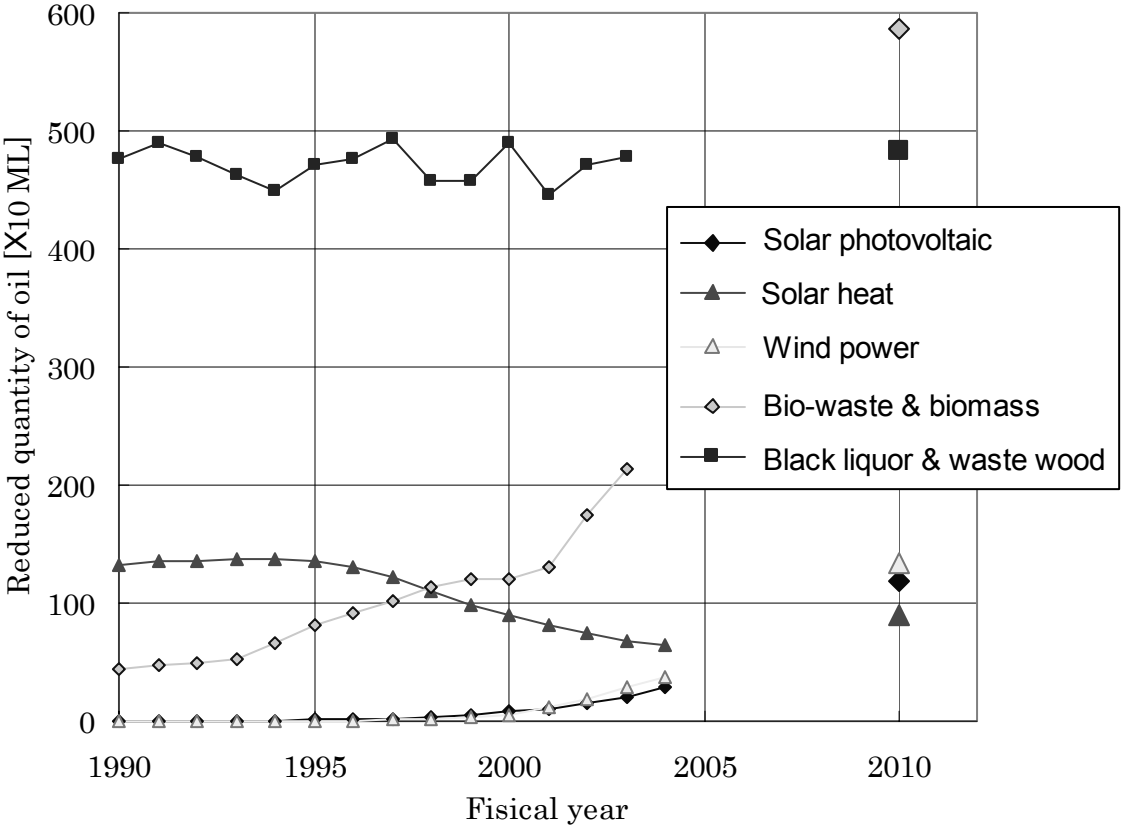

Figure 1.1 Introduced amounts of alternative energy (Technical information database on New Energy and Industrial Technology Development Organization (DB-NEDO))

Table 1.1 Prospective of the available amounts of alternative energy (DB-NEDO)

Solar photovoltaic	10,000～21,000 ML
Solar heat	8,000～16,000 ML
Wind power	1,000～2,000 ML
Bio-waste & biomass	6,600～10,000 ML
Black liquor & waste wood	6,000 ML

1.1.3 Composition of the available bio-waste & biomass in Japan

Figure 1.2 shows the composition of the available amounts of bio-waste & biomass in Japan in 2002. It should be noted that pulp biomass is not included in this pie chart. The available amounts are calculated by subtracting the amounts already used for material recycling from the total storages. As shown in this chart, the most abundant

source is wood biomass followed by food leftovers and animal manure, respectively. Wood biomass and agricultural residue, for instance rice straw, have a low moisture content, and are called dry biomass. Others, such as food leftovers, animal manure, and sewage sludge have high moisture content, and are called wet bio-waste. These wet bio-wastes occupy more than half of the total amount of bio-wastes & biomass as shown in Figure 1.2, and are expected to be used as alternative energy resources. Wet bio-wastes are hard to handle as fuels by themselves because they consume more heat energy to dry than they produce by incineration or by reforming into fuel gases in a high temperature gasification pit. Therefore, wet bio-wastes are usually fermented to produce methane, which is used in gas engines to generate electric power (Okuno et al., 2003). Some commercial methane fermentation plants have recently become operational (Yoneyama et al., 2004). At the same time, hydrothermal reactions have received attention among the viable treatment methods for wet bio-wastes.

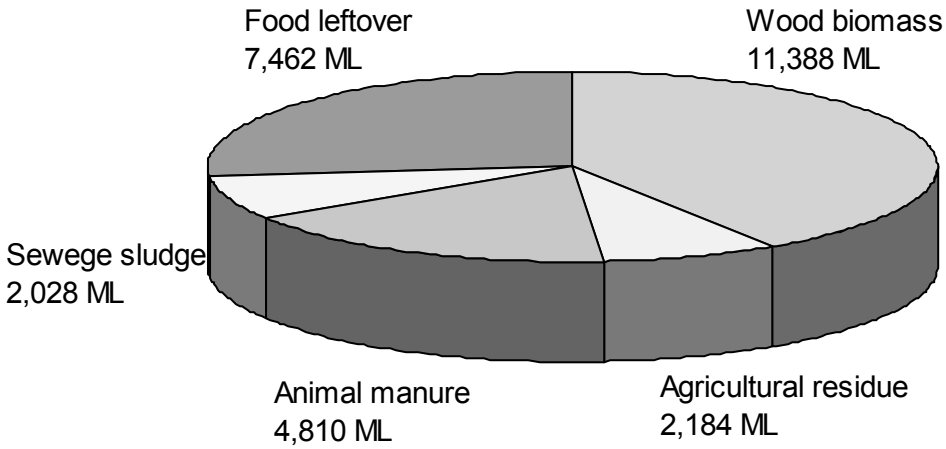

Figure 1.2 Composition of the available amounts of bio-waste & biomass (Agency for Natural Resources and Energy, Japan (ANRE documents), 2003)

1.1.4 Hydrothermal reaction and oxidation

A hydrothermal reaction is a chemical reaction in high-temperature and high-pressure water. The best advantage of using a hydrothermal reaction for wet bio-wastes treatment is that thermal energy is not needed in the drying process of wet bio-wastes because water is utilized as the reaction medium. Figure 1.3 illustrates the

phase diagram of water. The thermodynamic critical point of water exists under the conditions of 374 °C and 22.1 MPa. Hydrothermal reactions occur around this critical point, but hydrothermal reactions above the critical point are called supercritical water reactions. Hydrothermal reactions in liquid phase water below the critical point have several technical terms. However, in this study they are referred to as subcritical water reactions. Moreover, hydrothermal reactions in gas phase water below the critical point have several technical terms, but herein are called high-pressure steam reactions. When an oxidizer is added into the water medium, an oxidation reaction occurs in high-temperature and high-pressure water. This oxidation reaction is the subject of a special discipline of hydrothermal reactions, called hydrothermal oxidation. Hydrothermal oxidations are exothermic reactions that generate reaction heat. Therefore, thermal energy production from wet bio-wastes by hydrothermal oxidation is promising. Hydrothermal oxidations in supercritical water, subcritical water, and high-pressure steam are called supercritical water oxidation (SCWO), subcritical water oxidation, and high-pressure steam oxidation, respectively.

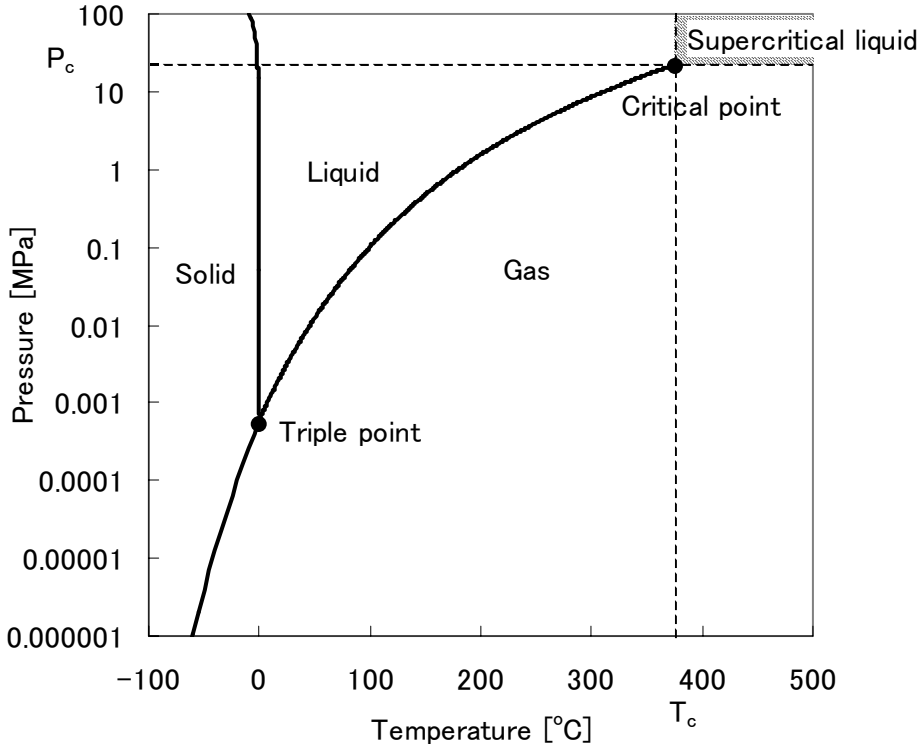

Figure 1.3 Phase diagram of water (by REFPROP)

1.1.5 Review of hydrothermal oxidation for waste material treatment

Hydrothermal oxidation such as SCWO is considered to be a promising treatment method for waste materials, particularly when the waste materials have high moisture content. Savage et al. (1995) and Shaw et al. (1991) have reported the potential of supercritical water as a chemical reaction field, and hence, SCWO has received attention from many researchers. Several works on SCWO are introduced in this section. The oxidation rate and the hydrolysis rate of H_2, CO, CH_4, and methanol have been measured in supercritical water (Webley and Tester, 1991; Holgatet and Tester, 1994; Rice et al., 1996; Brock et al., 1996). Particularly, the oxidation rates of ammonia and acetic acid have been measured in detail because these substances are the main intermediates when waste materials contain nitrogen and carbon (Li et al., 1991). In order to understand the SCWO mechanism more clearly, several studies have focused on the elementary reaction of methanol and ethanol oxidation in supercritical water (Alkam, 1996; Rice and Croiset, 2001).

As for applications to the treatment technology of waste materials, numerous studies such as the decomposition of hazardous and persistent waste materials (PCB, dioxin, incineration ash, and night soil) by SCWO, have been published. For example, Thomason and Modell (1984) have conducted a SCWO experiment using a bench scale apparatus. In their study, a methyl ethyl ketone solution, which included 3% nitrotoluene, was about 92.5% to 99.8% decomposed in accordance with the increase of reaction temperature from 404 °C to 513 °C during 20 to 30 s. Timberlake et al. (1982) have reported that urea was totally decomposed to N_2, CO_2, and H_2O at 650 °C in 22 s without nitrous oxide and only negligible amounts of ammonia nitrogen, nitrite nitrogen, and nitric nitrogen being detected in the exhaust gas. Staszak et al. (1987) have shown that more than 99.5% of nitrobenzene, chloroform, and PCB were decomposed in the SCWO process. Currently, a small number of SCWO commercial plants are operated as waste material treatments where the formation of primary pollutants, NO_x and SO_2, often produced during gas phase combustion are precluded and most waste materials are completely decomposed into non-toxic components such as N_2, CO_2, and H_2O. Several articles have reported innovative designs for a hydrothermal oxidation reactor for industrial applications (Fauvel et al., 2004; Marrone

et al., 2004). Due to these new concept reactors, some SCWO systems can generate heat by the oxidation of waste material in solution to preheat materials and can continuously operate with insignificant or no heat energy input (Barner et al., 1992; Suzuki et al., 1997; Cocero et al., 2002). Cocero et al. have suggested a hydrothermal reactor in which hot reactants after hydrothermal oxidation convey heat energy to preheat the cool incoming reactants. They have reported that operations without external heat input were possible if the drain water had a reaction enthalpy of 930 $kJ \cdot kg^{-1}$ when the drain water was decomposed at 2 $m^3 \cdot h^{-1}$ and a reaction temperature of 650 °C. The drain water, which contained 2 wt% n-hexane or 2.4 wt% 1-hexanol or 3.2 wt% hexanoic acid, satisfied this criteria and was disposed without any external heat input. If waste materials themselves contained a higher reaction enthalpy than the heat energy needed for preheating, then the additional heat energy generated by hydrothermal oxidation could be used as a heat source.

1.1.6 Advantages and disadvantages of SCWO

Most waste materials are completely decomposed in SCWO as described in Section 1.1.5. There are several reasons for the high reactivity of SCWO. 1) Reactions tend not to become diffusion-controlled because non-polar molecules such as gases (O_2) and organic substances are thoroughly dissolved in supercritical water due to its low static dielectric constant. Because the reaction field becomes one phase, substances do not need to be transported between two phases. 2) The ion product of supercritical water is low, and OH and HO_2 radical species, which originate from H_2O and O_2 molecules, are preferably formed during oxidation reactions. These radicals are believed to play an important role in SCWO through radical chain reactions. 3) The density of supercritical water is much higher than that of steam. 4) Molecular diffusivity of supercritical water is almost same as that of steam, but is much higher than that of water. The values of these physicochemical constants of water such as density, viscosity, diffusivity, heat transfer coefficient, static dielectric constant, and ion product with temperature and pressure are given in Appendix A.1. In Appendix A.2, several advantages for a hydrothermal reaction, including SCWO from an engineering viewpoint, are summarized.

However, limitations of SCWO have also been reported. Gloyna and Li (1993) noted that salt formation and corrosion on the inside wall of the reactor were among the most serious problems to be solved in SCWO systems. Salt formation, which is due to the low dielectric constant of supercritical water, causes a clogging problem in a reactor, and becomes a significant issue in the SCWO process when continuous operation is needed. Some studies have been conducted to overcome these limitations by specially designing reactors. For example, Hong et al. (1989) invented a two-zone reactor, which had a supercritical region where organic species were oxidized and a subcritical region where precipitated salts redissolved. Daman (1996) invented a transpiring wall reactor, which had a porous reactor liner near the wall through which solute-free water passed to prevent the wall from being exposed to hot reactants. A reactor with a wall made of a special alloy such as Hastelloy or Inconel that can endure the severe condition of SCWO, has also been suggested and manufactured.

1.1.7 Subcritical water oxidation

As explained in Sections 1.1.5 and 1.1.6, it has been confirmed that most waste materials are decomposed by SCWO, and certain amount of thermal energy is produced, but there are two problems from an engineering point of view, clogging and corrosion of the reactor. One of the easiest ways to overcome these two problems is to change the oxidation reaction field from supercritical water to subcritical water. Salt is better dissolved in subcritical water than in supercritical water due to the large difference in the static dielectric constant. Reactor corrosion caused by the high reactivity of SCWO is lessened with subcritical water oxidation because the advantages of SCWO mentioned in Section 1.1.6 (high solubility of non-polar materials such as O_2, high molecular diffusivity, etc.) are to some extent degraded in subcritical water oxidation, which means that subcritical water oxidation is a milder oxidation reaction than SCWO.

High-pressure steam oxidations also have a lower reactivity than SCWO when the reaction temperature is same. Thus, the corrosion problem can be alleviated in high-pressure steam oxidations. However, salt is not dissolved in high-pressure steam or in supercritical water. Hence, there is a high possibility that the clogging problem

will remain in high-pressure steam oxidations. In addition, the ion product of subcritical water is higher than that of supercritical water or high-pressure steam, and it is known that hydrolysis reactions, which reform substances with higher molecular weight to those with lower molecular weight, proceed faster in subcritical water (Yoshida et al., 1999; Yoshida and Tavakoli, 2004). Based on this knowledge, we decided to focus on subcritical water oxidation as a method of thermal energy production from bio-wastes with high moisture content.

However, it should be noted that when the state of subcritical water is far from the critical point, the reactivity of subcritical water oxidation becomes much lower and little oxidation reaction occurs. Thus, this situation must be avoided to achieve a beneficial use of wet bio-wastes as an energy resource. Therefore, it is necessary to conduct experiments that investigate and confirm efficient thermal energy production by subcritical water oxidation under certain conditions of temperatures and pressures.

1.1.8 Electric power generation by hydrothermal oxidation

Hydrothermal oxidation is an exothermic reaction, and a system to best use the thermal energy obtained by hydrothermal oxidation remains to be developed. A good example of such a system is an electric power generation system because electricity is more versatile than thermal energy itself. Additionally, the transmission of electricity is easier and more efficient than conveying thermal energy. A few studies have reported electric power generation systems using hydrothermal oxidation. Naito et al. (2001) have numerically simulated the efficiency of electric power generation by hydrothermal oxidation of ethanol solutions. However, their study only considered a system where a hot reactant after the hydrothermal oxidation flowed directly into a turbine. In addition, their simulation simplified the expansion process at the turbine by fixing the enthalpy at a turbine outlet to a saturated steam enthalpy at 35 °C.

If electric power generation systems from wet bio-wastes by hydrothermal oxidations are to be operated for industrial purposes, more intensive and precise evaluations of the systems must be conducted. For instance, introducing the adiabatic efficiency in the expansion process at the turbine changes the state of water at the turbine outlet, which is more realistic for practical situations. Another type of electric

power generation system where hot reactants from real bio-wastes by hydrothermal oxidation do not flow directly into a turbine also needs to be considered because real bio-wastes contain impure substances, which can cause serious problems to the turbine.

1.2. Objectives

We strived to study the feasibility of subcritical water oxidation for use as a thermal energy production method from bio-wastes with high moisture content. Experiments on subcritical water oxidation were conducted in order to confirm the occurrence of an exothermic reaction. Our experiment is unique because it focuses on subcritical water oxidation to produce thermal energy from wet bio-wastes. In the experiments, ethanol solutions were used as the test reactant. Although ethanol may not be considered a model reactant for bio-wastes with high moisture content because ethanol is miscible with water and most bio-wastes are immiscible, insoluble, two-phased, and highly buoyant in water, it has been reported that several bio-wastes are hydrolyzed in subcritical water to produce miscible substances such as alcohols and fatty acids (Hashaikeh et al., 2005; Holliday et al., 1997). Moreover, ethanol is among the simplest compounds containing C, H, and O atoms, all of which are prevalent in bio-wastes, and are non-toxic, which makes them easy to handle. Additionally a large amount of ethanol solutions have recently been produced from plant-based biomass such as corn or wood chips by fermentation. For this reason, ethanol solutions were selected as a model reactant.

Besides this feasibility study, electric power generation systems were evaluated by numerical simulations for the beneficial use of thermal energy obtained from wet bio-wastes by hydrothermal oxidation. The innovative point of this simulation is that the numerical studies were conducted with a more detailed simulation model than a previous work to the two electric power generation systems; one has already been reported and the other is the newly proposed. In the numerical simulations, ethanol, glucose, and peat solutions were selected as reactants for hydrothermal oxidation. Glucose solutions can be regarded as a model for biomass because glucose is a monomer of cellulose, which is found in a lot of wood biomass, while peat solutions are regarded as typical examples of real biomasses. To sum up, the objectives of this study are to

evaluate:

1) Thermal energy production by subcritical water oxidation of ethanol solutions using laboratory scale experimental apparatuses.

2) Electric power generation systems where thermal energy is obtained from wet bio-wastes by hydrothermal oxidation.

1.3. Organization of the thesis

This thesis consists of the following chapters: Chapter 2 describes the experimental results of subcritical water oxidation of ethanol solutions, including the production of hot water using laboratory scale apparatuses. Chapter 3 describes the kinetics of the ethanol oxidation reaction in subcritical water. A first-order oxidation rate and oxidation rate, which includes the oxygen concentration, are obtained. Chapter 4 describes a numerical study of subcritical water oxidation of ethanol solution. Moreover, in Chapter 4 these numerical results are compared with the experimental results in Chapter 2. Chapter 5 describes the numerical simulation to estimate electric power and energy conversion efficiency in power plants using hydrothermal oxidation. Two types of power plants, a direct type and indirect type, are considered. Ethanol, glucose, and peat solutions are assumed as the reactants. Chapter 6 summarizes the conclusions of this study and its future perspective. The contents in Chapters 2, 3, 4, and 5 are collected and organized from the content of three published papers (Hirosaka et al., 2007; Hirosaka et al., 2008[a]; Hirosaka et al., 2008[b]).

Chapter 2

Hot water production by subcritical water oxidation of ethanol

2.1 Purposes

Hot water production by subcritical water oxidation of ethanol (EtOH) solutions using laboratory scale flow type reactor is conducted in order to confirm that subcritical water oxidation can be used as a thermal energy production method from bio-wastes with high moisture content. EtOH solutions are selected as a reactant model in this experiment. The reason of this selection is explained in Section 1.2. It is considered that the production of hot water around 300 °C would be sufficient for this confirmation because the temperature range of subcritical water is below 374 °C.

In this experiment the following things are investigated. First of all, a preheating temperature at which subcritical water oxidation of EtOH solutions occurs is measured. The measurement of the temperature limit at which the subcritical water oxidation progress fast enough to produce heat energy is necessary because the thermal energy production system by subcritical water oxidation is the major objective in this study. Next, the temperature increases in product solutions by subcritical water oxidation in the reactor are measured to investigate the temperature of the produced hot water. At the same time, the oxidation products in the gas phase are analyzed to check what kind of reaction has occurred dominantly as well as to confirm that no harmful substances are produced.

2.2 Experiment

2.2.1 Experimental apparatus

Figure 2.1 shows the schematic diagram of experimental apparatus. A reactor is made of SUS316 tube with 825 mm in length, 11 mm in inner diameter and 4 mm in wall thickness. Two high-pressure pumps (Hitachi, L-6200) are employed to feed EtOH solution and hydrogen peroxide (H_2O_2) solution separately into the reactor. These high-pressure pumps are plunger type pumps (Figure 2.2). The pressure inside the reactor is maintained around 25 MPa by a buck pressure regulator at the end of the reactor. Three heaters are installed on the reactor tube in order to raise the temperature of the reactants. The temperature increase of the reactants was measured by four K-type thermocouples (Yamari Industries, Ltd.) installed in the reactor as shown in Figure 2.1. The distance between each thermocouple was 218 mm. The reactant is cooled down below 100 °C by a cooling unit so that the reaction is terminated after passing through the reactor. All flow channels except the reactor are made of SUS304 tube with 0.8 mm in inner diameter. Gas samples were collected in a water pool as shown in Figure 2.1. The gas samples and the liquid samples were analyzed by the gas chromatography (GC-FID: HP 4890A, GC-TCD: Yanaco G1880, Shimadzu GC-14B). Figures 2.3 and 2.4 illustrate the filling cylinder and the reactor and heater, respectively. Figure 2.5 and Figure 2.6 shows the schematic diagram of the cooling unit and the GC-FID, respectively. Table 2.1 and 2.2 indicate the analytical conditions and the scale of the capillary column for FID-GC and TCD-GC.

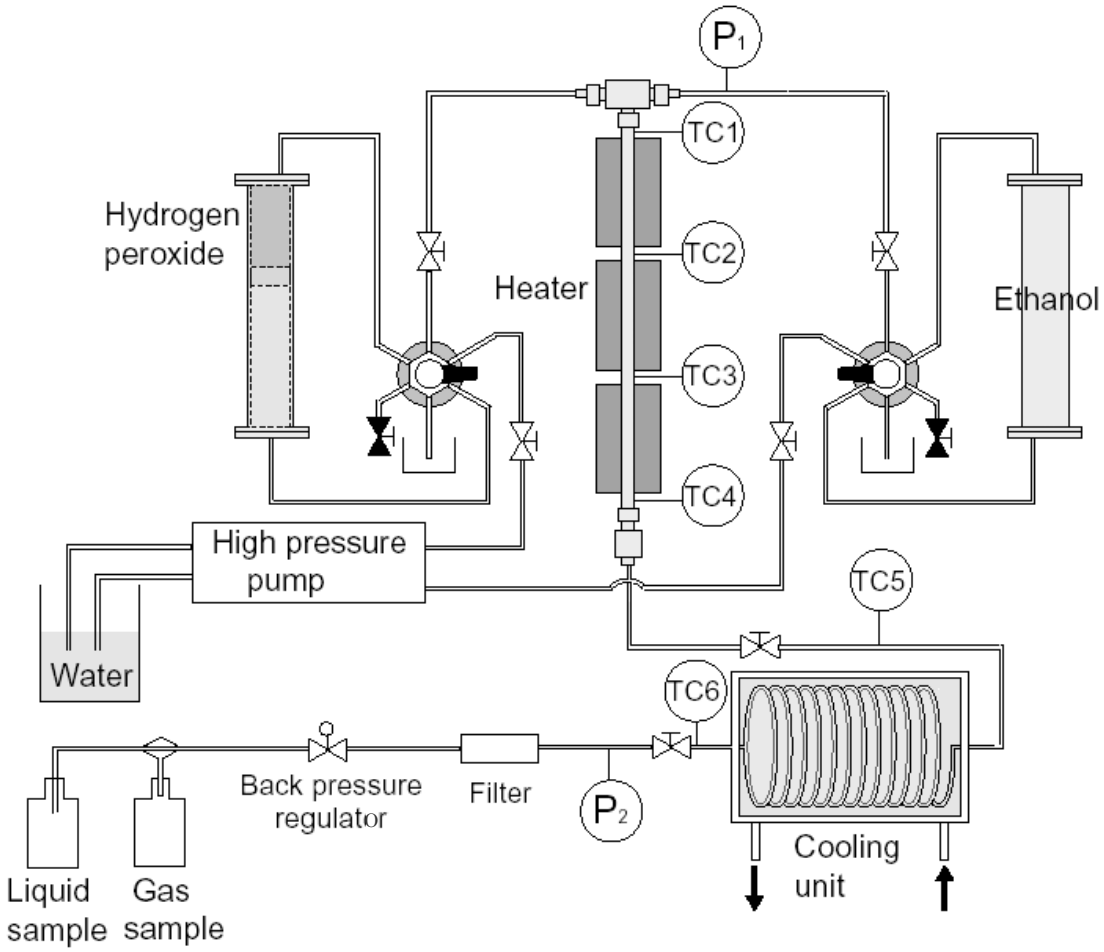

Figure 2.1 Experimental apparatus

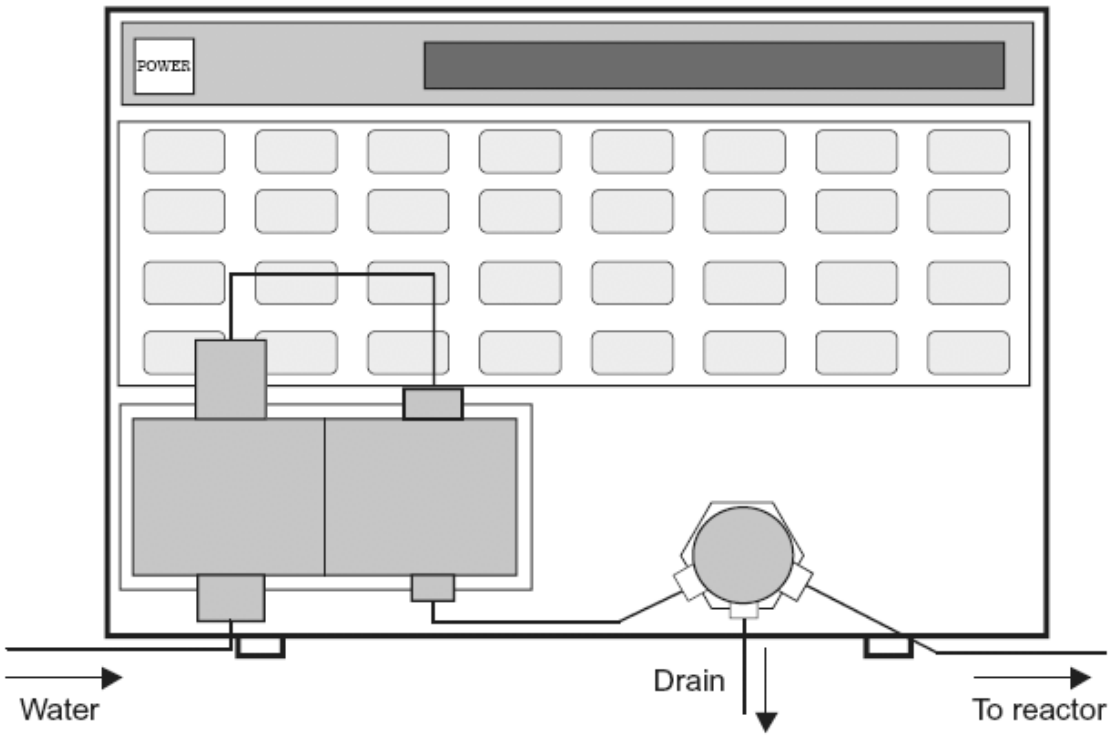

- Type Double plunger pumping
- Max pressure 400 kgf·cm^{-2} [39.2 MPa]
- Range of flow rate 0.01-9.99 ml·min^{-1}

Figure 2.2 High-pressure pump

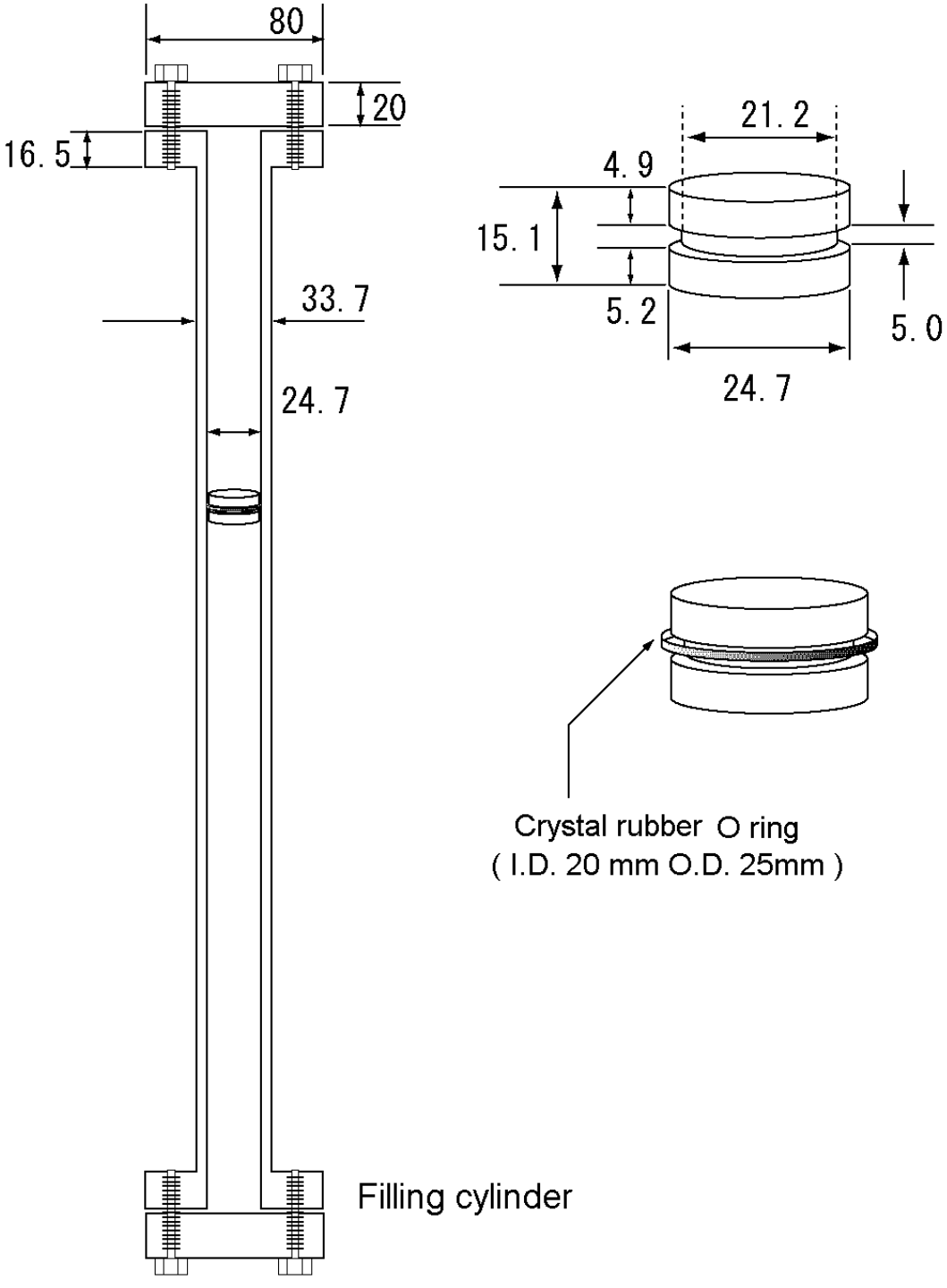

Figure 2.3 Filling cylinder

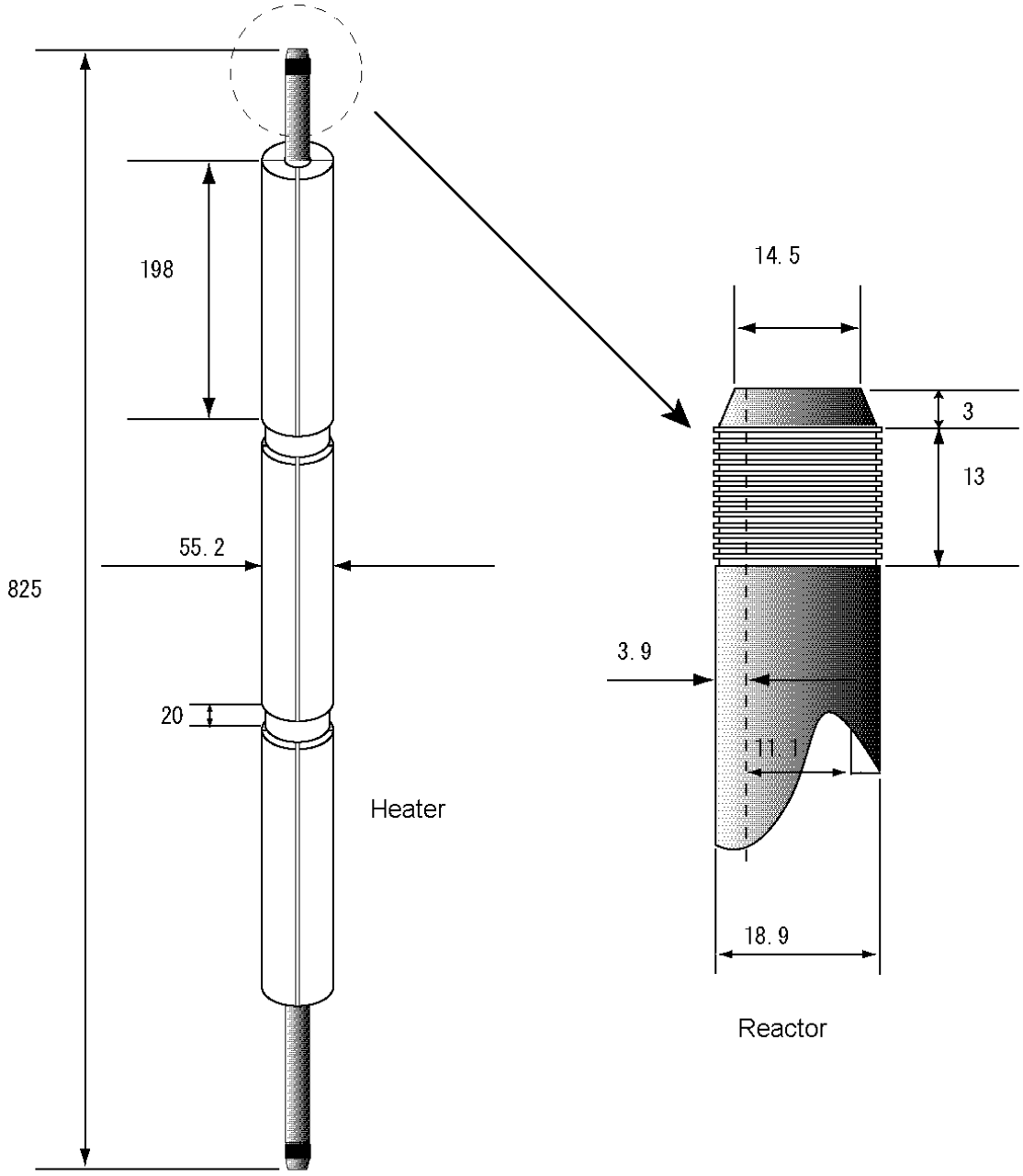

Figure 2.4 Reactor and heaters

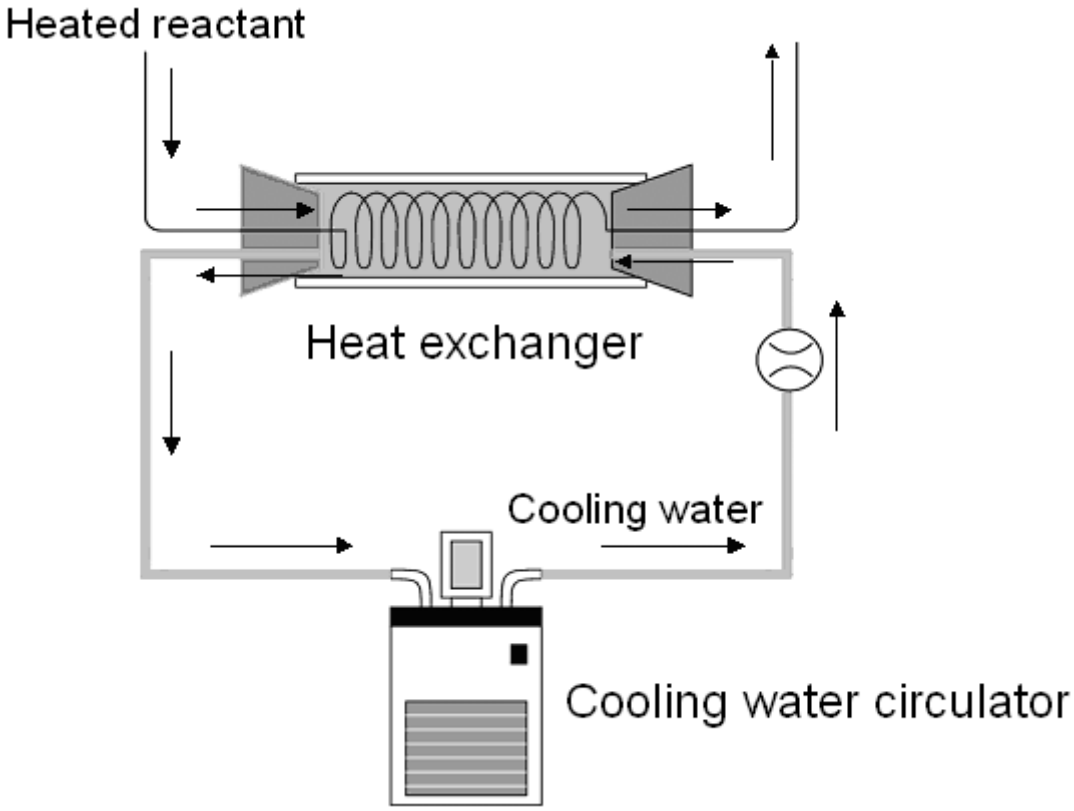

Figure 2.5 Cooling unit

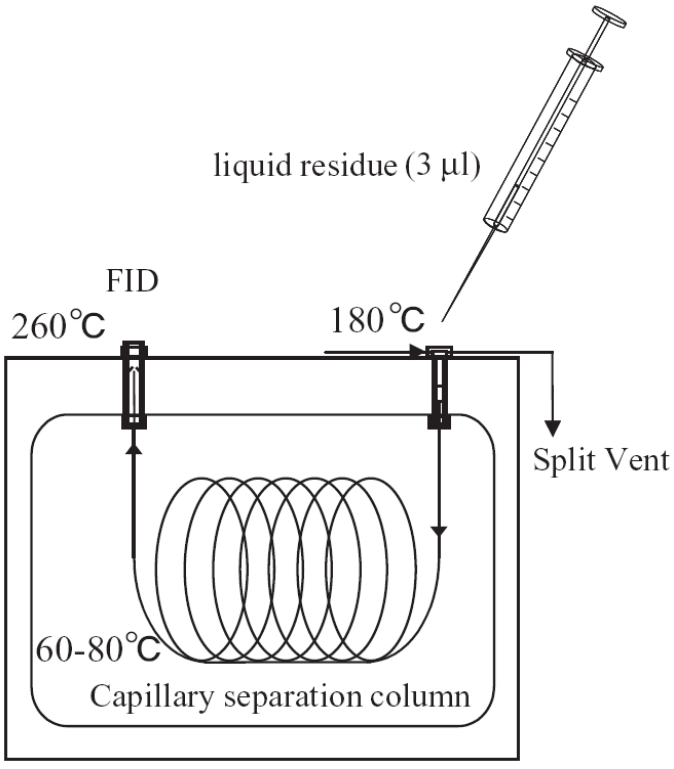

Figure 2.6 GC-FID

Table 2.1 System configuration of GC analysis for liquid sample

Detected substance	C_2H_5OH, CH_3COOH
Analysis equipment	HP-5890series Ⅱ (Hewlett-Packard)
Column	J&W Capillary Column, DB-225 (50%-Cyanopropylphenyl)- methylpolysiloxane, Middle/high-polarity Length = 30 m, I.D. = 0.25 mm, Film = 0.25 μm
Carrier gas	He
Detection method	FID
Analysis condition	Injection Temp. = 180 °C Detector Temp. = 260 °C Oven: Initial Temp. = 60 °C, Rate = 10 °C·min^{-1}, Final Temp. = 80 °C, Initial time = 2 mins, Final time = 2 mins
Injected quantity	3 μl

Table 2.2 System configuration of GC analysis for gas sample

Detected substance	H_2	O_2, CO, CH_4	CO_2, C_2H_4, C_2H_6
Analysis equipment	G1880 (YANACO)	GC-14B (SHIMADZU)	
Column	GL Packed Column (SUS) Length = 2 m, I.D. = 3 mm Molecular Sieve 5A 30/60		GL Packed Column (SUS) Length = 2 m, I.D. = 3 mm Porapak Q 30/60
Carrier gas	Ar	He	
Detection method	TCD		
Analysis condition	Oven Temp. = 60 °C Injection Temp. = 80 °C Detector Temp. = 80 °C		
Injected quantity	0.5ml		

2.2.2 Experimental conditions

Two kinds of experiments are conducted in this study. In one experiment, the effect of the preheating temperature of the reactants is investigated. In this case, the preheating temperature of the reactants is changed from 140 °C to 290 °C while the concentration of EtOH solution and that of H_2O_2 solution are fixed to 12 vol% and 6 vol%, respectively (equivalent ratio is 4.8, i.e. fuel-rich condition). In the other experiment, the effect of the oxidizer concentration is investigated. In this case, the concentration of H_2O_2 solution is changed from 2 vol% to 20 vol% (equivalent ratio is changed from 14 to 1.4) while the concentration of EtOH solution and the preheating temperature of the reactants are fixed to 12 vol% and 200 °C, respectively. Flowing rate of high-pressure pumps were 9.99 $ml \cdot min^{-1}$ for both EtOH and H_2O_2 solutions in both experiments.

2.2.3 Experimental procedure

First, only water was pumped into the reactor until the temperature of the water inside the reactor reached the preheating temperature by adjusting the electric power of the heater. This meant that the heat loss from the reactor could be compensated by the heat addition. Then, valves were switched to pump EtOH and H_2O_2 solutions into the reactor. Temperature increases of the reactant inside the reactor were measured by thermocouples (TC1 to TC4 in Figure 2.1).

2.3 Results and discussion

2.3.1 Effect of preheating temperature

Figure 2.7 shows the increase of temperature and enthalpy of the reactant caused by subcritical water oxidation at three measuring points (T2, T3, T4 from upper to bottom in order) in function of the preheating temperature. The temperature increase was larger at the bottom side of the reactor when the preheating temperature was 140 °C, but the temperature increase became larger at the upper side of the reactor when the preheating temperature became higher. This indicates that the reaction zone moved toward the inlet of the reactor from the downstream as the preheating temperature increased. Figure 2.8 shows the conversion of EtOH solution in function of the

preheating temperature. The conversion increased as the preheating temperature increased, and it saturated at 55% above 200 °C. This was caused by the lack of oxidant, i.e. the reactant was in fuel-rich condition (equivalent ratio was 4.8). From this result, it is shown that the preheating temperature of 200 °C is almost high enough for the subcritical water oxidation of 12 vol% EtOH solution to proceed sufficiently in this experimental apparatus.

2.3.2 Effect of oxidizer concentration

Figure 2.9 shows the increase of temperature and enthalpy of the reactant at three measuring points when the concentration of H_2O_2 solution changed from 2 vol% to 20 vol%, while the preheating temperature was fixed at 200 °C. The temperature increase due to hydrothermal oxidation occurred at the upper side of the reactor and reached up to 120 °C (corresponding increase of enthalpy was 576 $kJ \cdot kg^{-1}$) when the concentration of H_2O_2 solution became 20 vol% (equivalence ratio was 1.4). In this case, temperature of the obtained hot water became 320 °C because the preheating temperature was 200 °C and temperature increase was 120 °C. Thus it was found that the production of hot water around 300 °C was realized by subcritical water oxidation of EtOH solution. Figure 2.10 shows the conversion of EtOH solution in function of the concentration of H_2O_2 solution. The conversion increased as the concentration of H_2O_2 solution increased, and reached a constant value around 95% above 14 vol% of H_2O_2 solution. Figure 2.11 shows the composition of produced gas at different concentration of H_2O_2 solution. At a lower concentration of H_2O_2 solution, decomposition reaction was dominant and methane (CH_4), carbon monoxide (CO), and hydrogen (H_2) were produced. On the other hand, at a higher concentration of H_2O_2 solution, hydrothermal oxidation became dominant and carbon dioxide (CO_2) was mainly produced and the amount of CH_4, CO, and H_2 became smaller.

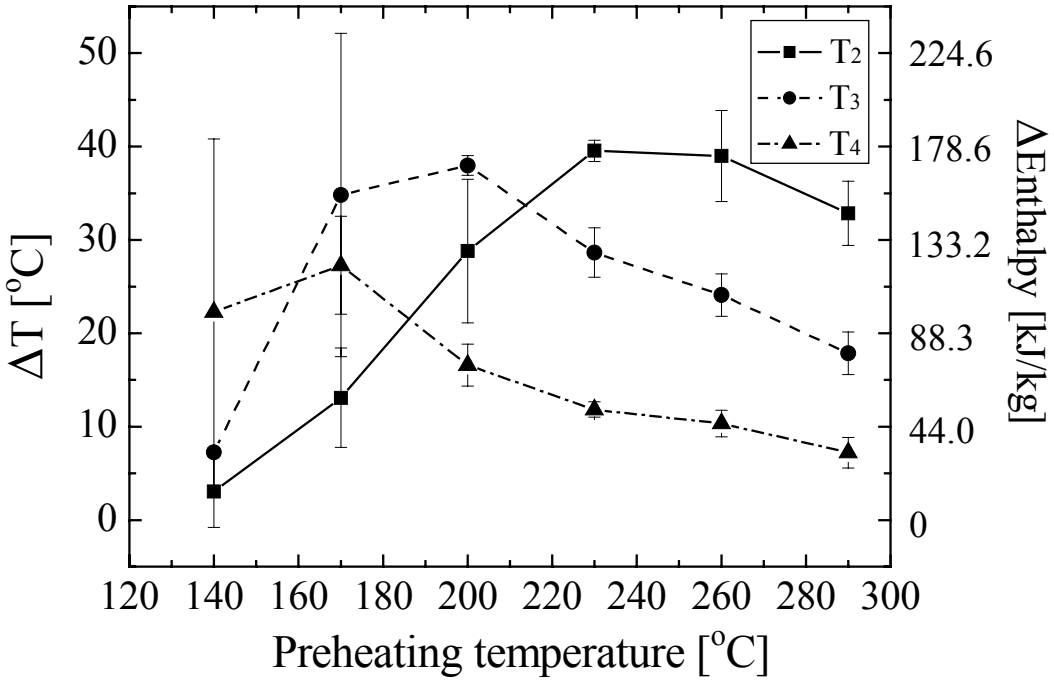

Figure 2.7 Temperature increase and enthalpy increase vs. preheating temperature

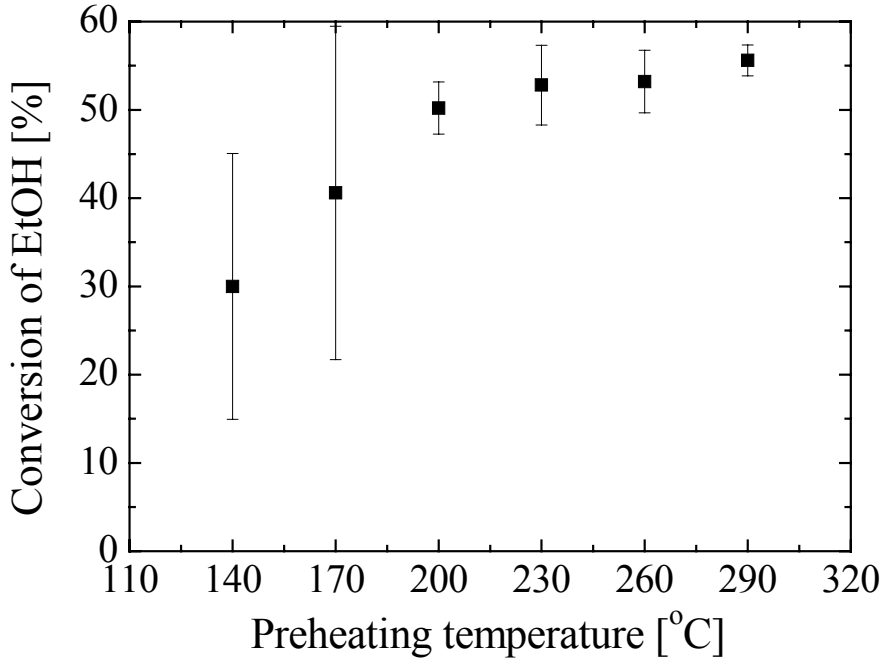

Figure 2.8 Conversion of EtOH vs. preheating temperature

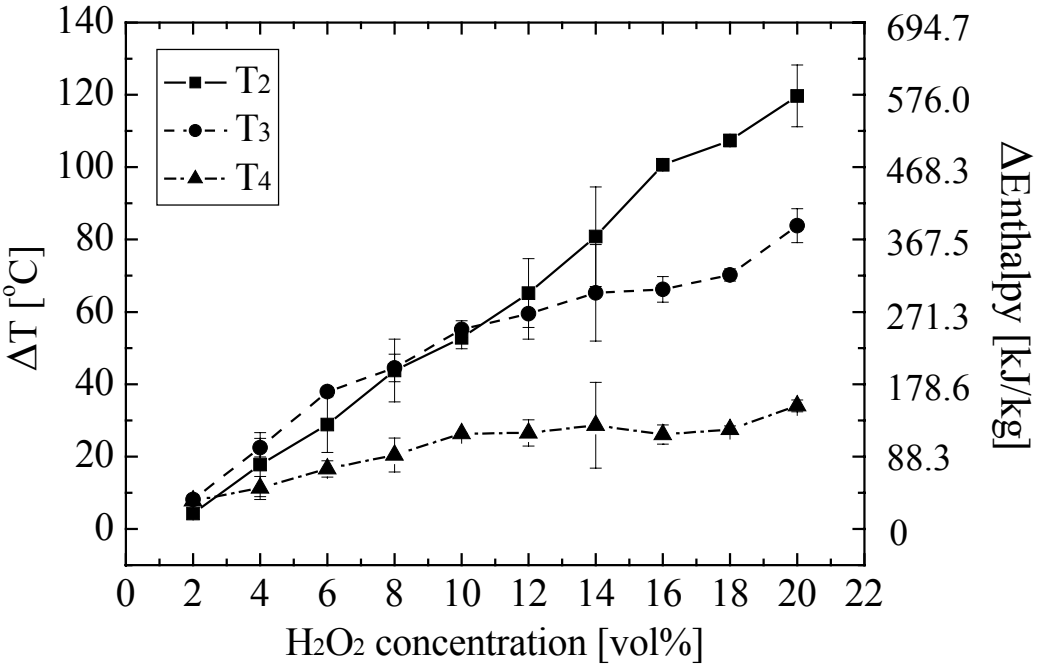

Figure 2.9 Temperature increase and enthalpy increase vs. H_2O_2 concentration

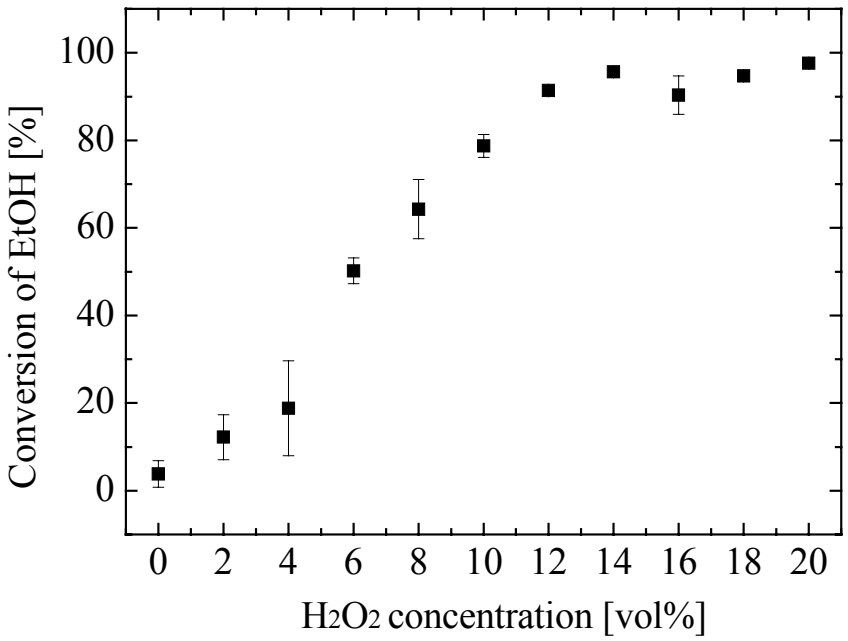

Figure 2.10 Conversion of EtOH vs. H_2O_2 concentration

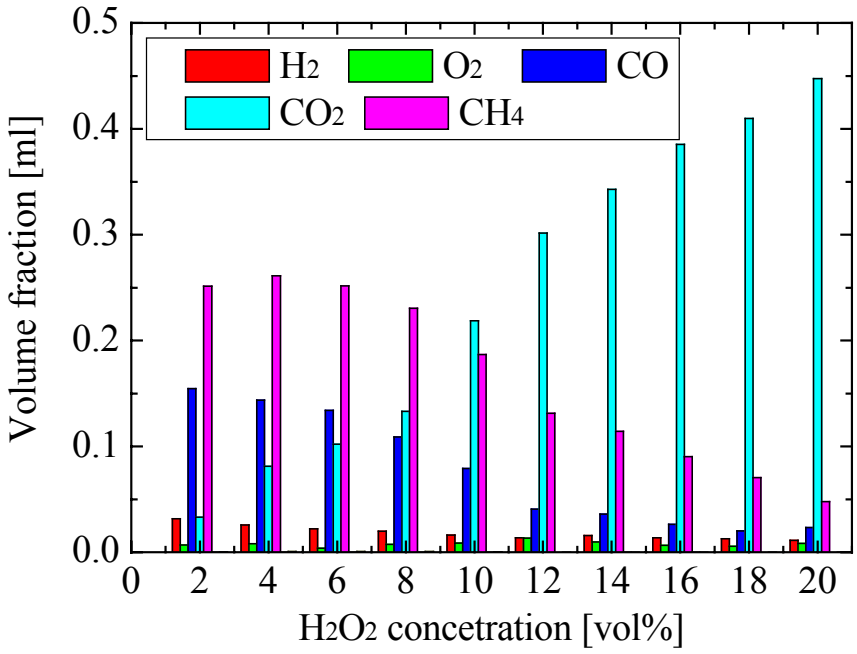

Figure 2.11 Volume fractions of H_2, O_2, CO, CO_2, and CH_4 vs. H_2O_2 concentration

2.4 Summary

Experiments on subcritical water oxidation of EtOH solution indicated that moderate exothermic reaction occurred and its conversion depended on the preheating temperature and the concentration of H_2O_2 solution. Results are summarized as follows:

1) The conversion of EtOH solution increased as the preheating temperature increased and it saturated above 200 °C.

2) The temperature increase and the enthalpy increase by EtOH oxidation reached up to 120 °C and 576 $kJ \cdot kg^{-1}$, respectively when the concentration of H_2O_2 solution was 20 vol%. This means that the production of hot water around 300 °C by subcritical water oxidation of EtOH is possible.

3) The conversion of EtOH solution increased as the concentration of H_2O_2 solution increased and it saturated around 95% above 14 vol%.

4) At a lower concentration of H_2O_2 solution, decomposition reaction of EtOH was dominant and CH_4, CO, H_2 were produced. At a higher concentration of H_2O_2 solution, oxidation reaction of EtOH was dominant and CO_2 was produced.

Chapter 3

Measurement of oxidation rate of ethanol in subcritical water

3.1 Purposes

It is necessary to measure the oxidation rate of ethanol in subcritical water, i.e. the pre-exponential factor and the activation energy in order to estimate a processing capacity of subcritical water oxidation as a thermal energy production method. Various studies about hydrothermal oxidation of ethanol have been reported until now. Schanzenbächer et al. (2002) and Helling and Tester (1988) have studied the oxidation rate of ethanol in supercritical water. Rice and Croiset (2001) have discussed the elementary reactions of SCWO of ethanol and modified the elementary reaction mechanism of ethanol by Marinov (1999) for SCWO conditions. However, oxidation rate of ethanol in subcritical water has not been reported yet. In this section, measurement of oxidation rate of ethanol in subcritical water was conducted using laboratory scale flow type reactor. Two types of oxidation rate, first-order oxidation rate and oxidation rate including oxygen concentration are obtained in these measurements. First-order oxidation rate are measured by the experiments under the fuel-lean condition (equivalence ratio of 0.5). Because actual heat source plants are usually operated around at equivalence ratio of 1, oxidation rate including oxygen concentration also need to be measured for a more accurate estimation of the processing capacity. The resulting oxidation rates are compared with those in supercritical water, which were obtained by Schanzenbächer et al. (2002).

3.2 Experiment

3.2.1 Experimental apparatus

For the measurement of the oxidation rate, we modified the apparatus in Figure 2.1. Figure 3.1 illustrates the experimental apparatus. Two high-pressure pumps are employed to feed aqueous solution of ethanol and H_2O_2 into the preheaters (300 mm in length and 12.25 mm in inner diameter). In these preheaters, aqueous solution of ethanol and H_2O_2 are heated up to the prescribed temperatures (170, 200, 230 °C), separately. Residence times of the aqueous solution of H_2O_2 in the preheater are estimated to be 388 and 360 s at 170 and 230 °C, respectively. The temperature and the density corresponding to it in the preheater are assumed to be constant since the aqueous solution of H_2O_2 is quickly heated up to around these prescribed temperatures near the inlet of the preheater. H_2O_2 needs to be decomposed into oxygen during passing through the preheater in order to measure the ethanol oxidation rate by oxygen not by H_2O_2. Croiset et al. (1997) and Takagi and Ishigure (1985) published the kinetic data for the thermal decomposition of H_2O_2 in high temperature water. On the basis of the kinetic data (Croiset et al., 1997) greater than 99% of H_2O_2 would be decomposed inside the preheater under these temperatures.

Three types of reactor made of SUS316 with different length (300 mm, 600 mm, 900 mm) but with the same inner diameter (12.25 mm) are prepared to measure the conversion of ethanol at different residence times. Residence time of the reactant inside the reactor is calculated using the flow rate and the tube volume, which is calculated from the known reactor tube diameter and length. The flow rate is obtained by considering the corresponding density (assuming pure water) at the reaction temperature and pressure. The temperature inside the reactor is maintained to the prescribed temperature (170, 200, 230 °C) by three heaters installed on the reactor, which are controlled by on-off controllers. From TC1 to TC4 in Figure 3.1 indicate the thermocouples, which measure the temperature inside the reactor. The experimental conditions are selected to meet plug-flow criteria (Cutler et al., 1988). The plug-flow reactor assumption holds even at the lowest Reynolds number of 104.4 corresponding to 170 °C and 10.9 $cm^3 \cdot min^{-1}$ since surface reactions in this reactor were assumed to be negligible (Arita et al., 2003). The reactant is cooled down below 100 °C by a cooling unit

so that the reaction is terminated. The pressure inside the reactor is measured by a pressure gauge, P in Figure 3.1. The reactant is collected after the backpressure regulator. All flow channels are made of SUS304 tube with 0.8 mm in inner diameter. Ethanol residuals in the liquid samples are measured by gas chromatography (GC-FID, HP 4890A), using internal standard method by adding 1-Butanol as a reference.

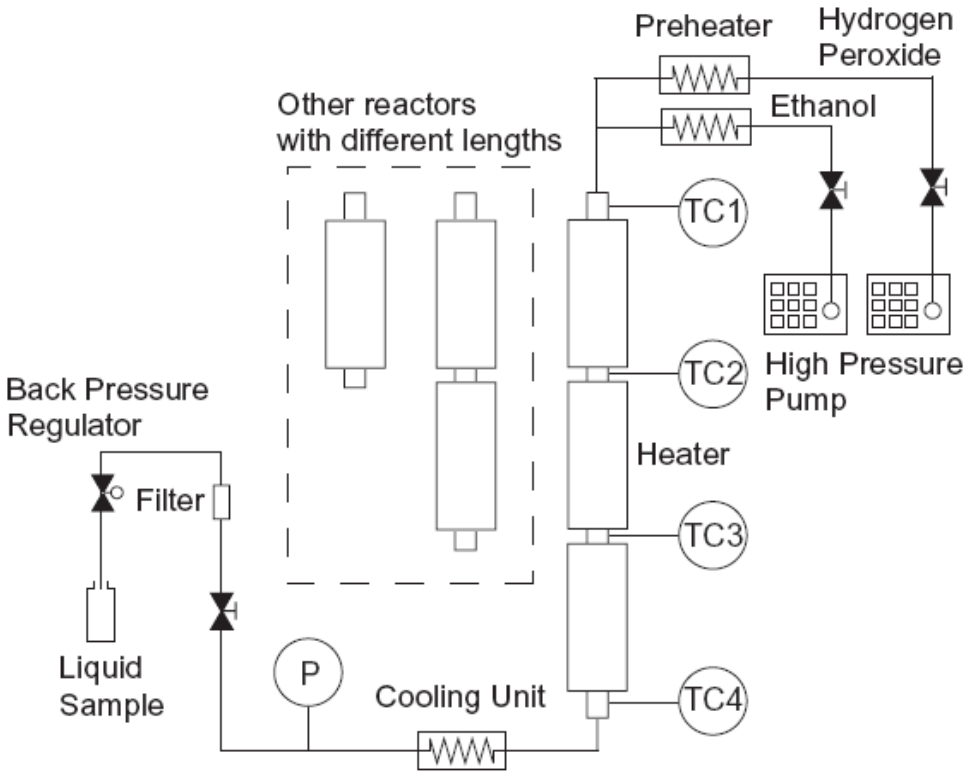

Figure 3.1 Modified experimental apparatus

3.2.2 Experimental conditions

Table 3.1 shows the experimental conditions. In this measurement, we focus on the subcritical water oxidation, thus temperature is set under the critical temperature and pressure is set over the critical pressure.

Two kinds of oxidation rate are measured. One is the first-order oxidation rate and the other is the oxidation rate including oxygen concentration. When first-order oxidation rate is investigated, equivalence ratio was set to 0.5, i.e. the oxidation occurred under the fuel-lean condition. Under this condition, influence of the oxygen concentration to the oxidation rate can be ignored. First-order oxidation is assumed

because the ethanol oxidation occurs under dilution condition. When oxidation rate including the oxygen concentration is investigated, equivalence ratio was varied from 0.5 to 1.5.

Table 3.1 Experimental conditions

Temperature [°C]	Pressure [MPa]	Flow Rate at 25 °C [1)]	Initial EtOH concentration	Initail O_2 concentration	Equivalence ratio
				150 mmol·l^{-1}	0.5
170, 200, 230	23.5	5.0 ml·min^{-1}	25 mmol·l^{-1}	75 mmol·l^{-1}	1.0
				50 mmol·l^{-1}	1.5

[1)] Flow rate is the same for both EtOH and H_2O_2 aqueous solutions.

3.3 Results and discussion

3.3.1 First-order oxidation rate

Ethanol conversions were measured at each prescribed temperature (170 °C, 200 °C, 230 °C). These measurements were conducted three times on each reactor. A summary of the measured conversion is shown in Table 3.2. Figure 3.2 shows the relation between $\ln([\mathrm{EtOH}]/[\mathrm{EtOH}]_0)$ and residence time at each temperature, where $[\mathrm{EtOH}]_0$ is the initial ethanol concentration. Error bar indicates the standard deviation. The oxidation rate was obtained by the negative slope of linear fit for each temperature as shown in Figure 3.2.

Figure 3.3 shows the Arrhenius plot of the oxidation rate k. Vertical and horizontal axes are $\ln k$ and $1/T$, respectively. The pre-exponential factor A and the activation energy E_a were obtained by the linear approximation of the Arrhenius plot. The resulting first-order oxidation rate is expressed as follows:

$$-\frac{d[\mathrm{EtOH}]}{dt} = 10^{2.64\pm0.07} \times \exp\left(\frac{-45.6\pm0.6\mathrm{kJ/mol}}{RT}\right)[\mathrm{EtOH}] \quad (1)$$

For supercritical conditions at 25.6 MPa and 430-490 °C, Schanzenbächer et al. (2002) obtained the oxidation rate of ethanol assuming the first-order oxidation of ethanol as

follows:

$$-\frac{d[\mathrm{EtOH}]}{dt} = 10^{11.1\pm4.5} \times \exp\left(\frac{-163.9 \pm 3.3\mathrm{kJ/mol}}{RT}\right)[\mathrm{EtOH}] \quad (2)$$

In Figure 3.4, the oxidation rate of ethanol obtained in our experiment is compared with that of Schanzenbächer et al. (2002). Temperature dependence was higher in supercritical region than in subcritical region, which is attributable the difference of the activation energy between subcritical water oxidation and SCWO. The activation energy is lower in subcritical water oxidation than in SCWO and this would be caused by the difference of reaction mechanism between both oxidations, i.e., H_2O molecules involve in the radical chain reactions more intensively in SCWO of ethanol than in its subcritical water oxidation. Pre-exponential factor is much larger in SCWO, which would indicate that radical and molecular collisions occur more frequently in SCWO. Overall, the reactivity is much higher in SCWO.

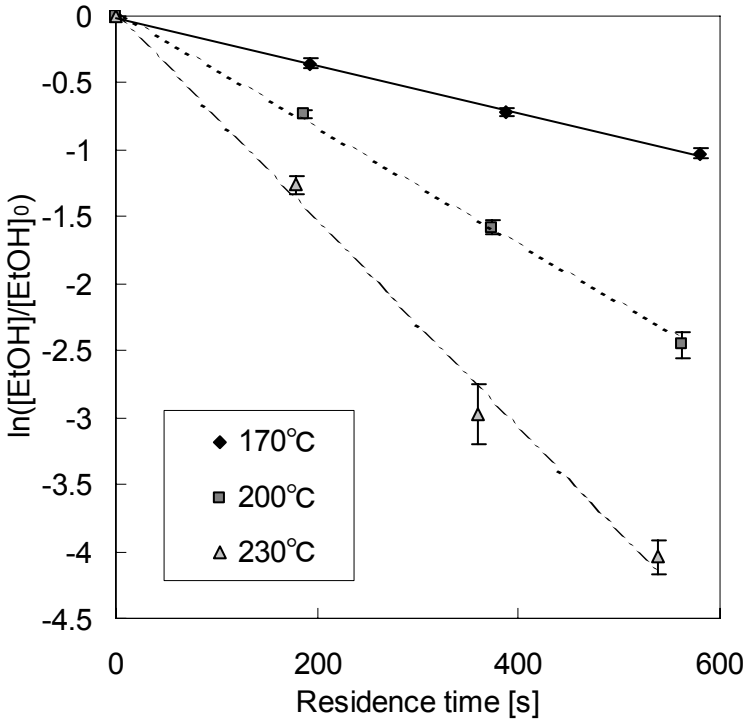

Figure 3.2 Plot of $\ln([\mathrm{EtOH}]/[\mathrm{EtOH}]_0)$ vs. residence time

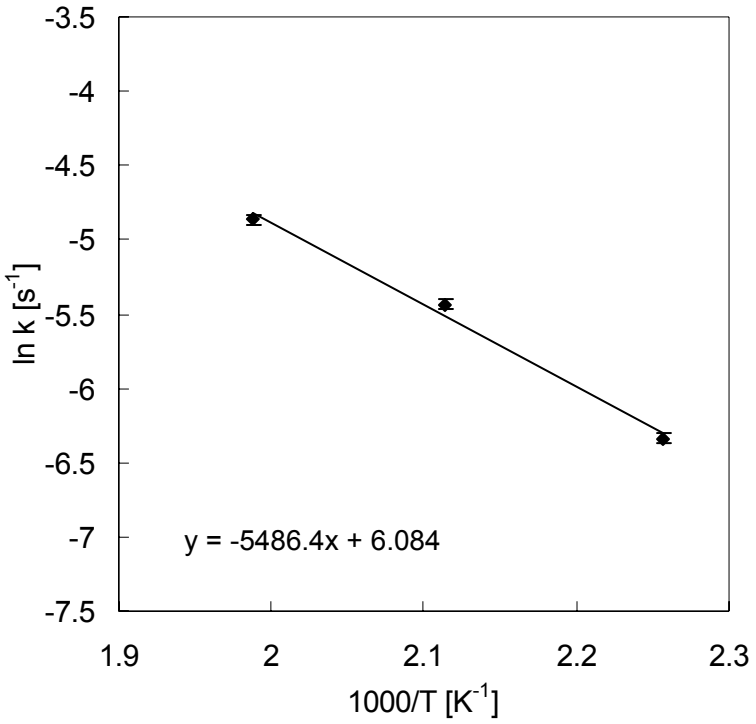

Figure 3.3 Arrhenius plot of $\ln k$ vs. reciprocal of temperature

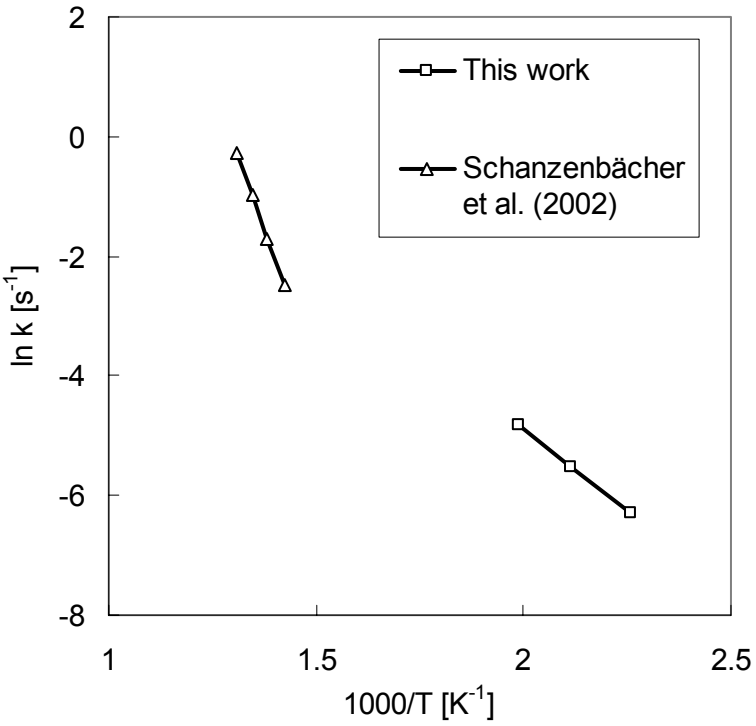

Figure 3.4 Comparison of oxidation rate of EtOH in subcritical and supercritical water

Table 3.2

Experimental conditions and results for EtOH oxidation in subcritical water at 23.5 MPa

(1) Equivalence ratio = 0.5

T [°C]	Residence time [s]	EtOH concentration [mmol·l^{-1}]	T [°C]	Residence time [s]	EtOH concentration [mmol·l^{-1}]
170	194	17.44±0.60	230	359	1.57±0.05
		18.30±0.86			1.29±0.04
		16.99±0.33			1.01±0.03
200	187	12.42±0.22	170	581	8.95±0.12
		11.92±0.38			9.24±0.36
		11.77±0.12			8.60±0.35
230	180	7.50±0.29	200	561	2.39±0.08
		7.14±0.43			2.08±0.07
		6.62±0.06			1.97±0.04
170	387	11.99±0.24	230	539	0.50±0.00
		12.56±0.40			0.44±0.03
		11.85±0.37			0.39±0.05
200	374	5.43±0.23			
		5.12±0.18			
		4.88±0.06			

(2) Equivalence ratio = 1.0

T [°C]	Residence time [s]	EtOH concentration [mmol·l^{-1}]	T [°C]	Residence time [s]	EtOH concentration [mmol·l^{-1}]
170	193	21.46±0.11	230	359	3.96±0.07
		22.32±0.48			4.62±0.20
		23.10±0.53			5.28±0.16
200	187	18.15±0.37	170	580	16.73±0.17
		18.47±0.19			17.55±0.52
		17.46±0.65			18.11±0.68
230	180	11.78±0.07	200	561	8.15±0.35
		12.16±0.35			9.43±0.36
		12.53±0.72			8.01±0.28
170	387	19.51±0.65	230	539	2.84±0.10
		19.55±0.41			3.58±0.11
		20.16±0.75			3.70±0.23
200	374	12.70±0.46			
		13.81±0.54			
		11.59±0.38			

(3) Equivalence ratio = 1.5

T [°C]	Residence time [s]	EtOH concentration [mmol·l^{-1}]	T [°C]	Residence time [s]	EtOH concentration [mmol·l^{-1}]
200	187	21.79±0.17	200	561	14.30±0.62
		21.25±0.33			13.75±0.72
		20.58±0.28			13.69±0.11
200	374	17.45±0.38			
		17.44±0.37			
		15.54±0.20			

3.3.2 Oxidation rate including oxygen concentration

Experiments were conducted at the equivalence ratio 0.5, 1.0 and 1.5 as shown in Table 3.1 in order to determine the influence of the oxygen concentration on the global oxidation rate. Table 3.2 shows the experimental data at these equivalence ratios. The global oxidation rate including oxygen concentration is expressed as follows:

$$\frac{d[\mathrm{EtOH}]}{dt} = A\exp\left(\frac{-E_a}{RT}\right)[\mathrm{EtOH}]^a[\mathrm{O_2}]^b \tag{3}$$

where a and b are the reaction order of the ethanol and oxygen, respectively. Equation (3) can be transformed into:

$$\int_0^x \frac{dx}{(1-x)^a(r_0-cx)} = A\exp\left(\frac{-E_a}{RT}\right)[\mathrm{EtOH}]_0^{a+b-1}t \tag{4}$$

where x is the ethanol conversion, r_0 is the ratio of the initial oxygen concentration to the initial ethanol concentration, t is the residence time, c is the mole number of consumed oxygen when one mole of ethanol is oxidized. If the entire amount of ethanol is oxidized completely to CO_2 and water, c would be 3.0. If some other products such as acetaldehyde or acetic acid are produced, c would be different number as shown in Table 3.3. In our exploratory experiments, most of the product in liquid phase was acetic acid as shown in Table 3.4. Based on the results in Table 3.4, we set c to 1.0. Schanzenbächer et al. (2002) also decided c equal to 1.0 in their study. Figure 3.5 shows the experimental data with the standard deviation at different equivalence ratios so that parameters a and b are obtained. Figure 3.6 shows the experimental data with the standard deviation at different temperatures so that parameters A and E_a are obtained. These parameters are obtained by least-square method by equation (4). The global oxidation rate is expressed as follows:

$$-\frac{d[\mathrm{EtOH}]}{dt} = 10^{2.05\pm0.24}\times\exp\left(\frac{-61\pm3\mathrm{kJ/mol}}{RT}\right)[\mathrm{EtOH}]^{0.86\pm0.03}[\mathrm{O_2}]^{1.15\pm0.05} \tag{5}$$

Lines in Figures 3.5 and 3.6 are calculated by equation (5). From these figures, it is found that the obtained parameters are accurate enough to describe the experimental results.

Schanzenbächer et al. (2002) obtained ethanol oxidation rate in supercritical water at the temperature from 433 to 494 °C and the pressure of 24.6 MPa as follows:

$$-\frac{d[\mathrm{EtOH}]}{dt} = 10^{17.23\pm1.65} \times \exp\left(\frac{-214\pm18\mathrm{kJ/mol}}{RT}\right) [\mathrm{EtOH}]^{1.34\pm0.11}[\mathrm{O_2}]^{0.55\pm0.19} \qquad (6)$$

The activation energy and the pre-exponential factor is larger in SCWO than in subcritical water oxidation same as in the case of the first-order oxidation rate. Figure 3.7 compares our ethanol kinetics (Equation (5)) with the Arrhenius plot developed by Schanzenbächer et al. (Equation (6)), and it is shown that the temperature dependence was higher in the supercritical region than in the subcritical region. When the reaction orders are compared between subcritical and supercritical water oxidation, the order of ethanol is higher in SCWO than in subcritical water oxidation, on the other hand, the order of oxygen is higher in subcritical water oxidation than in SCWO as shown in Equations (5) and (6).

In SCWO, ethanol oxidation reaction proceeds via a radical chain reaction, therefore ethanol is mainly oxidized by the reaction with active radicals such as OH radical, which is originated from O_2 and H_2O molecules, e.g., $H + O_2 = HO_2$, $H_2O + O = OH + OH$, $HO_2 + HO_2 = OH + H_2O_2$ (Akiya and Savage, 2002; Hippler et al. 1990). On the other hand, in subcritical water, chain branching reaction does not occur so considerably and ethanol oxidation proceeds via reactions such as hydrogen abstraction by O_2 molecules (Iyer et al., 1998). In other words, H_2O molecules play an important role in oxidation mechanism in SCWO, but do not in subcritical water oxidation. Therefore, the effect of oxygen molecules on the oxidation rate is less in SCWO than in subcritical water oxidation, while the effect of ethanol molecules on the oxidation rate is greater in SCWO than in subcritical water oxidation because EtOH oxidation can occur with less dependence on O_2 concentration in SCWO than in subcritical water oxidation. This is one of the reasons for the differences in the reaction orders of ethanol and oxygen. The

difference of the activation energy between subcritical water oxidation and SCWO is also attributable the difference in their oxidation mechanism. Croist et al. (1997) reported the activation energy in the decomposition rate of H_2O_2 molecules, which are intermediate products during the chain branching reaction, to two OH radicals (H_2O_2 + M = OH + OH + M) in supercritical water as 180 kJ·mol^{-1}. This value is similar to the activation energy in the oxidation rate of ethanol in supercritical water, 214 kJ·mol^{-1} (Equation (6)). The production of OH radical is one of the key elementary reactions in SCWO and would be one of the reasons which leads to the higher activation energy in SCWO (214 kJ·mol^{-1}) than in subcritical water oxidation (61 kJ·mol^{-1}).

Table 3.5 shows a few comparisons of the reaction kinetics parameters obtained in subcritical and supercritical water. The parameters in oxidation reaction of acetic acid and phenol, and those in decomposition reaction of H_2O_2 are tabulated. From this table, it is observed that the activation energy of these reactions in subcritical water is lower than those in supercritical water to a certain degree. These trends are same as the one observed in ethanol oxidation in subcritical and supercritical water.

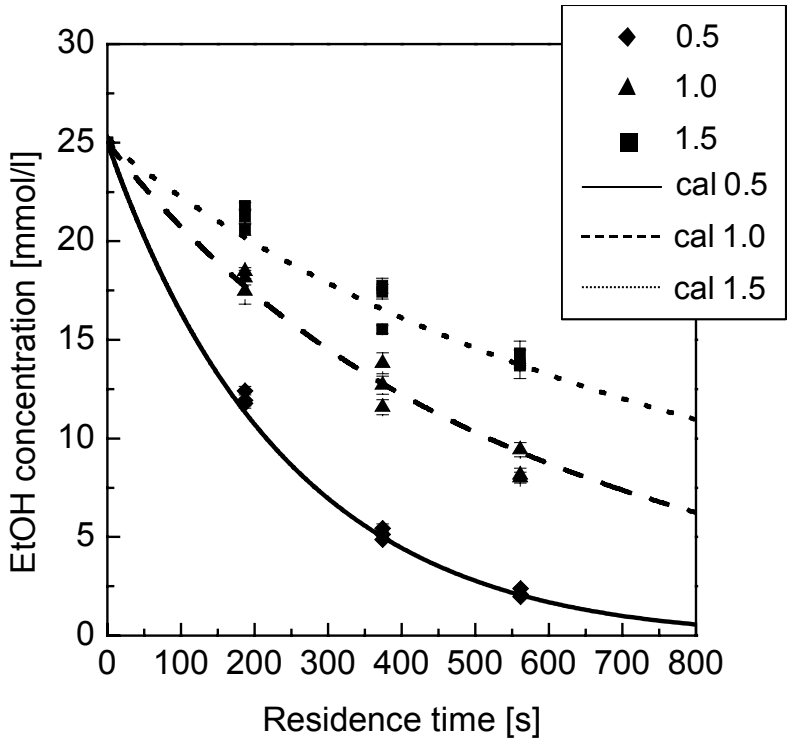

Figure 3.5 Ethanol conversions at 200 °C and 23.5 MPa

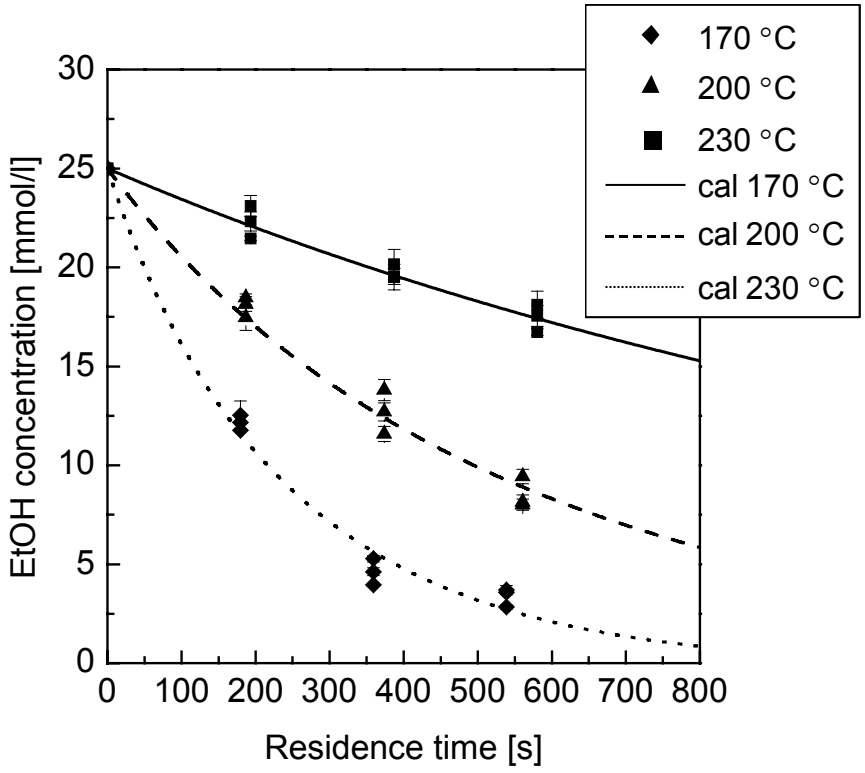

Figure 3.6 Ethanol conversions at 23.5 MPa and an equivalence ratio of 1.0

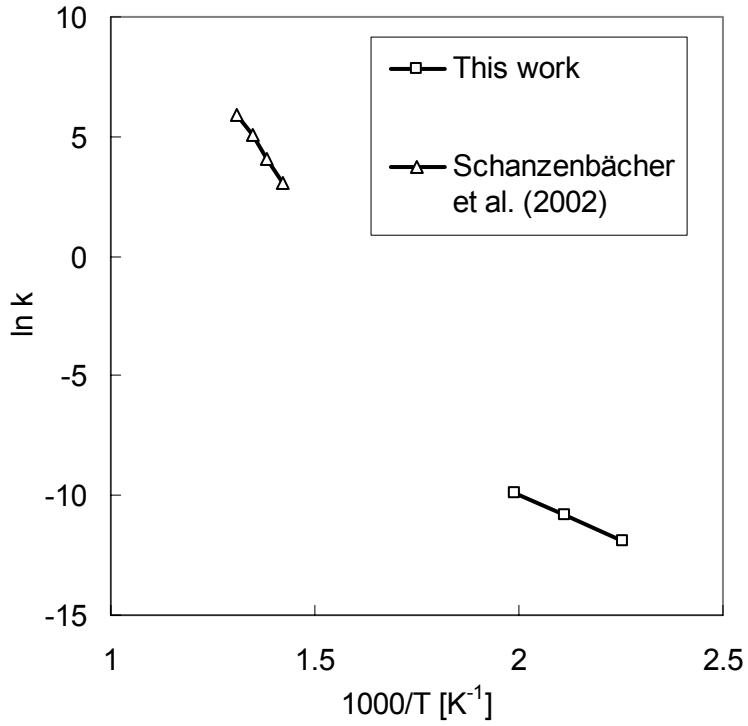

Figure 3.7 Arrhenius plot for hydrothermal oxidation of ethanol

Table 3.3 The value of c for some ethanol oxidation reactions

Reaction equations	c
$C_2H_5OH + 1/2O_2 \rightarrow CH_3COH + H_2O$	0.5
$C_2H_5OH + O_2 \rightarrow CH_3COOH + H_2O$	1.0
$C_2H_5OH + 3O_2 \rightarrow 2CO_2 + 3H_2O$	3.0

Table 3.4

Product yield by subcritical water oxidation of ethanol (200 °C and 23.5 MPa for No.1 and 2, 200 °C and 25 MPa for No.3)

No	Initial concentration		Equivalence ratio	Residence time [s]	[EtOH] (carbon ratio to initial [EtOH])	[Acetic acid] (carbon ratio to initial [EtOH])
	[EtOH]	[O_2]				
1	25 mmol·l^{-1}	150 mmol·l^{-1}	0.5	187	12.2 mmol·l^{-1} (0.45)	7.7 mmol·l^{-1} (0.31)
2	25 mmol·l^{-1}	50 mmol·l^{-1}	1.5	187	22.8 mmol·l^{-1} (0.91)	2.4 mmol·l^{-1} (0.10)
3	2050 mmol·l^{-1} (12 vol%)*	430 mmol·l^{-1} (2 vol% in [H_2O_2])*	14	212	1910 mmol·l^{-1} (0.93)	105 mmol·l^{-1} (0.05)

* For convenience in comparing with the condition in Chapter 2 (at 25 °C, 1 atm)

Table 3.5

Comparisons of kinetics parameters between in subcritical and supercritical water

Compounds	Reaction	Kinetic parameters*				Temp.	Pres.	Ref.
		A	E_a	a	b	[K]	[MPa]	
Acetic acid	Oxidation	5.60×10^{10}	167.7	1	0.37	543-593	2.0-20.0	Foussard et al., 1989
		9.82×10^{17}	231	1	1	611-718	39.4-43.8	Wightman, 1981
Phenol	Oxidation	4.71×10^{4}	45.1	1	1	473-523	5.5-15.2	Pruden and Le, 1976
		2.61×10^{5}	63.8	1	1	557-702	29.2-34.0	Wightman, 1981
H_2O_2	Decompo-sition	$10^{3.6}$	49	1	-	423-623	5-34	Croiset et al., 1997
		$10^{13.7}$	180	1	-	653-723	24.5-34	

* a and b are reaction orders for compounds and oxygen, respectively.

3.4 Summary

Ethanol oxidation rate in subcritical water is measured. The obtained oxidation rate is valid at the temperature from 170 °C to 230 °C and a pressure of 23.5 MPa. First-order oxidation rate is obtained by the experiment where equivalence ratio is fixed to 0.5. The parameters were determined to be $10^{2.64\pm0.07}$ for the pre-exponential factor, 45.6±0.6 kJ·mol^{-1} for the activation energy.

The oxygen dependence on the global oxidation rate of ethanol in subcritical water was also investigated. In this investigation, equivalence ratio was varied between 0.5 and 1.5. The parameters were determined to be $10^{2.05\pm0.24}$ for the pre-exponential factor, 61±3 kJ·mol^{-1} for the activation energy, and for the reaction orders, 0.86±0.03 for ethanol, and 1.15±0.05 for oxygen.

Chapter 4

Numerical study of subcritical water oxidation of ethanol

4.1 Purposes

In Chapter 2, a fundamental experiment of ethanol oxidation by H_2O_2 solution in subcritical water was performed and production of hot water whose temperature up to 320 °C was achieved. In Chapter 3, the ethanol oxidation rate in subcritical water was measured in order to estimate the processing capacity of subcritical water oxidation as a thermal energy production method.

When hydrothermal oxidation is used as a heat source, it is preferred to have a higher concentration of reactant since larger heat energy is obtained. Therefore concentration of ethanol solution was set to high value in Chapter 2 in order to achieve the higher temperature increase. For the measurement of the ethanol oxidation rate in Chapter 3, the concentration of ethanol solution needs to be low so that the temperature inside the reactor is kept constant with little oxidation heat. To check if the ethanol oxidation rate obtained in the experiments using low concentrations of ethanol solution can be applied to higher concentration of ethanol solution, 1-D numerical simulations of the subcritical water oxidation of ethanol using the oxidation rate obtained in Chapter 3 is conducted. The temperature increase and the conversion of ethanol solution by numerical simulations are compared with the experimental data in Chapter 2. For this simulation, a code developed by Koido et al. (2006) is used after partial modification. An explanation of this code is in Section 4.4.

4.2 Numerical

To check if the oxidation rate obtained at low ethanol concentration conditions (equation (5)) is applicable to high ethanol concentration conditions, numerical study of the hydrothermal oxidation of ethanol using equation (5) was conducted at the conditions in Chapter 2, that is, ethanol concentration was fixed to 12 vol% (2050 $mmol \cdot l^{-1}$) and H_2O_2 concentration was raised from 2 to 20 vol% (850 to 8530 $mmol \cdot l^{-1}$) which corresponded to a variation in equivalence ratio from 14 to 1.4.

4.2.1 Numerical model

For simulation, one-step irreversible reaction was assumed. Since equation (5) was obtained for conditions where quantity c equals 1.0 in the experimental part, Chapter 3, reaction product was assumed to be acetic acid as follows:

$$C_2H_5OH + O_2 \rightarrow CH_3COOH + H_2O \tag{7}$$

Main product of the ethanol oxidation was acetic acid at both high and low ethanol concentration as shown in Table 3.5, therefore it is reasonable to use equation (7) for numerical simulation of subcritical water oxidation at both high and low concentration ethanol solution as long as the reaction temperature is around 200 °C.

Figure 4.1 shows the reactor configuration in simulation. Tube length was 744 mm, which is similar to the reactor used in the experiment in Chapter 2. A heater was installed near the inlet of the tube to increase the reactant temperature. The heater length was almost the same as the heater used in the experiment in Chapter 2, 208 mm. The amount of heat loss from the reactor tube was assumed to be:

$$q_L[\mathrm{W/m^2}] = \begin{cases} h(T - T_{pre}) & (at\ T > T_{pre}) \\ 0 & (at\ T < T_{pre}) \end{cases} \tag{8}$$

where T_{pre} and h are the preheating temperature and heat transfer coefficient, respectively. Preheating temperature was defined as the temperature at the point just after the heater (x = 308 mm) when only water was fed into the reactor, i.e., for the

case where no reaction heat was produced. The value of the heat transfer coefficient was estimated to be 12.3 $W \cdot m^{-2} \cdot K^{-1}$. This estimation was done by approximating the temperatures at the points (x = 308, 524, 744 mm) in simulation to the experimental data in Chapter 2 at ethanol concentration of 12 vol%, H_2O_2 concentration of 6 vol%, and the preheating temperature of 200 °C. The value, 12.3, is within the range of the heat transfer coefficient of a natural convection gas mentioned in reference, 5-28 $W \cdot m^{-2} \cdot K^{-1}$ (Rohsenow and Choi, 1961) and considered to be reasonable.

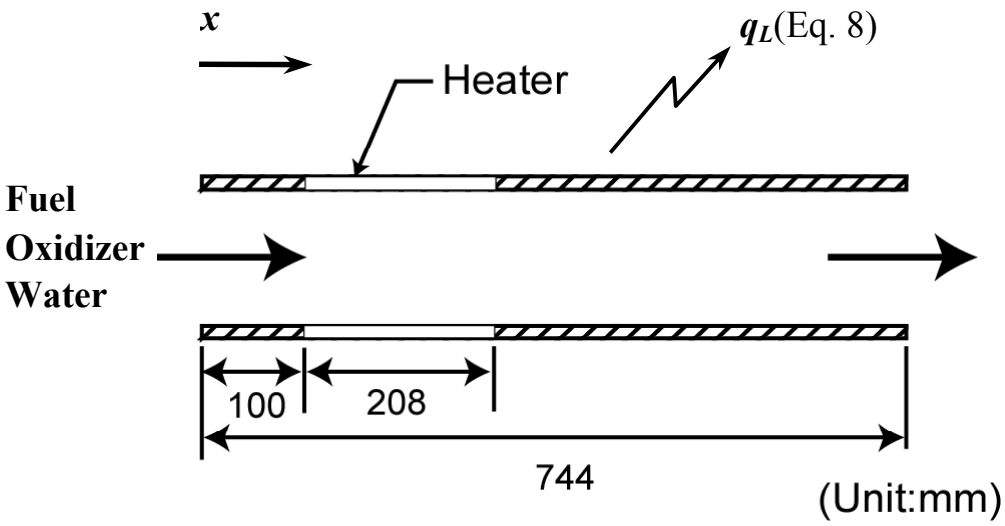

Figure 4.1 One-dimensional reactor model

4.2.2 Governing equations

The governing equations of the steady one-dimensional flow with hydrothermal oxidation reaction can be written by following equations (9)-(13). Thermal energy output by hydrothermal oxidation is described by the terms $-\sum_{i=1}^{4} h_i w_i$ in equation (12).

$$\frac{d\rho u}{dx} = 0 \tag{9}$$

$$\rho u \frac{du}{dx} = -\frac{dp}{dx} + \frac{d}{dx}\left(\frac{4}{3}\mu \frac{du}{dx}\right) \tag{10}$$

$$\rho u \frac{dY_i}{dx} = \frac{d}{dx}\left(\rho D_i \frac{dY_i}{dx} \right) + w_i \tag{11}$$

$$\rho u C_p \frac{dT}{dx} = \frac{d}{dx}\left(\lambda \frac{dT}{dx} \right) - \sum_{i=1}^{4} h_i w_i + Q(x) \tag{12}$$

$$\rho = f(p, T, Y_i) \tag{13}$$

4.2.3 Equation of state

4.2.3.1 Water

We use "IAPWS (The International Association for the Properties of Water and Steam) Industrial Formulation 1997" (IAPWS-IF97, 1997) as an equation of state of water. This formulation is based on the experimental data of properties of water. This formulation is valid for single-phase and saturation states from 273.15 K to 1073.15 K at pressures up to 100 MPa. By using this formulation, we can predict the thermodynamic properties of water such as density, isobaric specific heat and enthalpy precisely when we set a temperature and pressure.

4.2.3.2 Ethanol

For calculating the thermodynamic property of ethanol, we use the empirical formulation derived by Dillon and Penoncello (2004). This formulation is valid for single-phase and saturation states from 250 K to 650 K at pressures up to 280 MPa. We utilize this formulation to predict the thermodynamic properties of ethanol such as density, isobaric specific heat and enthalpy.

4.2.3.3 Lee-Kesler equation

For oxygen and acetic acid, we use an estimating formula derived by Lee and Kesler (1975). This equation should be valid for the substance when the reduced temperature ($T_r = T/T_c$) is between 0.3 and 4, where T_c is the critical temperature, and critical pressure (p_c) is between 0 and 10 MPa. Critical temperatures of oxygen and acetic acid are 154.6 K and 594.4 K respectively, and their critical pressures are 5.04 MPa and 5.78 MPa respectively. Hence Lee-Kesler equation is valid for oxygen and acetic acid at temperature between 20 °C and 345 °C. In order to calculate the isobaric

specific heat and enthalpy of substance by Lee-Kesler equation, we need isobaric specific heat of ideal gas (C_{pi}^{id}), which is estimated by the following polynomial equation:

$$C_{pi}^{id} = a + bT + cT^2 + dT^3 \tag{14}$$

where, a, b, c, and d are tabulated in Chemical Engineering Encyclopedia (1999) for each substance.

4.3 Transport properties and mixing law

For the estimation of transport properties of ethanol aqueous solution, equations derived by Chung et al. (1988) were used. An equation derived by Wilke and Chang (1955) can estimate a diffusion coefficient of a solute in water with validity and was used for the estimation of the diffusion coefficient of ethanol in water.

Since the reaction denoted in equation (7) occurs in water, the mixing law should be applied to density and isobaric specific heat obtained by equations of state, and also to transport properties such as thermal conductivity and viscosity. U. Plöcker et al (1978) suggested the mixing law for Lee-Kesler equation. However, in this study, we also use different equations of state for water and ethanol. So we cannot use the mixing law which is only applicable to Lee-Kesler equation. The mixing law which can be applied to different types of equation of state was also suggested by K. Arai et al. (1982). Currently, we just use most fundamental mixing law as follows, considering that density and isobaric specific heat are extensive values.

$$\rho = \sum M_i X_i \tag{15}$$

$$C_p = \sum Y_i C_{pi} \tag{16}$$

Mixing law of transport properties were obtained by Chung et al. (1988). When this mixing law is used, we set binary interaction parameter to unity followed by Chung et al. (1988).

4.4 Numerical method

Finite difference method was applied to solve equations (9)-(13). Backward difference scheme and central difference scheme were used for advection terms and diffusion terms, respectively, to solve the difference equations. This scheme is simple and available to obtain the 1-dimentional steady solutions (Anderson et al., 1984). Difference equations are as follows:

Mass conservation ($j = 1, \cdots, n$):

$$\rho_j u_j = \rho_0 u_0 \tag{9'}$$

Momentum conservation ($j = 1, \cdots, n$):

$$\rho_0 u_0 \frac{u_j - u_{j-1}}{\Delta x} = -\frac{p_j - p_{j-1}}{\Delta x} + \frac{4}{3}\left(\mu_j \frac{u_{j+1} - 2u_j + u_{j-1}}{\Delta x^2} + \frac{(\mu_j - \mu_{j-1})(u_j - u_{j-1})}{\Delta x^2} \right) \tag{10'}$$

Species conservation ($i = 1:\text{Oxygen},\ 2:\text{EtOH},\ 3:\text{Acetic acid}$) ($j = 1, \cdots, n$):

$$\begin{aligned} \rho_0 u_0 \frac{Y_{i,j} - Y_{i,j-1}}{\Delta x} = \rho_j D_{i,j} \frac{Y_{i,j+1} - 2Y_{i,j} + Y_{i,j-1}}{\Delta x^2} + \rho_j \frac{(D_{i,j} - D_{i,j-1})(Y_{i,j} - Y_{i,j-1})}{\Delta x^2} \\ + D_{i,j} \frac{(\rho_j - \rho_{j-1})(Y_{i,j} - Y_{i,j-1})}{\Delta x^2} + w_{i,j} \end{aligned} \tag{11'}$$

Energy conservation ($j = 1, \cdots, n$):

$$\begin{aligned} \rho_0 u_0 \ C_{pj} \frac{T_j - T_{j-1}}{\Delta x} = \lambda_j \frac{T_{j+1} - 2T_j + T_{j-1}}{\Delta x^2} + \frac{(\lambda_j - \lambda_{j-1})(T_j - T_{j-1})}{\Delta x^2} \\ - \sum h_{i,j} w_{i,j} + Q_j \end{aligned} \tag{12'}$$

Equation of state ($j = 1, \cdots, n$):

$$\rho_j = f(p_j, T_j, Y_{i,j}) \tag{13'}$$

Boundary conditions for velocity, density, pressure, temperature, and mass fraction at the inlet and the outlet of the reactor are given as follows:

$u = u_0$, $\rho = \rho_0$, $p = p_0$, $T = T_0$, $Y_i = Y_{i0}$ for inlet of the reactor (17)

$$\frac{du}{dx} = \frac{dT}{dx} = \frac{dY_i}{dx} = 0 \quad \text{for outlet of the reactor} \tag{18}$$

Above two boundary conditions are needed simultaneously because governing equations includes second-order derivatives such as $\left(d^2u/dx^2\right)$, $\left(d^2Y_i/dx^2\right)$, and $\left(d^2T/dx^2\right)$.

The total number of unknown variables is $n \times 8$, that is, $u_j (j = 1, \cdots, n)$, $\rho_j (j = 1, \cdots, n)$, $p_j (j = 1, \cdots, n)$, $Y_{i,j} (i = 0, \cdots 3 \;\; j = 1, \cdots, n)$, $T_j (j = 1, \cdots, n)$ because $u_{n+1}, T_{n+1}, Y_{i,n+1}$ are equal to u_n, T_n, $Y_{i,n}$, respectively by the boundary conditions (Equation (18)). The number of the equations (9)'-(13)' is $n \times 7$, thus the total number of algebraic equations is same as the number of unknown variables, $n \times 8$ with including the condition of mass fraction, $Y_{0,j} = 1 - \sum_{i=1}^{3} Y_{i,j}$ ($i = 0$: Water). Consequently equations (9)'-(13)' have unique solutions.

Calculation procedure is illustrated in Figure 4.2. First, velocity, density, pressure, temperature, and mass fraction of each chemical species were determined at the inlet of the reactor by boundary conditions. Second, pressure, temperature, and mass fraction of each chemical species were temporarily set to a certain value at a grid point of *j*. Then by difference equations, we recalculated the each value at *j* using these temporary values. The fully-converged answers at *j* were obtained by iteration method as shown in Figure 4.2. A temperature increase and a conversion of ethanol were calculated by the following equations.

$$\Delta T(x) = T(x) - T_{pre} \tag{19}$$

$$\text{Conversion of Ethanol} = \frac{X_{\text{EtOH}}(\text{initial}) - X_{\text{EtOH}}(\text{residue})}{X_{\text{EtOH}}(\text{initial})} \times 100 \tag{20}$$

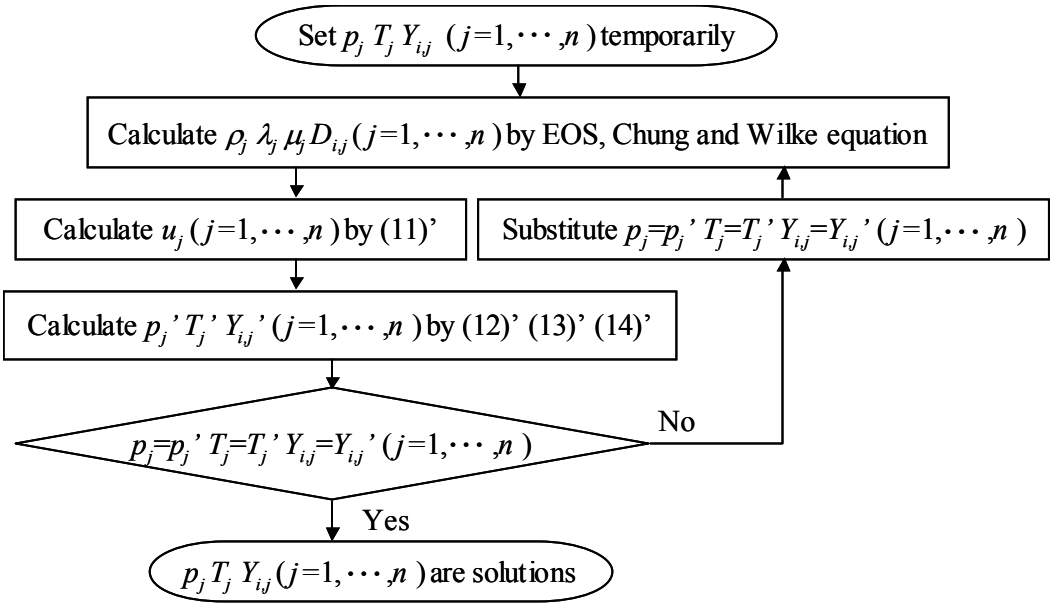

Figure 4.2 Numerical methods to obtain the value at grid point *j*

4.5 Results and discussion

4.5.1 Effect of preheating temperature

The concentration of ethanol and H_2O_2 at the inlet of the reactor were set to 12 vol% (2050 mmol·l^{-1}) and 6 vol% (2560 mmol·l^{-1}), respectively (equivalence ratio of 4.8) and the preheating temperature was changed from 140 °C to 290 °C at 30 °C interval corresponding to the experimental conditions in Chapter 2.

Figures 4.3 and 4.4 compare the conversion of ethanol and the temperature increase between simulation results and the experimental data in Chapter 2, respectively. The error bars in these figures indicate the standard deviations of the experimental data. Figure 4.3 shows that the conversion of ethanol in simulation is in agreement with the experimental data, though numerical results have slightly higher values than the experimental ones. The temperature increase is predicted well as shown in Figure 4.4. When the preheating temperature is low, the temperature increase is higher near the outlet of the reactor. On the other hand, the temperature increase becomes higher near the inlet of the reactor as the preheating temperature becomes higher. Same trend is observed in both simulation and the experimental data in Chapter 2.

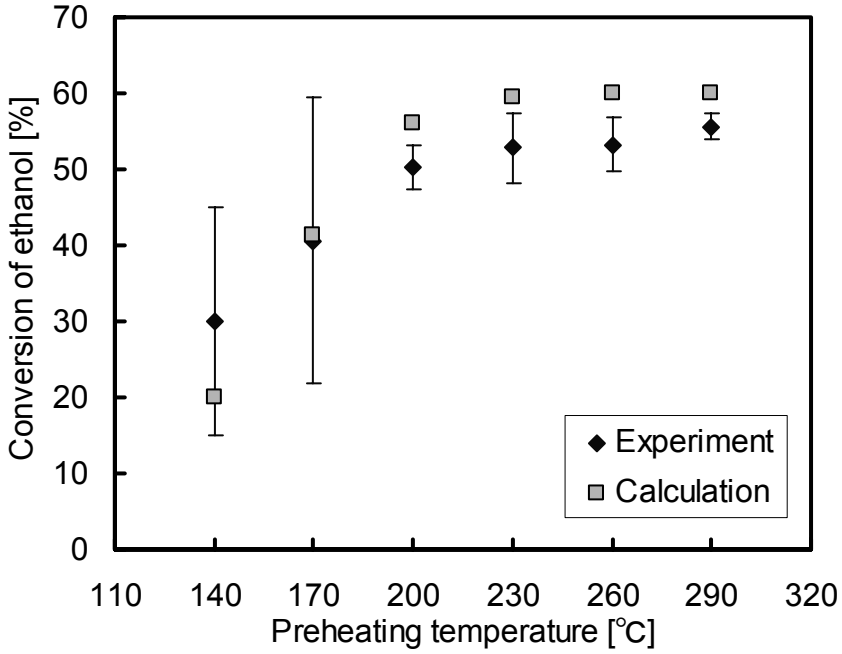

Figure 4.3 Conversion vs. preheating temperature at a pressure of 25 MPa

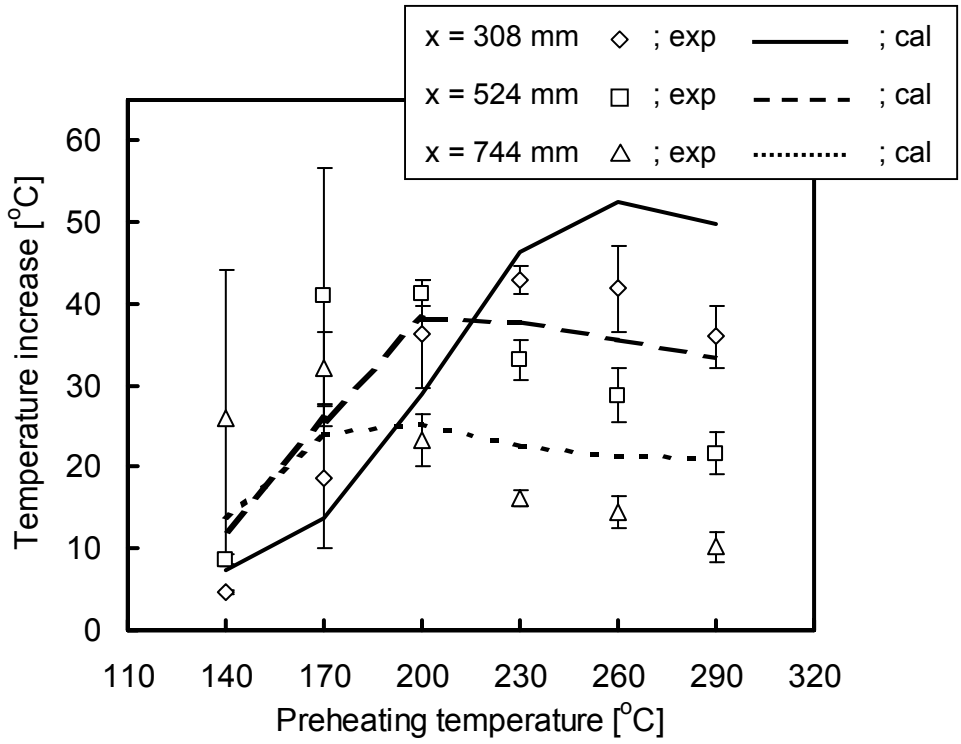

Figure 4.4 ΔT at each preheating temperature at a pressure of 25 MPa

4.5.2 Effect of oxidizer concentration

Effect of the concentration of oxygen was simulated at a fixed preheating temperature, 200 °C, and at a fixed concentration of ethanol, 12 vol% (2050 $mmol \cdot l^{-1}$). Concentration of H_2O_2 solution was changed from 2 to 20 vol% (850 to 8530 $mmol \cdot l^{-1}$) at 2 vol% interval corresponding to the experimental conditions in Chapter 2.

Figures 4.5 and 4.6 compare the conversion of ethanol and the temperature increase between simulation results and the experimental data in Chapter 2, respectively. The error bars in these figures indicate the standard deviations of the experimental data. It is shown that the conversion of ethanol in simulation compliments the experimental data (Figure 4.5). The temperature increase is predicted well at H_2O_2 concentration up to 10 vol%. However it does not have good agreement at higher H_2O_2 concentrations because it does not increase under these conditions for the simulation whereas it increases in experiment at x = 524 mm and x = 744 mm.

It was found in Figure 4.5 that almost all ethanol was oxidized to acetic acid at 10 vol% H_2O_2 solution in both simulation and experiment. Since we did not consider the oxidation of acetic acid in simulation, no more oxidation occurred even when higher H_2O_2 concentration solution, 14-20 vol% was used in simulation. On the other hand, the temperatures at the inlet of the reactor were around 300 °C in experiment in Chapter 2 as shown in Figure 4.6 due to the oxidation heat by ethanol when H_2O_2 solution of 14-20 vol% were used. Under these high temperatures, which were evidently different from the temperature range (170-230 °C) at the experiment in Chapter 3 of this study, acetic acid would be no more stable and oxidized to CO_2. Because of this further oxidation of acetic acid, more heat energy was generated and the temperature increase in experiment did occur at 14-20 vol% of H_2O_2 solution (Figure 4.6).

If the oxidation of acetic acid is considered in simulation, temperature increase will become higher. By roughly estimation at ethanol concentration of 12 vol% and H_2O_2 concentration of 20 vol%, where further oxidation of acetic acid is possible since oxygen is still remained after the ethanol oxidation to acetic acid, oxidation heat is about 2 times larger than that in the case without considering the oxidation of acetic acid to CO_2. Consequently the maximum temperature increase reaches around 160 °C when the oxidation of acetic acid to CO_2 is considered, which is much higher than the value in the

case without considering the oxidation of acetic acid to CO_2, 96 °C. In this calculation, remaining oxygen oxidizes about 55% of acetic acid and totally consumed. The oxidation enthalpy of ethanol to acetic acid is 486.3 $kJ \cdot mol^{-1}$ and that of acetic acid to CO_2 is 876.0 $kJ \cdot mol^{-1}$ at 200 °C and 25 MPa.

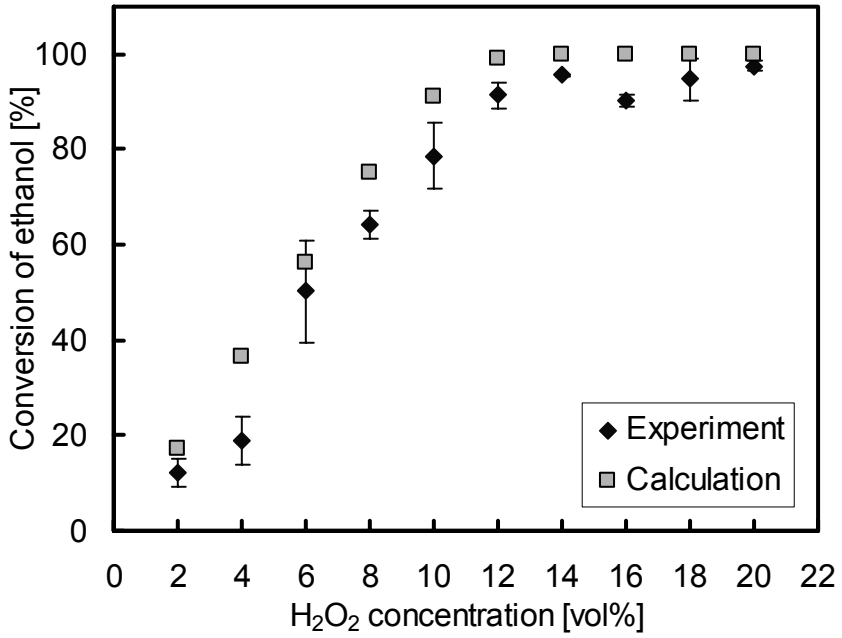

Figure 4.5 Conversion vs. H_2O_2 concentration at a pressure of 25 MPa

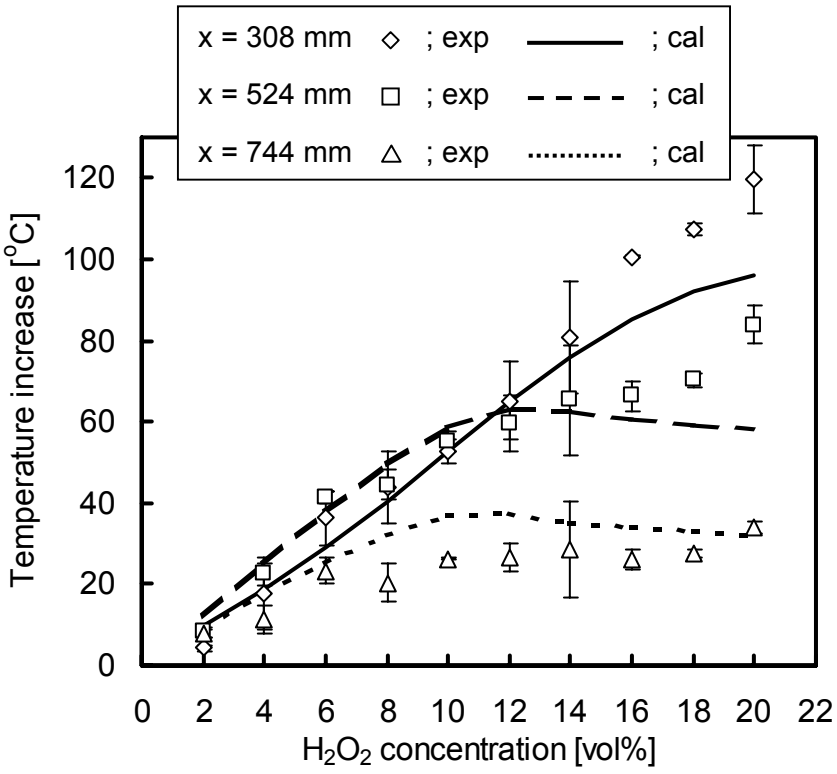

Figure 4.6 ΔT at each H_2O_2 concentration at a pressure of 25 MPa

4.6 Summary

Numerical study of hydrothermal oxidation of ethanol in subcritical water was conducted to confirm that the oxidation rate derived in Chapter 3 using low concentration of ethanol is applied to the hydrothermal oxidation by high concentration of ethanol solution in Chapter 2. The conversion of ethanol and the temperature increase in simulation agreed with the experimental data in Chapter 2 as long as the main product of the ethanol oxidation was acetic acid in experiment. The difference of the temperature increase at high concentration of H_2O_2, 14-20 vol% in simulation was caused by neglecting the further oxidation of acetic acid into CO_2, which generates more heat.

Chapter 5
Evaluation of power plants using hydrothermal oxidation

5.1 Purposes

In Chapters 2, 3, and 4, study on thermal energy production by subcritical water oxidation has been explained. Electricity is more convenient for use than heat itself since electricity is versatile for any purposes such as moving motor and lighting, and also easy to transmit. Therefore we focus on the power plants where thermal energy produced by hydrothermal oxidation is utilized in this section. We do not limit our focus on subcritical water oxidation, and SCWO and high-pressure steam oxidation are also included for this evaluation.

Generating electricity from thermal energy produced by hydrothermal oxidation of ethanol has been discussed concisely by system simulation by Naito et al. (2001). In this system evaluation by simulation, two other substances, glucose and peat solutions, are also selected besides ethanol solutions as reactants for hydrothermal oxidation power plants. The reasons of selecting these reactants are explained in Section 1.2: glucose solutions are regarded as a model biomass, and peat solutions are regarded as an example of real biomass. Composition and reaction enthalpies of each reactant are listed in Table 5.1. Electric power and energy conversion efficiency are calculated by the EgWin (2000), a general purpose program for analyzing efficiency of electric power generation system, produced by the Central Research Institute of Electric Power Industry (CRIEPI).

Table 5.1 Properties of reactants

	Composition	Reaction enthalpy
Ethanol	C_2H_5OH	29.73 kJ·g^{-1}
Glucose	$C_6O_{12}H_6$	15.55 kJ·g^{-1}
Peat *	C:46%, H:5%, N:1%, O:38%, Others:10%	17.46 kJ·g^{-1}

* Collected in Canada, New Brunswick Province.

5.2 Configuration of power plants

Two types of power plants are considered. One is a direct type and the other is an indirect type power plant. Figure 5.1 illustrates the direct type power plant using hydrothermal oxidation. Reactant and oxidizer are introduced into a reactor by a high-pressure pump and by a compressor, respectively. Hot and high-pressure steam is produced by hydrothermal oxidation and it is directly flowed into a turbine. Figure 5.2 illustrates the indirect type power plant using hydrothermal oxidation. The heat produced by hydrothermal oxidation in the reactor is conveyed to the main water by a heat exchanger and the produced steam is flowed into a turbine. Table 5.2 indicates merit and demerit of direct and indirect type power plants: direct type power plant is simple but remaining reactant could corrode the turbine blade while indirect type power plant has more complicated system with some heat and pressure loss and there is no concern about corrosion of turbine blade by remaining reactants.

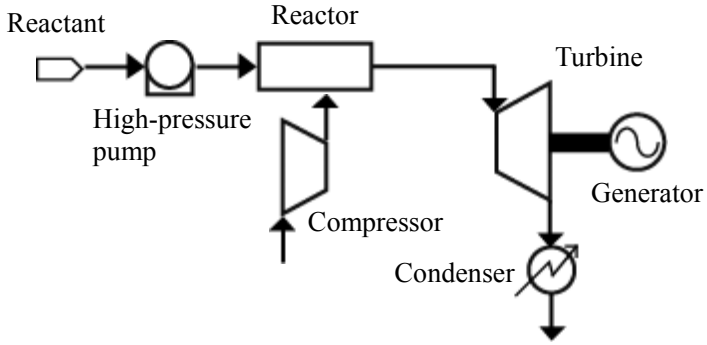

Figure 5.1 Direct type power plants

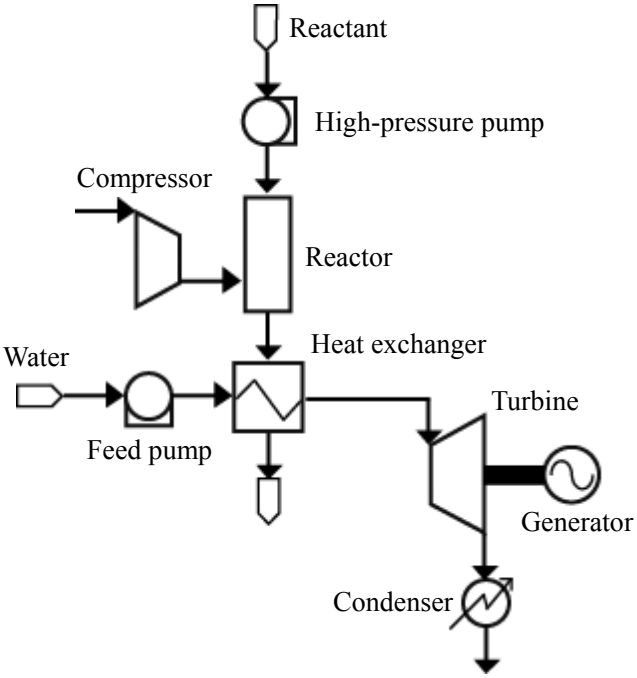

Figure 5.2 Indirect type power plants

Table 5.2 Merit and demerit of each type power plants

Type	Merit	Demerit
Direct	Simple system configuration	Residue of reactant could cause corrosion of a turbine
Indirect	Only water is flow into a turbine	Heat and pressure loss at a heat exchanger

5.3 Calculation conditions

Power plants considered in this study consist of two parts. One is a power generating part with a steam turbine and the other is a hydrothermal oxidation part to produce hot and high-pressure steam. These two parts are discussed separately in the following sections.

5.3.1 Power generating part

Figure 5.3 illustrates the power generating part commonly used for both direct and indirect type power plants. Only one steam turbine is considered here because the

reheat cycle using two or more turbines costs a lot and it would be enough to evaluate different type power plants with one turbine. The turbine inlet temperature (TIT) needs to be less than 650 °C because turbine blades would be eroded over 650 °C. Turbine output is calculated by the enthalpy difference between turbine inlet and outlet. In the previous study of Naito et al. (2001), the enthalpy at the outlet is fixed to a saturated steam enthalpy at 35 °C. Actually the enthalpy at the outlet depends on the expansion process at the turbine and not fixed. Therefore, in this study, expansion process is assumed to be irreversible with the adiabatic efficiency of 90%. Moreover the quality at the outlet of turbine should be more than 0.9 for preventing erosion of turbine blades. The temperature and the pressure of the condenser are assumed to be over 35 °C and its saturation pressure ($P_{35°C}$), respectively.

As an example, calculation of electric power at 600 °C of TIT and at 20 MPa of inlet pressure is demonstrated in Figure 5.4. The enthalpy (h_A) and the entropy (s_A) at the turbine inlet (point A) are known by the inlet conditions. Then point B' can be calculated by the following equation.

$$s_{B'} = s_A \tag{21}$$

This equation means that point B' is realized after adiabatic expansion from point A. Enthalpy and entropy at point B' are denoted by $h_{B'}$, $s_{B'}$, respectively. By assuming the pressure at the outlet of turbine P_B, $h_{B'}$ is obtained by the following equation.

$$h_{B'} = h(P_B,\ s_{B'}) \tag{22}$$

Then h_B at the outlet of turbine (point B) is obtained by equation (23) which is the definition of the adiabatic efficiency.

$$\frac{h_A - h_B}{h_A - h_{B'}} = 0.9 \tag{23}$$

If the quality at the turbine outlet (point B) calculated by equation (24) equals to 0.9, the assumed value of P_B is correct. Otherwise P_B is re-assumed again.

$$\frac{h_{B,gas} - h_B}{h_{B,gas} - h_{B,liq}} = 0.9 \tag{24}$$

In equation (24), $h_{B,gas}$ is the vapor enthalpy and $h_{B,liq}$ is the liquid enthalpy at the pressure P_B. The pressure at the turbine outlet, P_B, should be bigger than the pressure of the condenser, that is, the saturation pressure of 35 °C. When P_B becomes

same pressure as the condenser, P_B cannot be made lower even if the quality at the turbine outlet is more than 0.9. During these calculations, REFPROP (2002), which is developed by the NIST (National Institute of Standard and Technology), is used to obtain the properties of water.

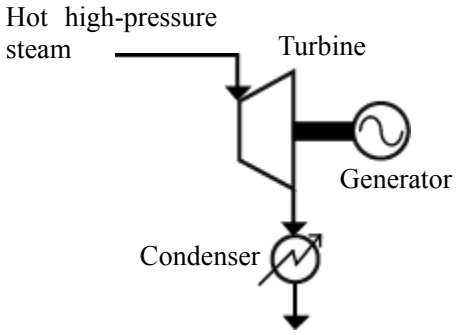

Figure 5.3 Power generating part

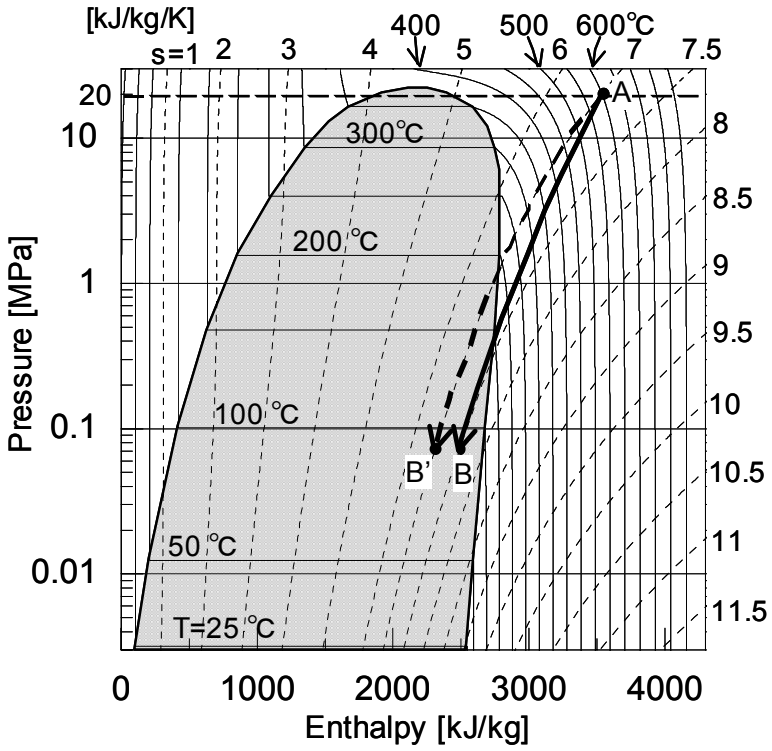

Figure 5.4 *p-h* diagram of expansion process

5.3.2 Hydrothermal oxidation part

Hydrothermal oxidation part of the direct type power plant and that of the indirect type power plant are considered. Both types are illustrated in Figures 5.1 and 5.2. In both types, oxygen separated from air is compressed into the reactor as an oxidizer. The work needed for separation of oxygen from air (W_{sep}) is 24.2 kJ·mol^{-1} (Naito et al., 2001). Air itself can be used as an oxidizer but total energy consumption for preparing oxidizer is higher when air is used as shown in Figure 5.5. This is because a lot of energy is consumed for compressing nitrogen, which is contained a lot in air. Thus oxygen is used as an oxidizer in this study. In the previous work done by Naito et al. (2001), it was also concluded that the energy consumption was higher when air was used instead of oxygen. The works needed for high-pressure liquid pump and feed pump could be ignored because they are much less than those of compressor and oxygen separation. The work needed for compression of oxygen (W_{com}) is calculated as follow by assuming an ideal gas. Adiabatic compression of oxygen is denoted by equation (25).

$$c_V dT + \frac{RT}{V} dV = 0 \tag{25}$$

Using Mayer's relation, the above equation becomes

$$\int \frac{c_p}{R} \frac{dT}{T} - \ln T + \ln V = const. \tag{26}$$

where the isobaric specific heat is calculated by the polynomial approximation.

$$c_p = a + bT + cT^2 + dT^3 \tag{14}$$

The values of a, b, c, and d are tabulated in Chemical Engineering Encyclopedia (1999). Substituting equation (14) into equation (26) leads to

$$\ln \frac{T^{\frac{a}{R}} \cdot R}{P} + \frac{1}{R}\left(bT + \frac{1}{2} cT^2 + \frac{1}{3} dT^3 \right) = const. \tag{27}$$

Once the pressure inside the reactor is decided, temperature after compression is calculated by equation (27). Then the compression work is calculated by

$$W_{com} = \frac{\int_{25^\circ C}^{T} c_p dT}{0.9} \tag{28}$$

where 0.9 is the adiabatic efficiency of the compressor.

Initial temperatures of reactant and that of water are 25 °C. Oxygen temperature before compression is also 25 °C and the initial pressure is 0.1013 MPa. For the indirect type power plant, drain temperature of heat exchanger assumed to be 35 °C in order to maintain the temperature difference of 10 °C between high and low temperature heat sources. Under these conditions, the calculated value of the heat transfer area per unit volume of heat exchanger is below 403 $m^2 \cdot m^{-3}$, which is similar to the value of normal heat exchanger (Tsubouchi, 1968). Thus it is concluded that this assumption is reasonable. The heat loss from the reactor and that from the heat exchanger are estimated to be 10%.

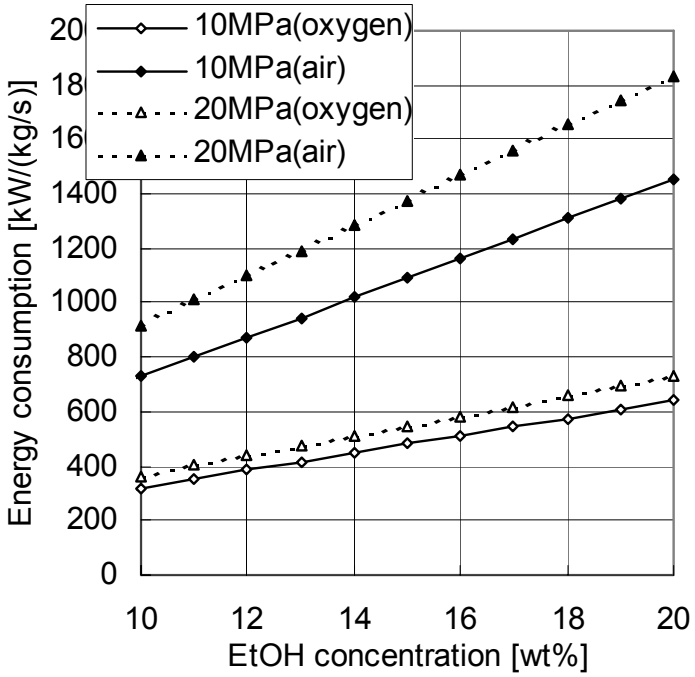

Figure 5.5 Energy consumption for preparation of high-pressure air and oxygen

5.3.3 Energy conversion efficiency

Energy conversion efficiency of power plants is calculated using the following equation.

$$\eta = \frac{E}{h_{re}} \tag{29}$$

$$E = E_{tb} - (W_{com} + W_{sep}) \tag{30}$$

Here, h_{re} is the reaction enthalpy of reactant, E is the electric power output, E_{tb} is

the turbine output, and W_{sep} and W_{com} are the work for oxygen separation and compression, respectively.

5.4 Results and discussions

5.4.1 Direct type power plant using ethanol

Figures 5.6 and 5.7 show the relationship between ethanol concentration and electric power and that between ethanol concentration and efficiency, respectively, for direct type power plant with reactor pressures of 5, 10, 15, 20, 25 MPa. From these figures, it is shown that electric power and efficiency become higher for higher concentration of ethanol, and that these values become higher for lower reactor pressure, though the difference is small. The maximum efficiency for the direct type power plant is about 26.4% for 17.6 wt% of ethanol with the reactor pressure of 10 MPa. The highest concentration of ethanol for each reactor pressure is restricted by the maximum TIT of 650 °C. The changes of slope at 16.5 wt% for 5 MPa is caused by the fact that the turbine outlet pressure reaches to the condenser pressure, i.e. even if the outlet steam has a higher temperature and its quality is more than 0.9 at the turbine outlet when higher concentration of ethanol is used, it is discarded because turbine outlet pressure cannot be lower than $P_{35°C}$. As a result, increases of the electric power and the efficiency are limited above 16.5 wt% for 5 MPa. Figure 5.8 shows *p-h* diagram of the direct type power plant for ethanol solution of 16 wt%. Lines A-B, B-C, and curve C-D indicate the pressurization of reactant by high-pressure pump up to 5 MPa, the hydrothermal oxidation in the reactor and the expansion at the turbine, respectively. Lines A-B', B'-C', and curve C'-D' indicate a similar process with the reactor pressure of 20 MPa. From Figure 5.8, it is found that turbine outputs at the reactor pressure of 5 MPa and 20 MPa are almost the same. As the reactor pressure becomes higher, the work for compression of oxygen is needed more. As a result, electric power becomes lower at higher reactor pressure. Figure 5.9 shows energy budget of direct type power plant using 17.6 wt% ethanol. A lot of heat is discarded in the condenser because reheat and regenerative cycle is not considered for the power generating part in this study. The work for preparing oxygen consumes large part of turbine output and makes the efficiency lower.

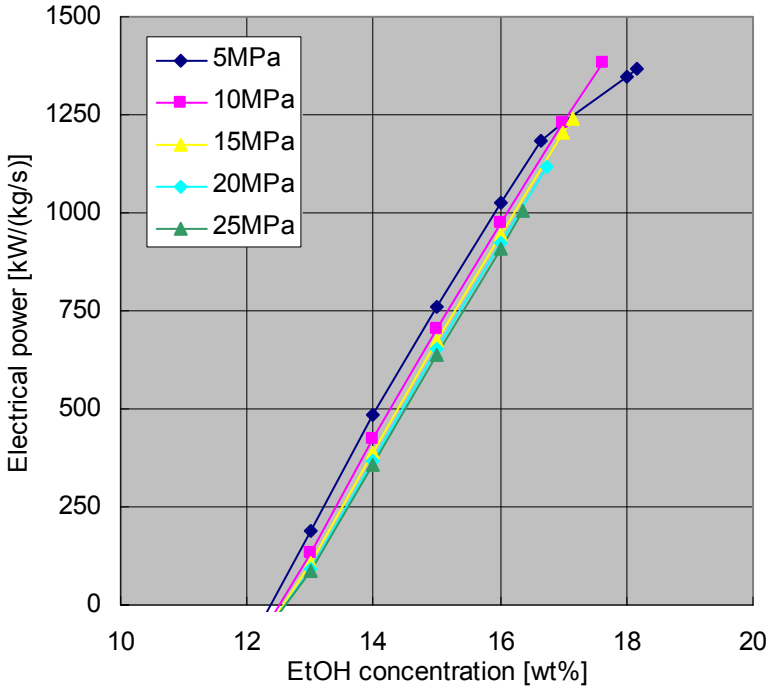

Figure 5.6 Electric power of direct type power plant using ethanol

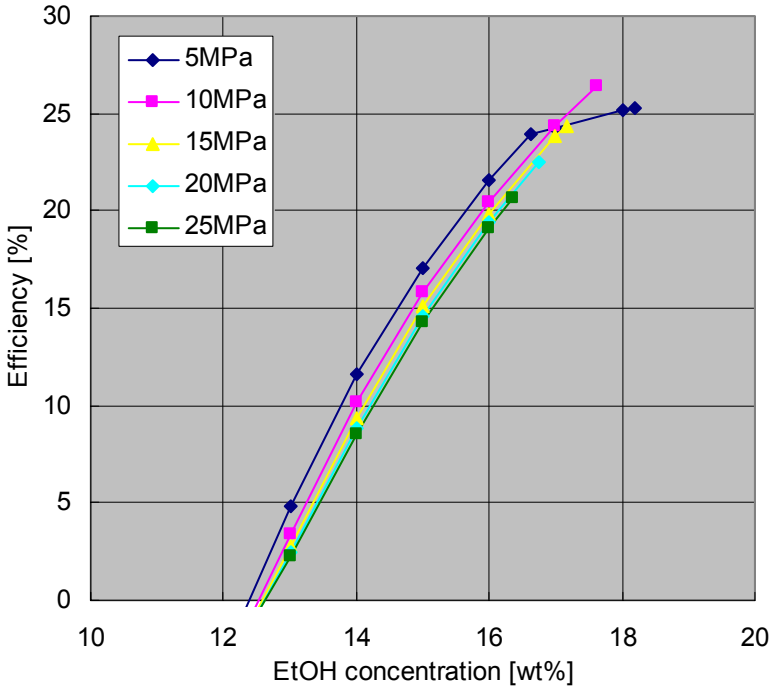

Figure 5.7 Efficiency of direct type power plant using ethanol

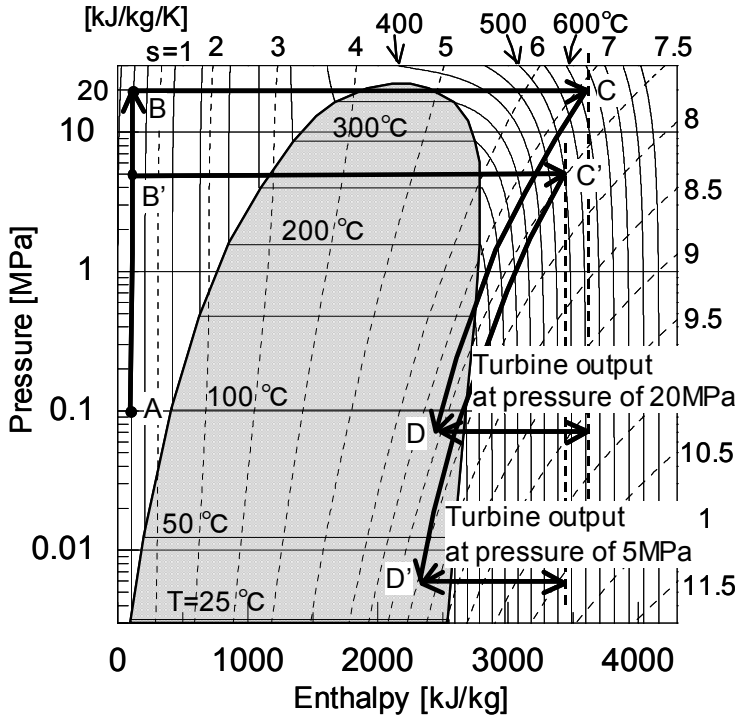

Figure 5.8 *p-h* diagram of direct type power plant

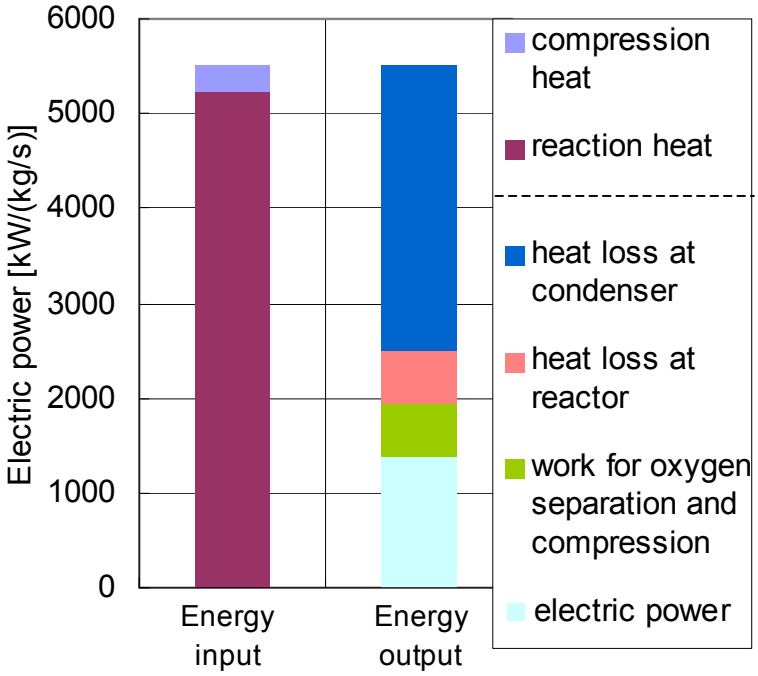

Figure 5.9 Energy budget of direct type power plant using 17.6 wt% ethanol

5.4.2 Indirect type power plant using ethanol

Figures 5.10 and 5.11 show the relationship between ethanol concentration and electric power and that between ethanol concentration and efficiency, respectively, for indirect type power plant with reactor pressures of 5, 10, 15, 20, 25 MPa. It is clear that the electric power and the efficiency are much lower than those of the direct type power plant. Both electric power and efficiency become higher at lower reactor pressure, because of the same reason as the direct type power plant, that is, more compressor work for compression of oxygen is needed for higher pressures. Figure 5.12 shows *p-h* diagram of the indirect type power plant using 16 wt% ethanol solution. Lines A-B, B-C, C-D indicate pressurization of reactant by high-pressure pump, hydrothermal oxidation in the reactor and heat transfer at the heat exchanger, respectively. Dashed line A-E and dashed curve E-F indicate heat receipt of the main water and expansion at turbine, respectively. From Figure 5.12, it is found that the pressure at the turbine inlet is lower than that in the direct type power plant shown in Figure 5.8. This results in lower electric power and lower efficiency for indirect type power plant. Even if coal or oil is used as a reactant, the efficiency is almost the same as ethanol for indirect type power plant with one turbine, though the amount of coal or oil is much less than that of ethanol because the calories of coal and oil are much higher than that of ethanol. Figure 5.13 shows the energy budget of indirect type power plant using 21.7 wt% ethanol. Heat loss dominates large part of the energy output because a lot of heat is discarded in the condenser. The amount of discarded heat is lager than that in the direct type power plant in Figure 5.9. This is because the lower pressure of main water causes the higher steam enthalpy at the turbine outlet. In commercial power plants, in order to enhance the efficiency, pressurization of main water is conducted. Therefore pressurization of the main water by feed pump is considered for the indirect type power plant in this study.

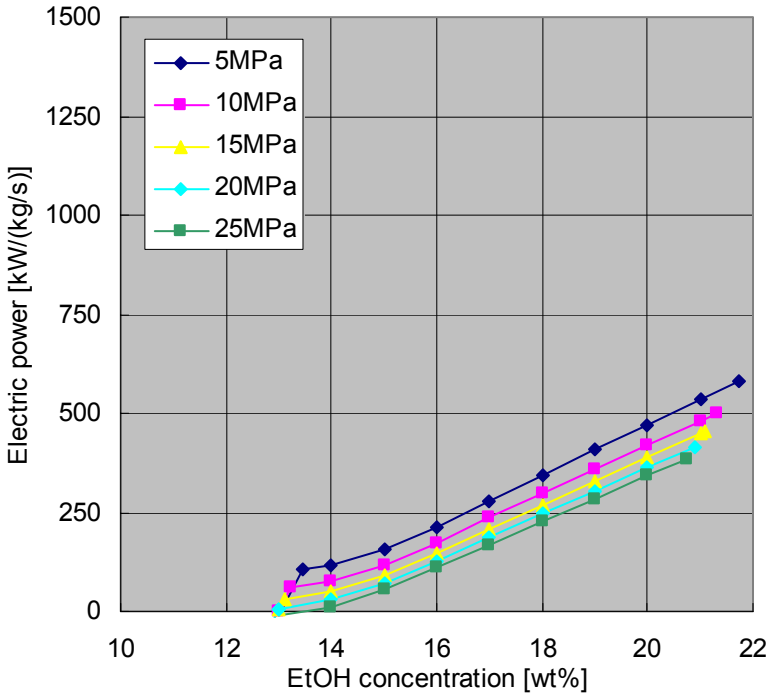

Figure 5.10 Electric power of indirect type power plant using ethanol

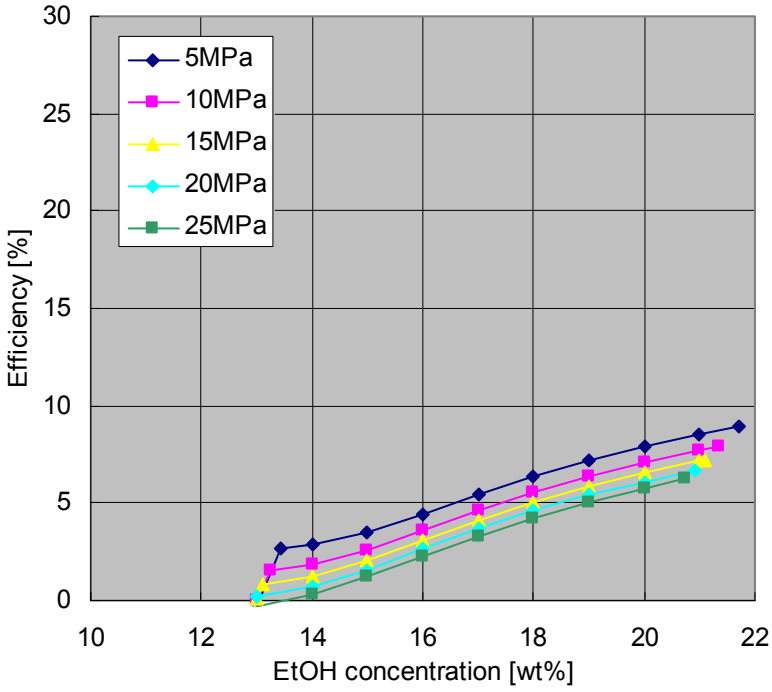

Figure 5.11 Efficiency of indirect type power plant using ethanol

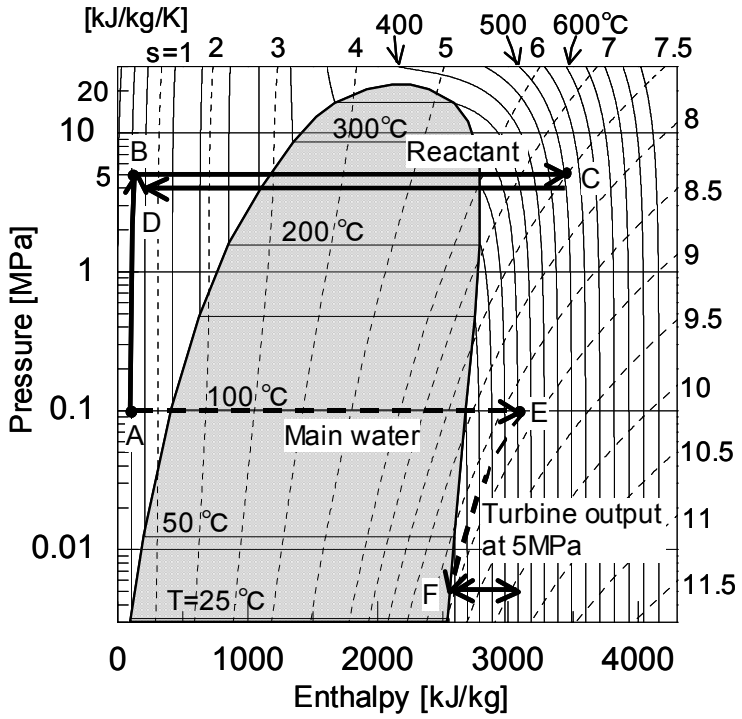

Figure 5.12 *p-h* diagram of indirect type power plant

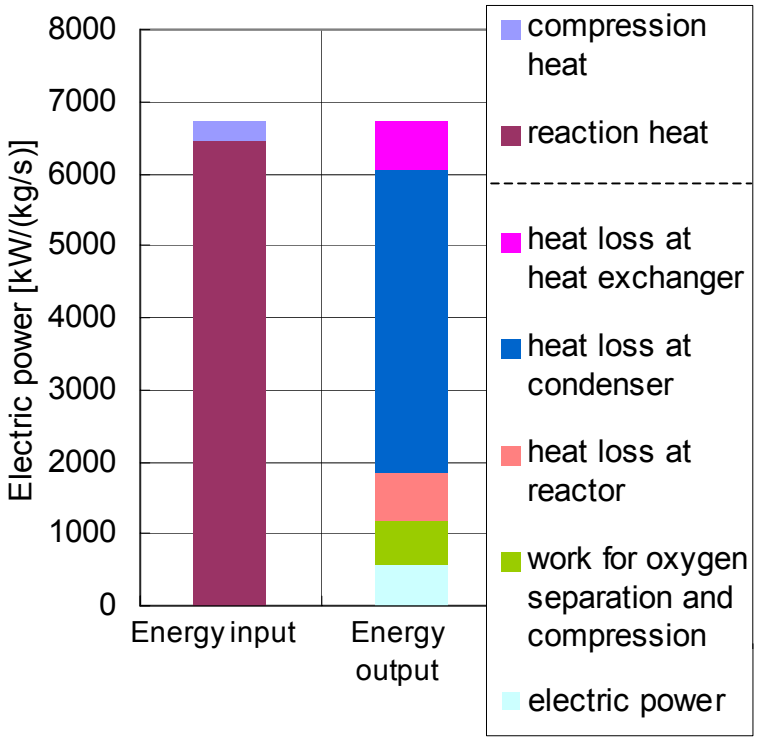

Figure 5.13 Energy budget of indirect type power plant using 21.7 wt% ethanol

5.4.3 Effect of the pressurization of inlet water in indirect type power plant

Saturation temperature at the pressure of main water needs to be lower than that of the reactor pressure by more than 10 °C in order to keep the temperature difference between high and low temperature fluids more than 10 °C at the heat exchanger. Figure 5.14 shows the change of the efficiency due to pressurization of main water with 16 wt% and 20 wt% ethanol solution at the reactor pressure of 5 MPa. From this figure, the efficiency increases from 7.9% to 20.1% as the pressure of the main water increases from 0.1 MPa to 4.2 MPa with 20 wt% solution. With 16 wt% solution, the efficiency increases from 4.5% to 11.6% as the pressure of the main water increases from 0.1 MPa to 0.8 MPa, though the efficiency decreases above 0.8 MPa. This indicates that over-pressurization causes the discarding of high quality steam at the turbine outlet and results in lower efficiency.

In Figures 5.15 and 5.16, electric power and efficiency of the direct type and the indirect type power plants using ethanol solution are compared at the reactor pressure of 5 MPa. If there is no pressurization, electric power and efficiency of the indirect type power plant are much lower than that of the direct type as mentioned before. However, with pressurization of 4 MPa, the difference between the direct and the indirect type power plants becomes smaller, though higher concentration of ethanol is still needed for the indirect type power plant.

As shown in Figures 5.15 and 5.16, the electric power and the efficiency around 15 wt% are lower with pressurization of 4 MPa than the case without pressurization. Under these conditions, optimal outputs are obtained in electric power and efficiency by adjusting the pressurization of main water as described by dashed line in Figures 5.15 and 5.16.

Thermal efficiency of commercial steam power plant is usually about 40%, because these power plants use reheat and regenerative cycle with 3 turbines and pressurization of main water. If this high efficient power generating part is connected to the hydrothermal oxidation part in Section 5.3.2, the maximum energy conversion efficiency for indirect type power plant becomes 32.2% for 20 wt% of ethanol at the reactor pressure of 5 MPa.

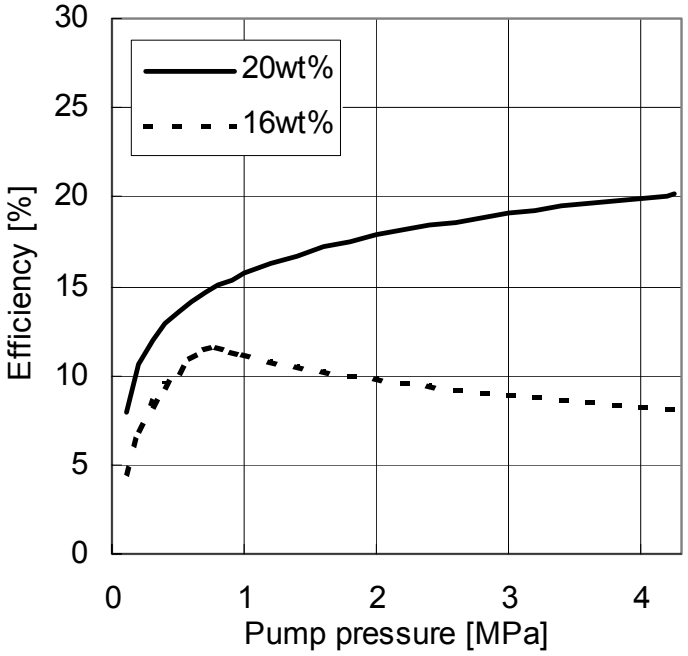

Figure 5.14 Effect of pressurization

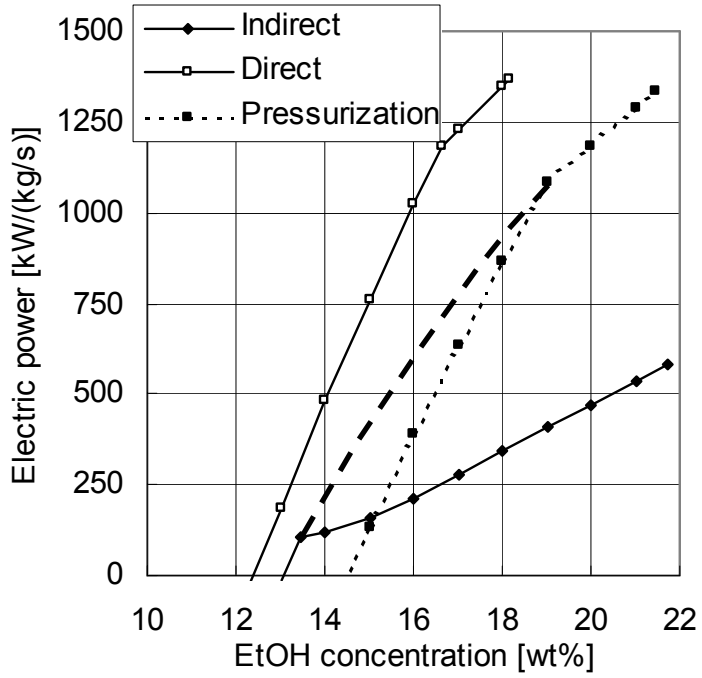

Figure 5.15 Comparison of electric power output

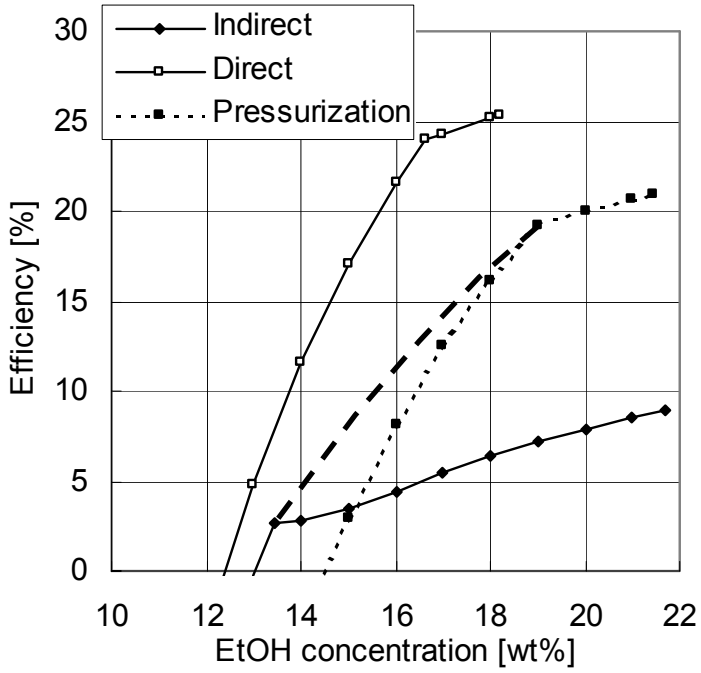

Figure 5.16 Comparison of efficiency

5.4.4 Power plant using glucose

Glucose solution is used as a model biomass fuel for direct and indirect type power plants. Reactor pressure of 5 MPa is selected because lower reactor pressure results in higher efficiency in the discussions in Sections 5.4.1 and 5.4.2. Figures 5.17 and 5.18 show the relationship between glucose concentration and electric power and that between glucose concentration and efficiency, respectively. In these figures, same tendency as shown in Figures 5.15 and 5.16, is observed in the relationship between direct and indirect type power plant, that is, higher efficiency is obtained in direct type power plant. Higher concentration of glucose is needed in order to obtain the same amount of electric power and efficiency as ethanol.

The maximum efficiency of the direct type power plant is about 25.5% with 34.5 wt% solution and that of the indirect type power plant with the pressurization of the main water of 4 MPa is about 21.1% with 40.7 wt% solution.

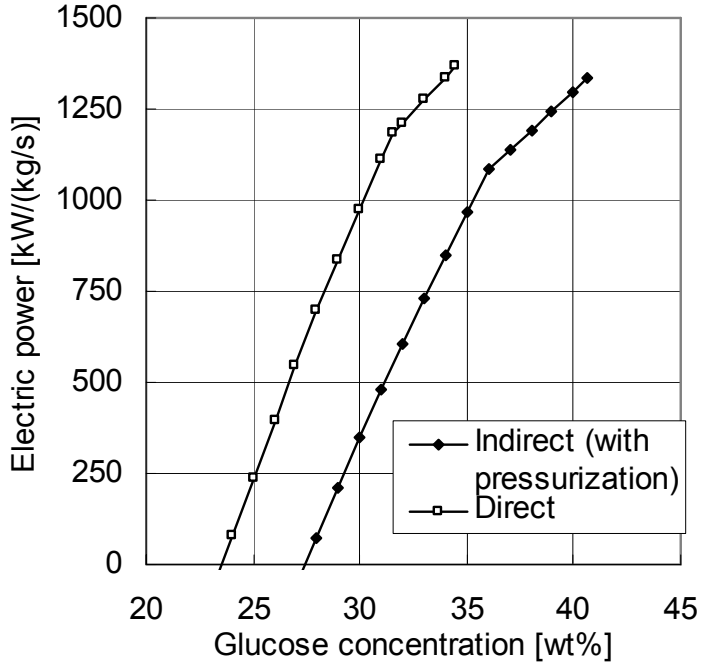

Figure 5.17 Electric power of direct and indirect type power plants using glucose

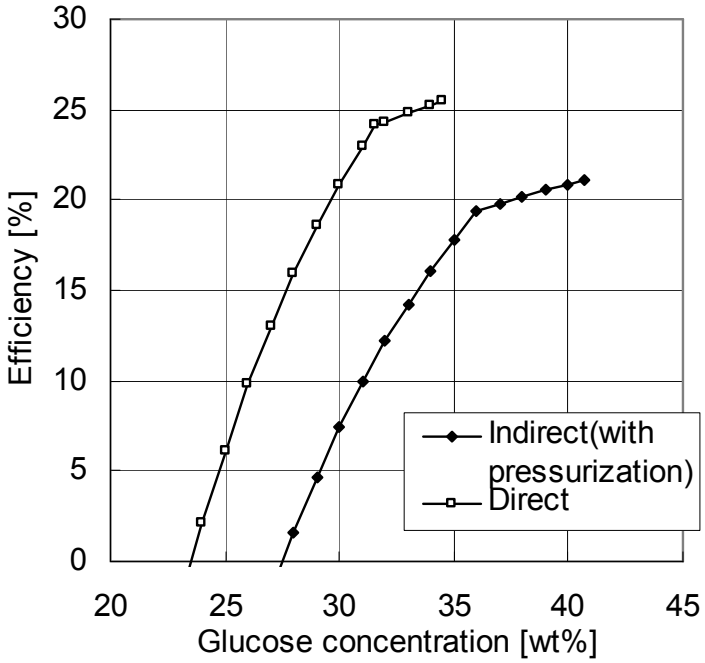

Figure 5.18 Efficiency of direct and indirect type power plants using glucose

5.4.5 Power plant using peat

When real biomass such as food leftovers, animal manure, and sewage sludge, are used for reactant, impure substances such as Na^+ and K^+ are included in the product solution, even if reactant is completely oxidized. Thus hot and high-pressure steam produced by hydrothermal oxidation cannot be directly introduced into turbine. Otherwise impure substance would corrode and adhere to the turbine blades. As a result, only the indirect type power plant is considered when real biomass is used. Here, peat solution is used as an example of real biomass. Low reactor pressure of 5 MPa is selected to maximize the efficiency. Figures 5.19 and 5.20 show the relationship between peat concentration and electric power and that between peat concentration and efficiency, respectively. The maximum efficiency for the indirect type power plant with the pressurization of the main water of 4 MPa is about 20.8% by 36.8 wt% peat solution. From this result, it is concluded that the electricity can be generated by hydrothermal oxidation using real wet biomass as well as using ethanol and glucose solutions.

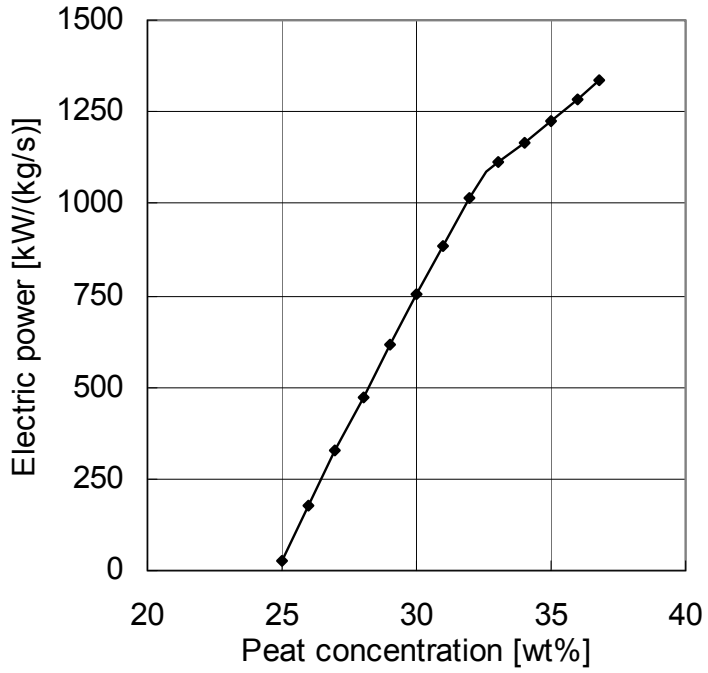

Figure 5.19 Electric power of indirect type power plant using peat

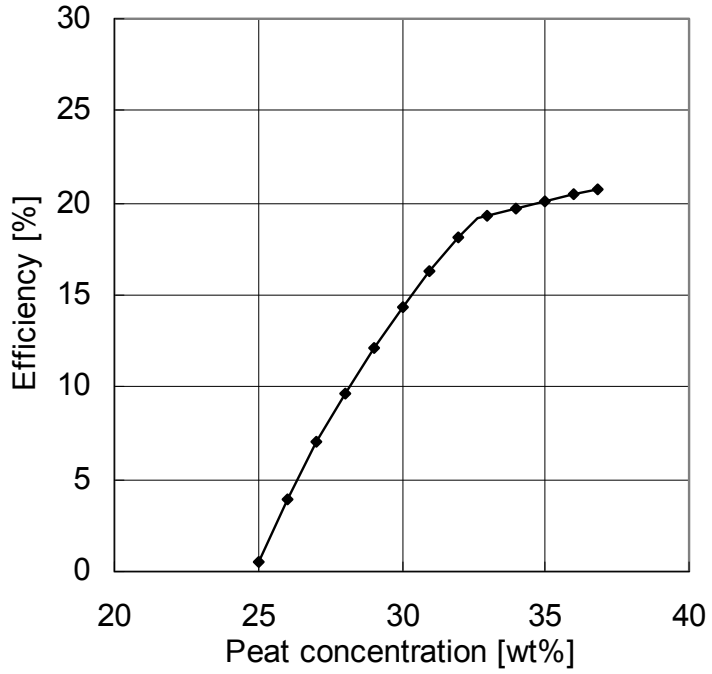

Figure 5.20 Efficiency of indirect type power plant using peat

5.5 Summary

Electric power and energy conversion efficiency of hydrothermal oxidation power plants using ethanol, glucose, and peat solutions are investigated. Findings from this study are listed as follows:

1) As an oxidizer, oxygen separated from air is used instead of air itself because compressing nitrogen in air consumes a lot of energy.

2) In both direct and indirect type power plants, electric power and efficiency become higher as the reactor pressure decreases, because energy needed for oxygen compression becomes larger as the reactor pressure becomes higher.

3) Electric power and efficiency of the direct type power plant is higher than that of the indirect type power plant.

4) The energy conversion efficiency of the direct type power plant using 17.6 wt% ethanol solution is about 26.4% at the reactor pressure of 10 MPa. By observing energy budget, a lot of heat energy is discarded in a condenser because reheat and regenerative cycles are not applied.

5) The energy conversion efficiency of the indirect type power plant using 21.7 wt%

ethanol solution is about 9.0% at the reactor pressure of 5 MPa. By observing energy budget, a lot of heat energy is discarded in a condenser. This is because reheat and regenerative cycles are not applied and the main water is not pressurized.

6) The electric power and the efficiency of the indirect type power plant can be improved a lot by pressurizing the main water, and optimal pressurization values exist at each concentration of ethanol. The energy conversion efficiency using 21.5 wt% ethanol solution with the pressurization of the main water of 4 MPa is about 20.9% at the reactor pressure of 5 MPa.

7) The energy conversion efficiency of the direct type power plant using 34.5 wt% glucose solution is about 25.5% at the reactor pressure of 5 MPa and the efficiency of the indirect type power plant using 40.7 wt% glucose solution with pressurization of the main water to 4 MPa is about 21.1% at the reactor pressure of 5 MPa.

8) The energy conversion efficiency of the indirect type power plant using 36.8 wt% peat solution with pressurization of the main water to 4 MPa is about 20.8% at the reactor pressure of 5 MPa.

Chapter 6

Conclusion

Hydrothermal oxidation has several advantages as a treatment method for wet bio-wastes. When wet bio-wastes contain a large reaction enthalpy, they produce thermal energy during their disposal by hydrothermal oxidation. In this study, the feasibility of thermal energy production from bio-wastes with high moisture content by subcritical water oxidation was investigated. From the experimental results using ethanol solutions, it was confirmed that ethanol solutions become hot water by subcritical water oxidation. The oxidation rates of ethanol in subcritical water were also measured experimentally and numerical simulations were conducted using the experimentally determined oxidation rate, which included the oxygen concentration. Consequently, the simulation results are qualitatively in good agreement with the experimental data. As a test to employ the thermal energy produced by hydrothermal oxidation, electric power plants were considered and their energy conversion efficiencies were calculated. We conclude that thermal energy production by subcritical water oxidation from wet bio-wastes is promising and that electric power generation from the resulting thermal energy is plausible. The results obtained in this study are summarized below.

An experimental study using an aqueous solution of ethanol was conducted with various preheating temperatures, 140-290 °C, and H_2O_2 concentrations, 2-20 vol%. The exothermic oxidation reaction was confirmed, and hot water around 300 °C was produced under the conditions of a preheating temperature of 200 °C, an ethanol concentration of 12 vol%, and a H_2O_2 concentration of 20 vol%. The conversion of

ethanol increases as the preheating temperature and the concentration of the oxidizer increase. In addition, the temperature increase of the water produced becomes larger as the concentration of the oxidizer increases. If there is a shortage of the oxidizer in the reactant, the decomposition reaction, rather than oxidation reaction, becomes dominant and less thermal energy was produced.

The ethanol oxidation rate in subcritical water was measured to estimate the processing capacity of subcritical water oxidation of the ethanol solutions. These measurements were conducted in a temperature range of 170 °C to 230 °C and a pressure of 23.5 MPa. To maintain a constant temperature inside the reactor, a low concentration of ethanol solution was used in the oxidation measurements. A first-order oxidation rate was obtained as follows:

$$-\frac{d[\mathrm{EtOH}]}{dt} = 10^{2.64\pm0.07} \times \exp\left(\frac{-45.6 \pm 0.6\mathrm{kJ/mol}}{RT}\right)[\mathrm{EtOH}].$$

The oxygen dependence on the global oxidation rate of ethanol was also investigated. The ethanol oxidation rate, including the oxygen concentration, was:

$$-\frac{d[\mathrm{EtOH}]}{dt} = 10^{2.05\pm0.24} \times \exp\left(\frac{-61 \pm 3\mathrm{kJ/mol}}{RT}\right)[\mathrm{EtOH}]^{0.86\pm0.03}[\mathrm{O_2}]^{1.15\pm0.05}.$$

A numerical study of subcritical water oxidation of ethanol was conducted to investigate whether the obtained ethanol oxidation rate, which was derived from experiments with the low concentration of ethanol, is applicable to subcritical water oxidation with a high concentration of ethanol. The conversion of ethanol and the temperature increase in the numerical simulation agree with the experimental data using a high concentration of ethanol as long as the main product of ethanol oxidation is acetic acid. This agreement indicated that the obtained ethanol oxidation rate is used at both high and low concentrations of ethanol. The difference in the temperature increase at a high concentration of H_2O_2, 14-20 vol% in the simulation is caused by neglecting the further oxidation of acetic acid into CO_2, which generates more heat in the

experiment.

Electric power plants where thermal energy produced by hydrothermal oxidation is used for electric power generation were also evaluated. The amount of electric power and the energy conversion efficiency in these power plants were calculated. The electric power and the efficiency become higher as the reactor pressure decreases in both direct and indirect type power plants because the energy consumption for oxygen compression becomes larger as the reactor pressure becomes higher. In the indirect type power plants, the electric power and efficiency are lower than those of direct type power plants. However, pressurizing the main water improves the low efficiencies of indirect type power plants. The highest efficiencies with ethanol solution are 26.4% and 20.9% in the direct and indirect power plants, respectively. Hence, this evaluation showed that the electric power plants using hydrothermal oxidation have high potential as electric power generation systems from wet bio-wastes as well as their decompositions.

In this study, experiments using the clean ethanol solutions as reactants were conducted. However, thermal energy production from dirty reactants, which more closely resemble real wet bio-wastes & biomass, needs to be realized. Because food leftovers are well hydrolyzed in subcritical water, the solutions obtained after hydrolysis are appropriate reactants to be tested in experiments prior to establishing industrial plants with subcritical water oxidation using real dirty bio-wastes. Drains from livestock houses, which contain animal manure, are also suitable reactants to be examined. As explained in Section 1.1.3, the total amount of thermal energy contained in wet bio-wastes & biomass disposed in Japan accounted for 14,300 ML in oil equivalents in the fiscal year of 2002. Thus, it is strongly anticipated that in the future, hydrothermal oxidation will beneficially use the thermal energy from these wastes.

Moreover, there are large amounts of thermal energy exhausted from factories in Japan. The total amount of such a exhausted thermal energy, which consists of high temperature gases over 250 °C, hot water over 80 °C, and hot solid materials over 200 °C, was about 6,200 ML in oil equivalents in the fiscal year of 2000 (ECCJ report, 2000). Utilizing this wasted thermal energy for preheating in hydrothermal oxidation systems is one practical method to boost the thermal efficiency of hydrothermal oxidation systems. Thus, the integration of the hydrothermal oxidation process and thermal

energy recovery process from exhausted heats is an important research topic toward advanced systems. Additionally, because hydrothermal oxidation is operated under high pressure, separation and underground disposal of CO_2 can be conducted easily. From an environmental point of view, this feature of hydrothermal oxidation also needs to be scrutinized, technically and economically, as an aggressive method to prevent an increase in atmospheric CO_2.

I hope that the thermal energy production from wet bio-wastes & biomass is realized with high efficiency by hydrothermal oxidation. Moreover, I am optimistic that electric power generation from wet bio-wastes & biomass will be realized in the near future. These break-through technologies will definitely contribute to the increase in the amount of alternative energy from wet bio-wastes & biomass introduced in Japan. Furthermore, there is no doubt that the intensive use of alternative energy will decrease the amount of fossil fuels imported into Japan, and will also be one solution to global warming.

Bibliography

Akiya, N., Savage, P. E., Roles of Water for Chemical Reactions in High-Temperature Water, *Chem. Rev.*, **102** (2002) 2725-2750.

Alkam, M. K., Pai, V. M., Butler, P. B., Pitz, W. J., Methanol and Hydrogen Oxidation Kinetics in Water at Supercritical States, *Combustion and Flame*, **106** (1996) 110-130.

Anderson, D. A., Tannehill, J. C., Pletcher, R. H., Computational fluid mechanics and heat transfer, McGraw-Hill book company, New York, 1984.

ANRE document: Documents distributed at the 10th New Energy Subcommittee of the Advisory Committee on Natural Resources and Energy, Agency for Natural Resources and Energy, Japan, 2003, http://www.meti.go.jp/report/downloadfiles/g21122d045j.pdf

Antal, Jr., M. J., Allen, S. G., Schulman, D., Xu, X., Divilio, R. J., Biomass Gasification in Supercritical Water, *Ind. Eng. Chem. Res.* **39** (2000) 4040-4053.

Arai, K., Inomata, H., Saito, S., Vapor-liquid equilibrium calculations using new mixing rules combining functionally different equations of state, *J. Chem. Eng. Japan*, **15**-1, (1982) 1-5.

Arita, T., Nakahara, K., Nagami, K., Kazimoto, O., Hydrogen generation from ethanol in supercritical water without catalyst. *Tetrahedron Letters*, **44** (2003) 1083-1086.

Barner, H. E., Huang, C. Y., Johnson, T., Jacobs, G., Martch, M. A., Killilea, W. R., Supercritical water oxidation: An emerging technology. *J. Haz. Mat.*, **31** (1992) l-17.

Brock, E. E., Oshima, Y., Savage, P. E., Barker, J. R., Kinetics and Mechanism of Methanol Oxidation in Supercritical Water, *J. Phys. Chem.*, **100** (1996) 15834-15842.

Chemical Engineering Encyclopedia 6th Edition, The Society of Chemical Engineers Japan, Tokyo, Japan, 1999, 18-23. (in Japanese)

Chung, T. H., Ajlan, M., Lee, L. L., Starling, K. E., Generalized multiparameter

correlation for nonpolar and polar fluid transport properties, *Ind. Eng. Chem. Res.*, **27** (1988) 671-679.

Climate Change 2001: The Scientific Basis, Intergovernmental Panel on Climate Change, Third Assessment Report, 2001.

Cocero, M. J., Alonso, E., Sanz, M. T., Fdz-Polanco, F., Supercritical water oxidation process under energetically self-sufficient operation, *J. Supercritical Fluids*, **24** (2002) 37-46.

Croiset, E., Rice, S. F., Hanush, R. G., Hydrogen peroxide decomposition in supercritical water. *AIChE J.*, **43** (1997) 2343-2352.

Cutler, A. H., Antal, Jr., M. J., John, Jr., M., A critical evaluation of the plug-flow idealization of tubular-flow reactor data, *Ind. Eng. Chem. Res.*, **27** (1988) 691-697.

Daman, E. L., Process and apparatus for supercritical water oxidation, U.S. Patent #5571423 (1996).

DB-NEDO: Technical information database on New Energy and Industrial Technology Development Organization, Japan, http://www.nedo.go.jp/nedata/17fy/index.html

Dillon, H. E., Penoncello, S. G., A Fundamental Equation for Calculation of the Thermodynamic Properties of Ethanol. *Int. J. Thermophys.*, **25** (2004) 321-335.

Dittus, F. W., Boelter, L. M. K., Heat Transfer in Automobile Radiators of the Tubular Type, *Publications in Engineering*, **2**-13 University of California, Berkeley, (1930), 443-461; reprinted in *International Communications in Heat and Mass Transfer*, **12** (1985) 3-22.

ECCJ report: The Energy Conservation Center, Japan, 2000. http://www.eccj.or.jp/ wasteheat/index.html

EgWin: Koda, E., Takahashi, T., Mimaki, T., Development of General-purpose Computer Program to analyze the Steady State of Power Generation System, Central Research Institute of Electric Power Industry Research Report, W99034, (2000) (in Japanese)

Energy Information Administration International Energy Outlook, U.S. Department of Energy, Washington, DC, 2007.

Foussard, J. -N., Debellefontaine, H., Besombes-Vailhé, J., Efficient Elimination of Organic Liquid Wastes: Wet Air Oxidation, *J. Environ. Eng.*, **115**-2, (1989) 367-385.

Fauvel, E., Dubien, C. J., Guichardon, P., Charbit, G., Charbit, F., Sarrade, S., A

double-wall reactor for hydrothermal oxidation with supercritical water flow across the inner porous tube, *J. Supercritical Fluids*, **28** (2004) 47-56.

Gloyna, E. F., Li, L., *Waste Management*, **13** (1993) 374-394.

Hashaikeh, R., Fang, Z., Butler, I. S., Kozinski, J. A., Sequential hydrothermal gasification of biomass to hydrogen. *Proceedings of the Combustion Institute*, **30** (2005) 2231-2237.

Helling, R. K., Tester, J. W., Oxidation of simple compounds and mixtures in supercritical water: carbon monoxide, ammonia, and ethanol, *Environ. Sci. Technol.*, **22** (1988) 1319-1324.

Hippler, H., Troe, J., Willner, J., Shock Wave Study of the Reaction $HO_2 + HO_2 \rightarrow H_2O_2 + O_2$: Confirmation of a Rate Constant Minimum Near 700 K, *J. Chem. Phys.*, **93**-3, (1990) 1755-1760.

Hirosaka, K., Fukayama, M., Wakamatsu, K., Ishida, Y., Kitagawa, K., Hasegawa, T., Combustion of ethanol by hydrothermal oxidation. *Proceedings of the Combustion Institute*, 31 (2007) 3361-3367

Hirosaka, K., Koido, K., Fukayama, M., Ouryoji, K., Hasegawa, T., Experimental and Numerical Study of Ethanol Oxidation in Sub-critical Water, *J. Supercritical Fluids*, (2008[a]) doi:10.1016/j.supflu.2007.09.009

Hirosaka, K., Yuvamitra, K., Ishikawa, A., Hasegawa, T., Efficiencies of power plants using hydrothermal oxidation, *Thermal Science and Engineering*, **16**-1 (2008[b]) (in printing)

Holgatet, H. R., Tester, J. W., Oxidation of Hydrogen and Carbon Monoxide in Sub- and Supercritical Water: Reaction Kinetics, Pathways, and Water-Density Effects. 1. Experimental Results, *J. Phys. Chem.*, **98** (1994) 800-809.

Holliday, R. L., King, J. W., List, G. R., Hydrolysis of vegetable oils in sub- and supercritical water. *Ind. Eng. Chem. Res.*, **36** (1997) 932-935.

Hong, G. T., Killilea, W. R., Thomason, T. B., Method for solids separation in a wet oxidation type process, U.S. Patent #4822497 (1989).

IAPWS equation[1]: Release on the Static Dielectric Constant of Ordinary Water Substance for Temperatures from 238 K to 873 K and Pressures up to 1000 MPa, The International Association for the Properties of Water and Steam, Germany, 1997.

IAPWS equation[2]: Release on the Ionization Constant of H_2O, The International Association for the Properties of Water and Steam, Switzerland, 2007.

IAPWS-IF97: Release on the IAPWS Industrial Formulation 1997 for the Thermodynamic Properties of Water and Steam, The International Association for the Properties of Water and Steam, Germany, 1997.

Iyer, S. D., Joshi, P. V., Klein, M. T., Automated model building and modeling of alcohol oxidation in high temperature water, *Environmental Progress*, **17**-4 (1998) 221-233.

Koido, K., Hirosaka, K., Kubo, T., Fukayama, M., Ouryouji, K., Hasegawa, T., Numerical study on hydrothermal oxidation in a tube reactor. 4th International Energy Conversion Engineering Conference, AIAA-2006-4156, 2006.

Lamb, W. J., Hoffman, G. A., Jonas, J., Self-diffusion in compressed supercritical water, *J. Chem. Phys.*, **74**-12 (1981) 6875-6880.

Lee, B. I., Kesler, M. G., A generalized thermodynamic correlation based on three-parameter corresponding state, *AIChE J.*, **21** (1975) 510-527.

Li, L., Chen, P., Gloyna, E. F., Generalized Kinetic Model for Wet Oxidation of Organic Compounds, *AIChE J.*, **37**-11 (1991) 1687-1697.

Marinov, N. M., A detailed chemical kinetics model for high temperature ethanol oxidation, *Int. J. Chem. Kinetics*, **31** (1999) 183-220.

Marrone, P. A., Hodes, M., Smith, K. A., Tester, J. W., Salt precipitation and scale control in supercritical water oxidation- part B: commercial/full-scale applications, *J. Supercritical Fluids*, **29** (2004) 289-312.

Medium-Term Oil Market Report, International Energy Agency, Paris, 2006. (Handbook of energy & Statistics, Energy data and modeling center, Japan, 2006.)

Mills, R., Self-Diffusion in Normal and Heavy Water in the Range 1-45°, *J. Phys. Chem.*, **77**-5 (1973) 685-688.

Naito, K., Huang, K., Endo, A., Nakaiwa, M., Akiya, T., Yanagishita, H., Nakane, T., New system for electric power generation by wet oxidation of biomass ethanol, *J. Chem. Eng. Japan*, **34**-12, (2001), 1545-1548.

Okuno, Y., Li, Y., Sasaki, H., Seki, K., Kamigochi, I., Influence of the sludge ratio on the high-solids thermophilic methane fermentation of the organic fraction of municipal solid waste and bio-sludge, *J. Japan Society of Waste Management Experts*, **14**-1

(2003) 27-35 (in Japanese).

Plöcker, U., Knapp, H., Prausnitz, J., Calculation of high-pressure vapor-liquid equilibria from a corresponding-states correlation with emphasis on asymmetric mixtures, *Ind. Eng. Chem. Process. Des. Dev.*, **17**-3, (1978) 324-332.

Pruden, B. B., Le, H., Wet Air Oxidation of Soluble Components in Waste Water, *Can. J. Chem. Eng.*, **54**, (1976) 319-325.

REFPROP: Lemmon, E. W., McLinden, M. O., Huber, M. L., Reference Fluid Thermodynamic and Transport Properties, NIST Standard Reference Database 23 Version 7.0, Physical and Chemical Properties Division, NIST, 2002

Renewables Information, International Energy Agency, Paris, 2006. (Handbook of energy & Statistics, Energy data and modeling center, Japan, 2006.)

Rice, S. F., Croiset, E., Oxidation of simple alcohols in supercritical water III. Formation of Intermediates from Ethanol, *Ind. Eng. Chem. Res.*, **40** (2001) 86-93.

Rice, S. F., Hunter, T. B., Ryden, A. C., Hanush, R. G., Raman Spectroscopic Measurement of Oxidation in Supercritical water. 1. Conversion of Methanol to Formaldehyde, *Ind. Eng. Chem. Res.,* **35** (1996) 2161-2171.

Robelius, F., Giant Oil Fields - The Highway to Oil, Ph.D. Thesis, Uppsala University, Sweden, 2007.

Rohsenow, W. M., Choi, H., Heat mass and momentum transfer, Prentice-Hall Inc., New Jersey, 1961, p.102.

Savage, P. E., Gopalan, S., Mizan, T. I., Martino, C. J., Brock, E. E., *AIChE J.*, **41** (1995) 1723-1778.

Schanzenbächer, J., Taylor, J. D., Tester, J. W., Ethanol oxidation and hydrolysis rates in supercritical water, *J. Supercritical Fluids*, **22** (2002) 139-147.

Shaw, R. W., Brill, T. B., Clifford, A. A., Eckert, C. A., Franck, E. U., *Chem. Eng. News* **69**-51 (1991) 26-39.

Staszak, C. N., Malinowski, K. C., Killilea, W. R., The pilot-scale demonstration of the MODAR oxidation process for the destruction of hazardous organic waste materials. *Environmental Progress*, **6** (1987) 39-43.

Suzuki, A., Oe, T., Anjo, N., Suzugaki, H., Nakamura, T., Commercialization of supercritical water oxidation. *Proc. 4th Int. Symp. Supercritical Fluids*, (1997)

895-899.

Takagi, J., Ishigure, K., Thermal decomposition of hydrogen peroxide and its effect on reactor water monitoring of boiling water reactors, *Nucl. Sci. Eng.*, **89** (1985) 177-186.

Thomason, T., Modell, M., Supercritical water destruction of aqueous wastes. *Hazardous Waste*, **1** (1984) 453-466.

Timberlake, S. H., Hong, G. T., Simson, M., Modell, M., Supercritical water oxidation for wastewater treatment: Preliminary study of urea destruction. 12th Intersociety Conference on Environmental Systems, SAE technical paper #820872, (1982) 19-21.

Tsubouchi, T., comp., Heat exchanger, Asakura Publishing Co., Inc., Tokyo, Japan, 1968, 140. (in Japanese)

Webley, P. A., Tester, J. W., Fundamental Kinetics of Methane Oxidation in Supercritical Water, *Energy & Fuels*, **5**-3 (1991) 411-419.

Wightman, T. J., Studies in Supercritical Wet Air Oxidation, MS Thesis, Chem. Eng. Dept., MIT, Cambridge, MA, 1981.

Wilke, C. R., Chang, P., Correlation of diffusion coefficients in dilute solutions, *AIChE J.*, **1** (1955) 264-270.

Yoneyama, Y., Takeno, K., Shimizu, K., Naito, T., Itagaki, F., Yasuhara, Y., Nakada, M., Cogeneration through the Processing of Domestic Kitchen Waste and night soil sludge in a full-scale treatment plant, *J. Japan Society of Waste Management Experts*, **15**-3 (2004) 155-164 (in Japanese).

Yoshida, H., Tavakoli, O., Sub-critical Water Hydrolysis Treatment for Waste Squid Entrails and Production of Amino Acids, Organic Acids, and Fatty Acids, *J. Chem. Eng. Japan*, **37**-2 (2004) 253-260.

Yoshida, H., Terashima, M., Takahashi, Y., Production of Organic Acids and Amino Acids from Fish Meat by Sub-Critical Water Hydrolysis, *Biotechnol. Prog.*, **15** (1999) 1090-1094.

Appendix

A.1. Physical and chemical features of high-temperature and high-pressure water

Physicochemical constants of high-temperature and high-pressure water near the critical point of water are described. Figure A.1 demonstrates the density of water. It is noteworthy that the density decreases as the temperature increases, but the density increases as the pressure increases. Table A.1 compares the rough values of the density of water, steam, and supercritical water. The density of supercritical water is one order of magnitude smaller than that of the water, but is much larger than that of steam. Figure A.2 shows the dependence of the viscosity of water on temperature and pressure. The viscosity of supercritical water is almost same as that of steam, but is one order of magnitude smaller than that of water (Table A.1). Figure A.3 demonstrates the dependence of the molecular diffusion coefficient on temperature and pressure. These values are calculated on the basis of the equation of Lamb et al. (1981). This equation is derived from the experimental data obtained at temperatures between 400 °C and 700 °C and pressures between 19.9 MPa and 145.9 MPa. Hence, some of the extrapolated values differ from the measured values. Particularly, the value measured at 25 °C and 0.1013 MPa is 2.3×10^{-5} $cm^2 \cdot s^{-1}$ (Mills, 1973), which differs from the calculated value by about one order of magnitude. The molecular diffusion coefficient of supercritical water is much larger than that of water (Table A.1) due to the lower density and viscosity of supercritical water.

Figure A.4 shows the dependency of the heat transfer coefficient on the temperature and pressure. The heat transfer coefficient is affected not only by the properties, but also by the flow condition. These values are calculated under a condition of 100 $g \cdot s^{-1}$ flow inside a 1/8 inch concentric annulus. The heat transfer coefficients are

estimated using the Dittus-Boelter equation (Dittus and Boelter, 1930). This equation is derived from experimental data of a one-phase flow, which is the condition where supercritical water flow meets. Therefore, although the values in Figure A.4 are not accurate, they provide valuable qualitative information on the heat transfer coefficient. It should be noted that the heat transfer coefficient has a peak at the critical point and that the water near the critical point has a higher heat transfer. Figure A.5 shows the behavior of the static dielectric constant. It is noteworthy that the static dielectric constant in the liquid phase is high, which leads to a high miscibility of water with polar materials. In contrast, the static dielectric constants in the supercritical and gas phases are low and the miscibility of water with non-polar materials is high. Figure A.6 shows the feature of the ion product. The ion product at 25 °C and 1 atm is about -14 and increases as the temperature increases. However, when water turns to supercritical water or steam, the ion product drops rapidly. On the other hand, it does not decrease as much if the pressure is much higher. In short, water molecules tend to be ionized in the liquid phase, but tend to be non-ionized in the supercritical or gas phase, except in cases of ultrahigh pressures.

Table A.1 Comparison of steam, supercritical water, and water properties (Savage et al., 1995)

	Steam	Supercritical water	Water
Density [g·cm^{-3}]	10^{-3}	10^{-1}	1
Viscosity [Pa·s]	10^{-5}	10^{-4}-10^{-5}	10^{-3}
Diffusivity [cm^2·s^{-1}]	10^{-1}	10^{-3}	10^{-5}

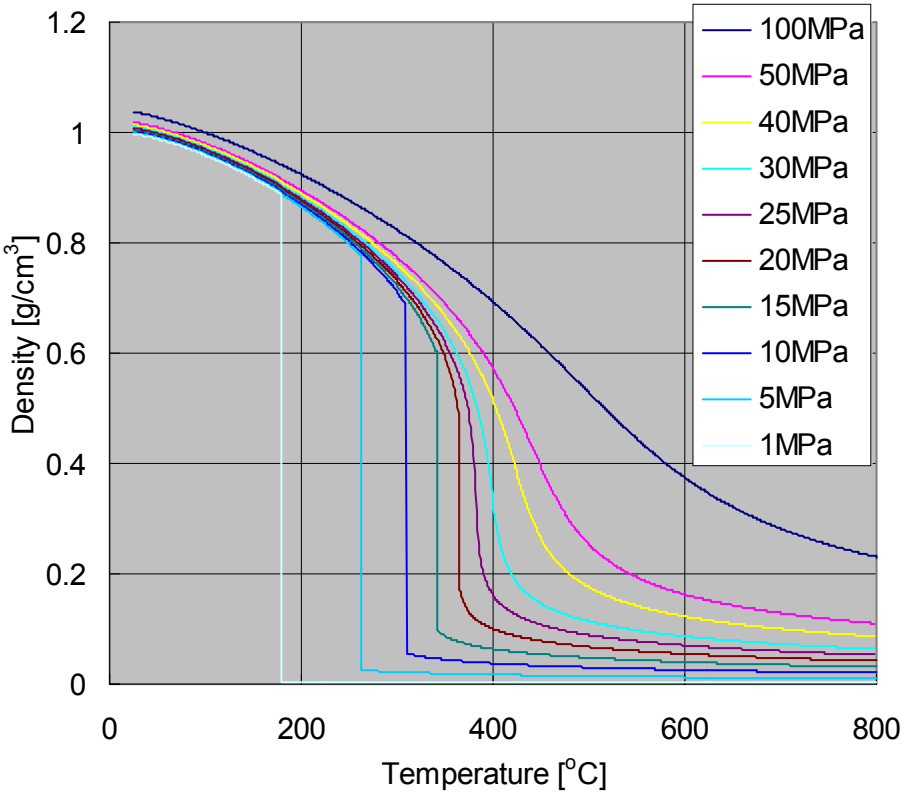

Figure A.1 Density under the conditions of 25-800 °C and 1-100 MPa (by REFPROP)

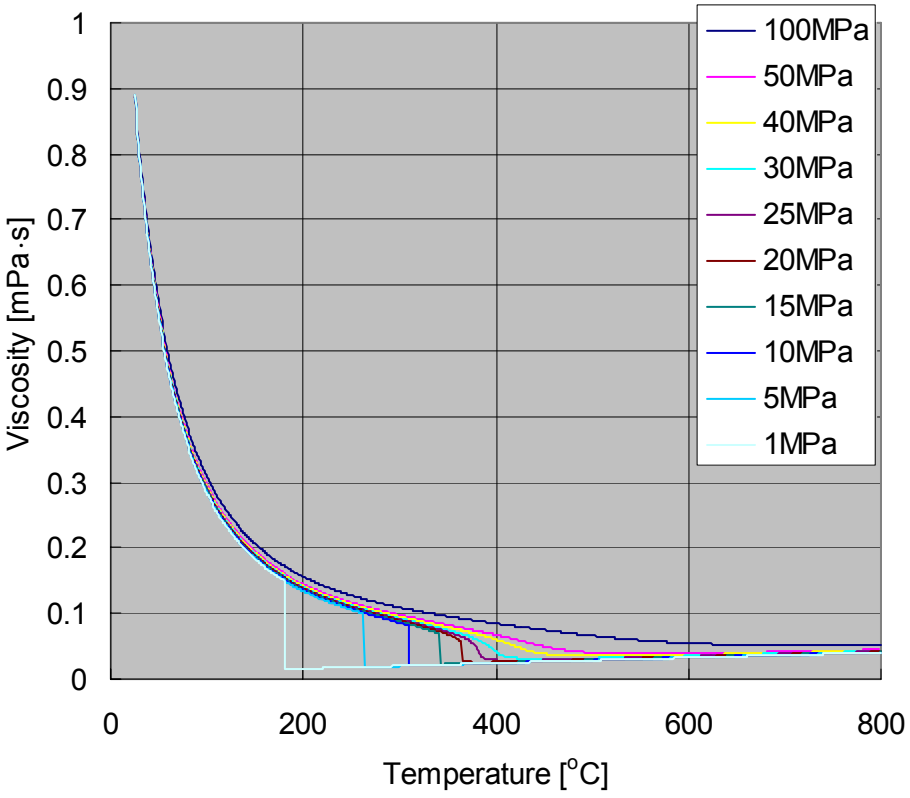

Figure A.2 Viscosity under the conditions of 25-800 °C and 1-100 MPa (by REFPROP)

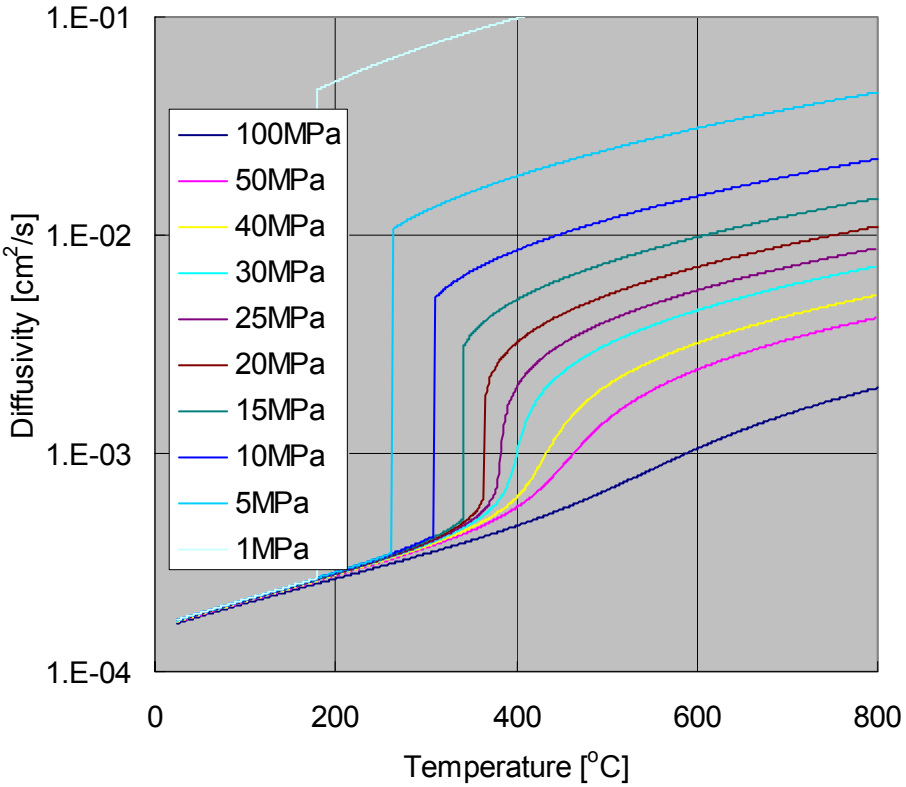

Figure A.3 Diffusivity under the conditions of 25-800 °C and 1-100 MPa (using the equation from Lamb et al.)

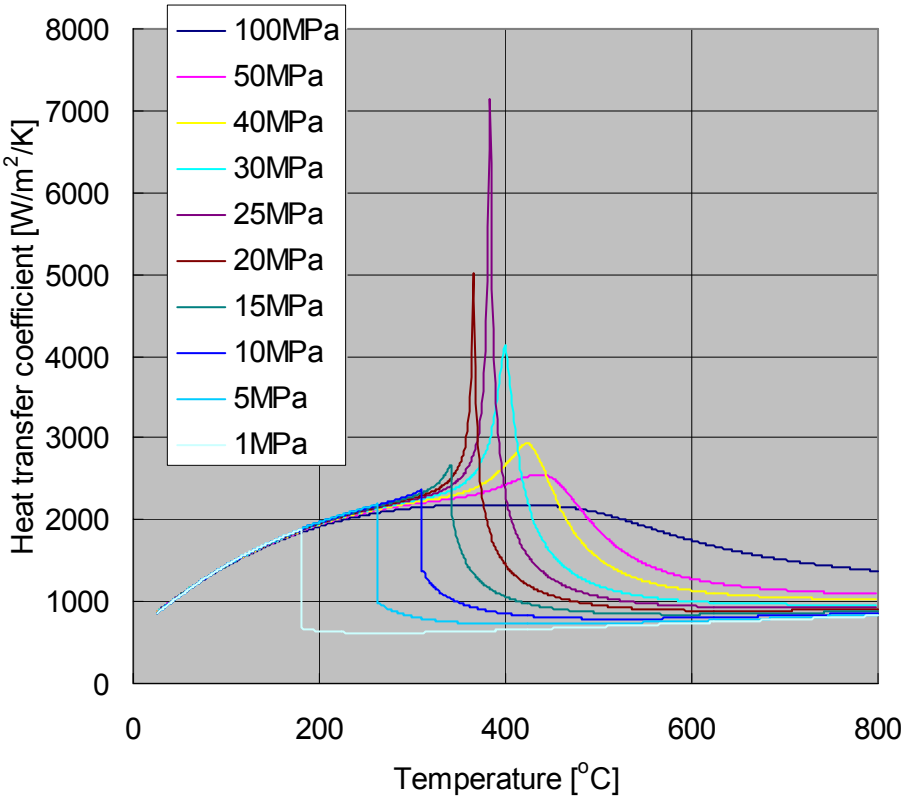

Figure A.4 Heat transfer coefficient under the conditions of 25-800 °C and 1-100 MPa (using Dittus-Boelter equation)

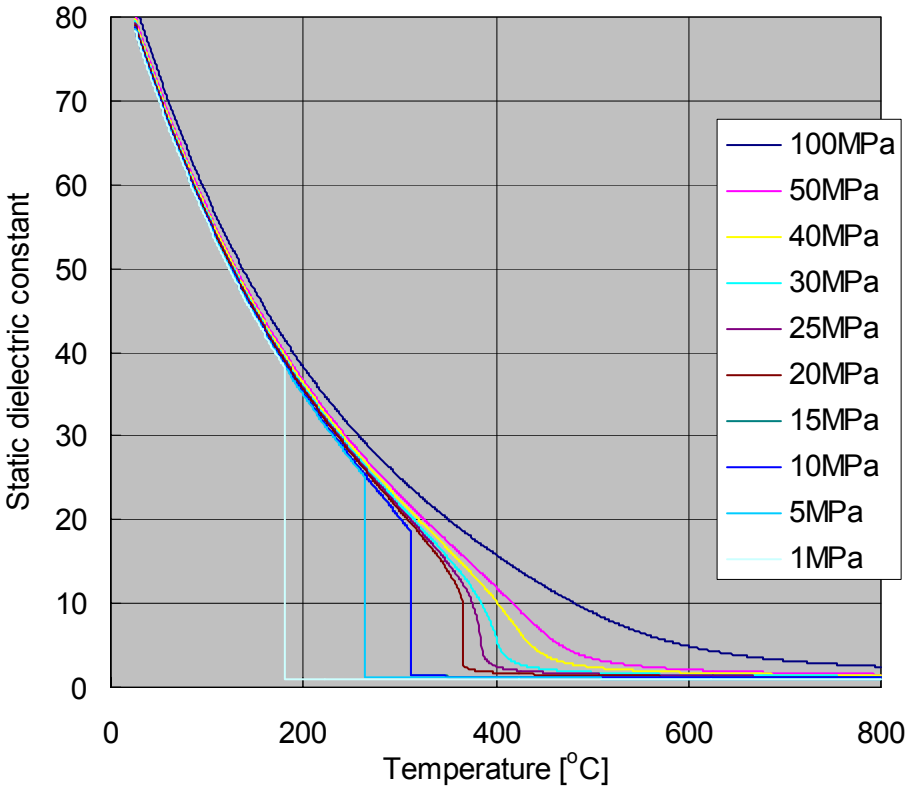

Figure A.5 Static dielectric constant under the conditions of 25-800 °C and 1-100 MPa (using IAPWS equation[1])

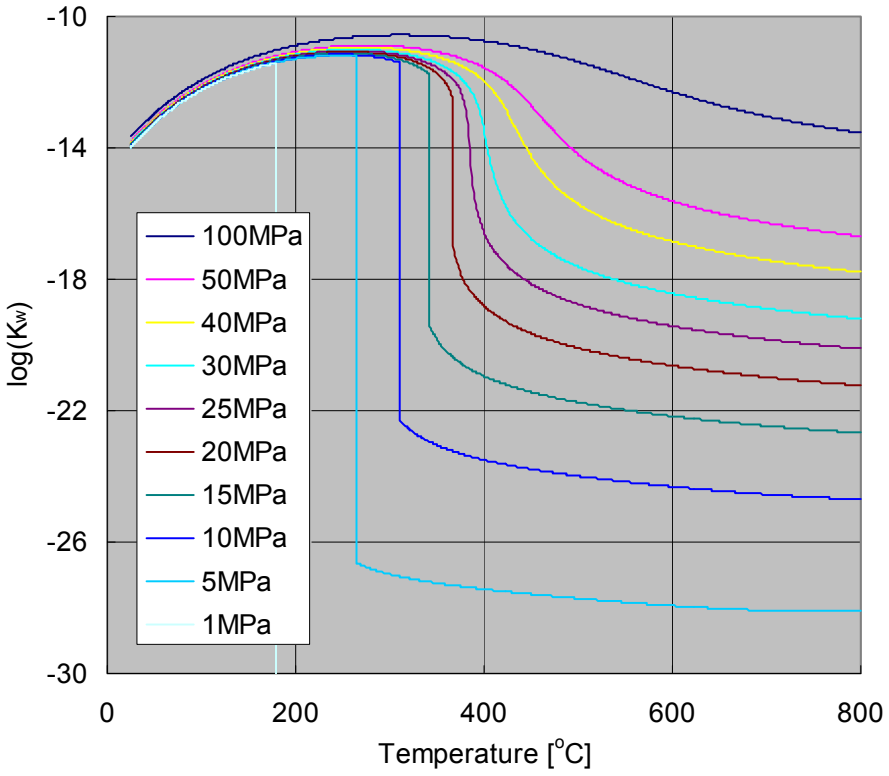

Figure A.6 Ion product under the conditions of 25-800 °C and 1-100 MPa (using IAPWS equation[2])

A.2 Advantages of a hydrothermal reaction from an engineering viewpoint

Section A.1 describes the physical and chemical features of high-temperature and high-pressure water: high density, high diffusivity, high heat transference, and a drastic change in the static constant and ion products. These features lead to several advantages for a hydrothermal reaction from an engineering point of view. Some of them are as follows. 1) High reaction controllability due to the drastic change in the static dielectric constant and the ion product at the critical point. For instance, salt precipitation and separation can be conducted by taking advantage of the drastic change in the static dielectric constant of water with temperature. Another example, which takes advantage of the drastic change in the ion product of water with temperature, is the alternation of the reaction field where ions are preferably formed to a field where radicals are preferably formed, or vice versa.

More concrete explanations can be given using the example of hydrogen production from wood biomass in supercritical water. Steam reforming of wood biomass under atmospheric pressure produces significant amounts of tars, chars, and gases containing large amounts of hydrocarbons with a higher molecular weight and small amount of hydrogen. On the other hand, the effective conversion of wood biomass to useful gases (H_2, CO, CH_4, etc.) in supercritical water has been reported with a little amount of tars and no chars (Antal, Jr. et al., 2000). The reason for this lies in measurements of the pyrolysis kinetics of wood biomass materials. The constituents of wood biomass are mainly cellulose, hemi-cellulose, and lignin. Cellulose is not gasified, and tends to become char at high temperatures, but is easily hydrolyzed in hot temperature (subcritical) water. When wood biomass is heated with water along path (1) in Figure A.7, most of the cellulose turns into char, but heating along path (2) causes the cellulose to hydrolyze in water at temperatures below the critical temperature of water. Then the cellulose is gasified or decomposed to form useful gases (H_2, CO, CH_4, etc.) and tars above the critical temperature. One of the reasons for the alternate reaction mechanism from hydrolysis to gasification is the changes in the static dielectric constant and ion product. Thus, hydrogen production from wood biomass in supercritical water takes advantage of the changes in these properties. Although the reaction along path (3) may seem to suffice and that high pressure would be

unnecessary, this is only true if only the changes of static dielectric constant and ion product are important. However, when hydrogen gasification is conducted in, for example, a batch process, a large enthalpy difference exists between the liquid phase and the gas phase as shown in Figure A.8 along path (3), and this amount of enthalpy would be wasted in order to turn the water medium from the liquid phase into the gas phase each time. In contrast, along path (2), the enthalpy difference is small, and the wasted enthalpy is reduced. This is why high-temperature and high-pressure water around the critical point has high reaction controllability.

2) Heat loss from a reactor and, if any, the heat exchanger is reduced. One reason is the reaction time is shortened due to the high reactivity of hydrothermal reaction. 3) Exhaust heat (around 300 to 400 °C) from certain factories can be used for preheating. Generally, the reaction temperature in the gas phase is high, and between 600 to 800 °C. However, the reaction temperature of a hydrothermal reaction is around 350 to 500 °C, which is much lower than a gas phase reaction. If the temperature of exhausted heat is around 300 to 400 °C, then this thermal energy can be more easily used for preheating in hydrothermal reactions. 4) Hydrothermal reactions utilize water as the reaction media. It is noteworthy that water is not harmful to the environment and the hydrothermal reaction is chemically benign to the environment.

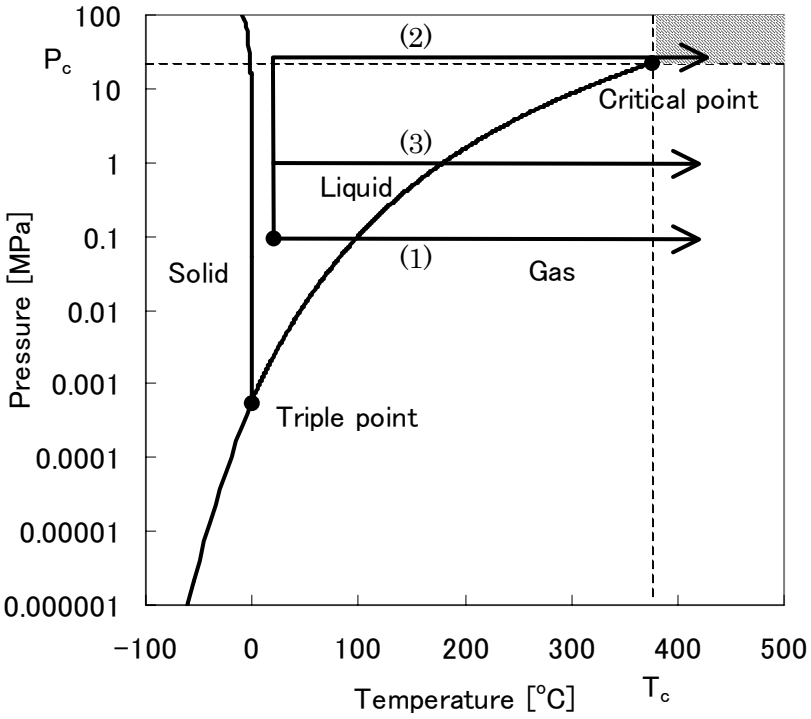

Figure A.7 Reaction paths for hydrogen production from wood biomass

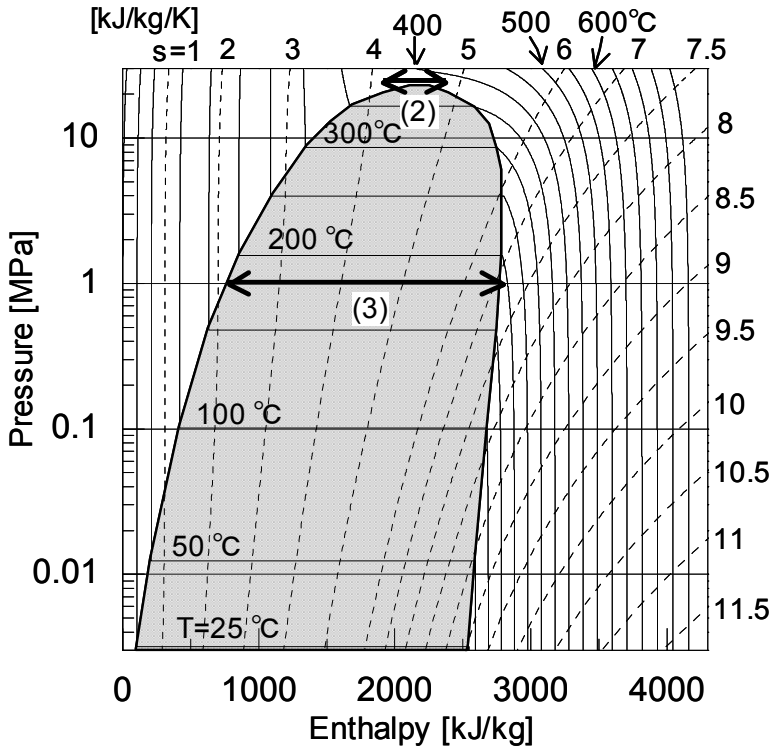

Figure A.8 Enthalpy differences between the liquid and gas phase in paths (2) and (3)